SPIKE OUTPUT AND SYNAPTIC PLASTICITY IN A FEED-FORWARD INHIBITORY MICROCIRCUIT IN THE CEREBELLAR CORTEX

Thesis submitted for the degree of
Doctor of Philosophy of London University

Wolfgang Matthias Oliver Mittmann

Department of Physiology & Wolfson Institute for Biomedical Research

UNIVERSITY COLLEGE LONDON

2006

ProQuest LLC
789 East Eisenhower Parkway
P.O. Box 1346
Ann Arbor, MI 48106-1346

Abstract

Feed-forward inhibitory circuits are common building blocks in the mammalian brain and lead to excitatory input also activating inhibitory input to a common postsynaptic neuron. Such circuits are important for regulating neuronal excitability and timing of activity in the brain. In this thesis I have explored the mechanisms and consequences of feed-forward inhibition in the rat cerebellar cortex, which is known to be involved in coordination and timing of movement.

Voltage clamp recordings from Purkinje cells in cerebellar slices exhibit a biphasic current waveform in response to stimulation of parallel fibres, consisting of an excitatory postsynaptic current (EPSC) followed by an inhibitory postsynaptic current (IPSC). The latency difference between the two components – only 1.4 ms – and the complete block of the biphasic response by glutamate receptor antagonists confirmed the second component as feed-forward inhibition (FFI). The rapid onset of FFI shortens EPSPs, which enhances spike precision and limits summation of independent inputs. Next, I showed that the latency of FFI does not change with distance along active parallel fibres. This suggests that desynchronisation of action potentials travelling along the parallel fibres is insufficient to cause feed-forward inhibition to arrive ahead of excitation, a theory previously used to explain the observed lack of 'beams' of active Purkinje cells along the parallel fibres. Instead, it is argued that this may result from spatial or temporal spread of activity in the granule cell layer leading to early arrival of inhibition.

Both excitation and inhibition in Purkinje cells are subject to plastic changes induced by climbing fibre activation. In a feed-forward network, what is the net effect of this plasticity on the output of the cerebellar cortex? First I showed that both inhibition and excitation undergo long-term depression (LTD) to a similar extent when paired with climbing fibre input. This plasticity was reflected in corresponding changes in Purkinje cell spike output triggered by independent inhibitory and excitatory inputs: parallel fibre LTD reduced, and LTD of inhibition increased the number of spikes evoked by the respective inputs. To examine the net effect of simultaneous plasticity of inhibition and excitation on Purkinje

cell output with a feed-forward input, I simulated synaptic inputs with dynamic clamp and systematically changed the ratio of excitation and inhibition as well as the amplitude of both components. Depressing both components as observed when pairing the isolated components with the climbing fibre, reduced spike output for feed-forward inputs with small inhibitory components, while for inputs with stronger inhibition the spike output increased. Finally, I showed that pauses after spike bursts evoked by strong parallel fibre inputs in the absence of inhibition scaled with input strength. A classical climbing fibre LTD protocol reduced these pauses, which thus encode information stored by synaptic plasticity for downstream neurons. These findings are discussed in the context of classical theories of cerebellar learning, which are concluded to require revision or refinement.

Acknowledgements

First of all I want to thank my boss, Michael Häusser. He provided a great breeding ground for scientists and ideas, not only through a lab packed with amazing people and the newest toys but also by encouraging discussion with great scientists in lab meetings, retreats and conferences all around our hemisphere.

Pablo Monsivais, Troy Margrie and Mickey London helped and motivated me at crunch times. A thousand thanks.

David Attwell, Jesper Sjöström, Arnd Roth, Beverley Clark, Jason Rothman, Julian Jack and Latha Ramakrishnan were always happy and able to help.

Paul Chadderton, Severine Mahon, Kamilla Angelo and Jenny Davie have been the best office mates ever, gifted footballers, less gifted drivers, reliable MA nachos companions, firm English teachers and they were always up for discussing how the cerebellum works. Ede Rancz helped me to rid myself of negative thoughts and emotions by inducing cell death of the responsible neurons.

Special thanks to my curly editor for her hard work, her support and her loving honesty.

The old Rockefeller students, the Freiburg connection and my family played a big part in keeping me reasonably sane.

"There are known knowns. There are things we know that we know. There are known unknowns. That is to say, there are things that we now know we don't know. But there are also unknown unknowns. There are things that we do not know we don't know."

Donald Rumsfeld

1 Introduction

Since Holmes' early work examining shrapnel victims of World War I (Holmes, 1939) it has been known that the cerebellum is crucial for motor control. While movements are possible despite cerebellar damage, cerebellar function is necessary for smooth, temporally and spatially precise movements. The cerebellum is thought to control the timing of muscle activation necessary for smooth movements and is also responsible learning new motor tasks.

The cerebellum consists of a cortex and the deep cerebellar nuclei in its center. The only output of the cortex are the axons of Purkinje cells, which target the deep cerebellar nuclei, which in turn form the output of the cerebellum. Purkinje cells receive inhibitory input from interneurons, which strongly influence spiking in Purkinje cells. I show that these interneurons are part of a microcircuit, in which inhibition from interneurons is activated by parallel fibres, the same fibres that also provide Purkinje cell excitation. This thesis is focused on this microcircuit and its influence on Purkinje cell spiking, as well as changes of the microcircuit introduced by synaptic plasticity, the cellular correlate for learning.

Here I will introduce inhibitory synaptic transmission and the common building blocks in which inhibition is found, namely feedback and feed-forward inhibitory microcircuits. This is followed by an introduction to the cerebellar circuitry, and the different forms of synaptic plasticity of Purkinje cell inputs linked to motor learning in the cerebellum.

1.1 Inhibition

Chemical synaptic transmission is mediated by neurotransmitters released from presynaptic boutons. The majority of receptors for those neurotransmitters are located on the postsynaptic side of the synapse and are part of ion channels, which transiently open in response to activation of the receptor. These ligand-gated channels are selectively permeant to one or several ions. Whether the synaptic current resulting from channel opening hyperpolarizes or depolarizes the postsynaptic cell depends on the relative permeability to different ion species, the reversal potential of the permeant ions and the membrane potential of the cell. Glutamate receptors that are also activated by α-amino-3-hydroxy-5-methylisoxazoleproprionic acid (AMPA) are cation specific and have reversal potentials around 0 mV. Application of agonist therefore brings the cell closer to 0 mV. Since the threshold for action potential generation is more negative, activation of these channels promotes action potential firing and AMPA receptors (AMPARs), their agonists and synapses containing AMPARs are called excitatory.

That some connections between cells reduce excitation and therefore are inhibitory was already recognized before electrical correlates for neural activity were known (Sherrington, 1906). Fast synaptic inhibition is mediated by two neurotransmitters, glycine and γ-aminobutyric acid (GABA). The receptor-channel complexes for glycine and GABA are selectively permeable to chloride (and to a lesser extent to bicarbonate), which in most neurons has a reversal potential more negative than the resting potential (Hille, 2001). GABA receptors permeant to chloride are called $GABA_A$ receptors (or $GABA_AR$s) to distinguish them from non-conducting metabotropic $GABA_B$ receptors ($GABA_BR$). Therefore, activation of glycine or GABA receptors typically leads to hyperpolarisation of the postsynaptic cell and to a reduction of spike probability. Glycine is the predominant inhibitory neurotransmitter of the spinal cord, GABA is predominant in the brain although there is some overlap, particularly in the

brainstem (Nolte, 1999). Glycinergic inhibition has also been shown in the cerebellum where Lugaro cells co-release GABA and glycine onto potsynaptic Golgi cells (Dumoulin *et al.*, 2001). Golgi cell → unipolar brush cell synapses and some inputs to deep cerebellar nucleus neurons are also glycinergic (Kawa, 2003; Dugue *et al.*, 2005). However, synaptic inhibition stemming from cells of the molecular layer of the cerebellum is exclusively GABAergic.

1.1.1 GABA mediated inhibition

Local interneurons are usually the source of GABA in the brain. These cells display a puzzling variety of different morphologies indicating diverse cell-type specific functions although the structure function relationship is incompletely understood (e.g. in hippocampus Freund & Buzsaki, 1996; Miles *et al.*, 1996). Presynaptic terminals of interneurons look similar to glutamatergic terminals in electron-microscopic images (Cowan *et al.*, 2001). Small clear vesicles contain several thousand molecules of GABA. Upon invasion of an action potential calcium influx leads to fusion of these vesicles with the presynaptic membrane and release of GABA into the synaptic cleft.

The postsynaptic side of GABAergic synapses differs from glutamatergic synapses. In electron microscopic images glutamatergic synapses show a fuzzy dense thickening of the postsynaptic membrane, termed the postsynaptic density. This gives glutamatergic synapses an asymmetric appearance with electron-dense material confined to the postsynaptic side. In contrast, GABAergic synapses lack a strongly developed postsynaptic density and thus look symmetric. The postsynaptic density is comprised of fibres of the cytoskeleton and a large number of proteins involved in scaffolding and modulation of postsynaptic receptor sensitivity, kinetics and number. Differential expression of these components is thought to be the basis for the microscopically detectable differences in the postsynaptic densities of glutamatergic and GABAergic synapses (Cowan *et al.*, 2001).

Functional $GABA_A$Rs are comprised of five subunits. Those subunits contain four transmembrane domains and a ligand-binding domain in the extracellular

N-terminus. The architecture of the subunits and their pentameric organisation is similar to other ligand-gated channels, including the inhibitory glycine channel and the nicotinic acetylcholine receptor (Hille, 2001). $GABA_AR$s require the binding of two GABA molecules to open and the continued presence of GABA leads to desensitisation, which is thought to be a state of the channel in which the receptors are occupied but the channel stays closed.

A confusing multitude of different subunits exists which is further complicated by different splice variants of some subunits. Six different α subunits, three β, three γ as well as δ, ε, θ, π and ρ subunits have been cloned (Farrant & Nusser, 2005). Not all combination of subunits are possible and some rules for assembly are known. The combination of subunits in the pentamer endows $GABA_AR$s with a whole range of different properties. A common combination is likely to contain two α_1 , two β_2 and a single γ_2 subunit. Expression of a γ_2 subunit seems to be responsible for targeting and clustering of $GABA_AR$ to a synaptic location, whereas receptors containing δ subunits instead of γ_2 and/or α_6 subunits are located extrasynaptically (Moss & Smart, 2001; Brunig *et al.*, 2002). GABA sensitivity is determined by the α subunits and the δ subunit if present. These subunits also determine the extent of desensitisation during continued presence of GABA and the time the channel stays open is much longer for channels where the γ subunit are replaced by a δ subunit. Sensitivity and kinetics of $GABA_AR$s can be modulated by endogenous steroids, barbiturates, benzodiazepines, alcohol and other substances and this modulation also depends on the subunit composition (Hille, 2001; Farrant & Nusser, 2005).

Taken together, the diversity of $GABA_AR$ properties are likely to be the result of specialisation to distinct functional requirements. Especially interesting is the phenomenon of tonic inhibition caused by ambient levels of GABA. Tonic inhibition decreases the input resistance of cells and therefore changes synaptic integration of excitation and phasic inhibition (Mitchell & Silver, 2003). Phasic inhibition is, at least partially, mediated by $GABA_AR$s containing α_1 , β_2 and γ_2 subunits whereas tonic inhibition is often mediated by channels containing a δ instead of a γ_2 subunit. The γ subunit containing channels are located synaptically and their sensitivity to GABA is much lower compared to

extrasynaptic δ subunit containing channels. This enables the extrasynaptic $GABA_A$Rs to be responsive to micromolar (or maybe even nanomolar) ambient GABA concentrations, whereas the synaptic $GABA_A$Rs will not be saturated by millimolar GABA concentration in the synaptic cleft during synaptic transmission and thus stay responsive to trains of presynaptic activity. Synaptic γ subunit-containing $GABA_A$Rs also desensitise faster and have shorter opening times compared to extrasynaptic $GABA_A$Rs which, again, might serve to keep these receptors operating within a dynamic range to allow different rates of synaptic transmission to be 'read out'. In contrast, long opening times and reduced desensitisation serves to maintain a steady conductance of extrasynaptic $GABA_A$Rs containing a δ subunit. Interestingly, the modulation of $GABA_A$Rs by benzodiazepines and endogenous steroids depends not only on the γ or δ subunits, but also on the species of α subunit in the channel which could be part of an extrasynaptic δ subunit containing channel or synaptic γ containing channel. Thus tonic and phasic inhibition could be regulated independently or in concert by different modulators indicating a complex regulation of two computationally distinct functions of $GABA_A$Rs (Farrant & Nusser, 2005).

The reversal potential of $GABA_A$Rs depends on the intracellular chloride concentration. The chloride concentration in the cell is kept low by the potassium chloride co-transporter (KCC2), resulting in chloride reversal potentials more negative than resting potential. In immature neurons the potassium chloride co-transporters is often not expressed and chloride is accumulated inside the cell by Na^+/K^+ coupled cotransporters (NKCC1). Therefore $GABA_A$Rs activation leads to inward chloride currents with reversal potentials higher than the action potential threshold. GABAergic transmission can therefore be excitatory in immature neuronal networks (Ben-Ari, 2002).

Later in development, and also in some mature neurons, the reversal potential of current through $GABA_A$Rs often lies between the resting potential and the action potential threshold. In this situation GABAergic responses are depolarising but not excitatory as they do not trigger or aid the triggering of spikes: although the depolarising GABAergic potential brings the cell closer to threshold, coincident excitatory input will have reduced probability of reaching

threshold. This is because as soon as the membrane potential exceeds the reversal potential, current through $GABA_A$Rs will reverse and will be hyperpolarising. Thus, the GABAergic conductance clamps the cell to a voltage below threshold and is inhibitory despite depolarising potentials at rest (Hille, 2001).

Some exceptions to this scenario have recently emerged. GABAergic inputs have been shown to aid spike generation although the reversal potential was in between membrane potential and spike threshold. This occurs when the GABAergic inputs are isolated from excitation. This separation can be temporal, such that depolarising IPSPs outlasting the conductance sum with excitation (Gulledge & Stuart, 2003). Alternatively, spatial separation of inputs can lead to dendritic GABAergic conductances acting like currents if the local voltage at the inhibitory synapse is only weakly influenced by electrically remote excitatory input (Gulledge & Stuart, 2003). Another mechanism of excitatory action of GABA in cells with reversal potentials in between rest and threshold can happen by activation of voltage-gated channels or NMDA receptors by depolarising IPSPs (Leinekugel *et al.*, 1997).

1.1.2 Microcircuits

Neurons are not randomly connected. On the scale of many thousands of neurons this is evident even from the gross anatomy of the brain. Most nuclei of the brain have their neurons connect to other specified nuclei or specific areas of the brain, usually to specific cell types. This is a logical consequence of regional specialisation of brain function. Local connections often do not follow similarly clear connection patterns. However, local connections are not random. Layer V neurons in the visual cortex have been found to be more reciprocally connected than expected for random connections. Furthermore, two connected neurons are much more likely to receive input from the same pyramidal cell and are also more likely to have a common target than expected for random connectivity (Song *et al.*, 2005). Such building blocks are often called microcircuits although there is no principal difference between those local

circuits and connections between different nuclei other than the distance of the connection.

Microcircuits containing inhibitory cells are especially interesting because interpretation of their functional significance is more intuitive compared to excitatory microcircuits. The most basic feedback inhibitory circuit consists of only two neurons: an excitatory neuron (or principal neuron) that activates an inhibitory neuron, which in turn inhibits its input, the principal neuron. The purpose of such a circuit is likely to be the regulation of activity of the principal neuron. This control is dynamic as the level of activity determines the amount of inhibition. This inhibitory control may play a role in avoiding high, sustained firing frequencies linked to excitotoxicity. As already mentioned, many local excitatory connections are reciprocal and feedback inhibition is a mechanism to dampen such intrinsically unstable circuits and prevent synchronized activity reminiscent of epilepsy. Negative feedback control is a mechanism not restricted to the nervous system. It is found in many other contexts such as biochemical metabolic pathways (e.g. the pyrimidine biosynthesis ; Voet & Voet, 1995), mechanical contexts like a toilet cistern, in electronics and many other areas.

In neural systems such as the hippocampus, control of firing rate by inhibitory feedback can be very fast. If a spike in a principal pyramidal cell triggers a spike in a feedback inhibitory interneuron the time between spike and feedback inhibition is only slightly longer than the delay of the two synapses involved in this pathway and feedback inhibition lags the spike by only a few milliseconds (Andersen *et al.*, 1963). EPSPs in hippocampal pyramidal neurons last tens of milliseconds, (Purves *et al.*, 2004) therefore feedback inhibition can limit the number of spikes fired in response to an input and can confine the timing of spikes to a few milliseconds after onset of the excitation that drives the microcircuit. Recently, such action was observed for feedback inhibition terminating on the soma of hippocampal pyramidal cells (Pouille & Scanziani, 2004). Strikingly, within the same cell, feedback inhibition terminating on the dendrite was much weaker. However, sustained firing of the pyramidal cell led to increasingly strong dendritic inhibition due to facilitation of pyramidal cell inputs to interneurons which mediate dendritic inhibition. Initially weak dendritic

inhibition that facilitates with increasing pyramidal cell spike rate might counteract dendritic excitation that in a physiological scenario would be the cause for high spike frequencies of the pyramidal cell. This was suggested to prevent excitotoxicity through excessive calcium influx (Mittmann *et al.*, 2004) as has been shown previously (Miles *et al.*, 1996). In this example, two distinct inhibitory feedback circuits of the same pyramidal cell are tuned to perform two different operations: the synaptic properties of somatic feedback inhibition ensure precise timing of output spikes whereas dendritic inhibition is tuned to counteract the side effects of strong excitatory input to the pyramidal cell. This example highlights how the exact properties of such simple inhibitory feedback circuits could be designed to perform specific tasks. It is plausible that with synapses and cells displaying various forms of plasticity, such hardwired circuits could show a rich dynamic behaviour in response to different activity states of the network.

While feedback inhibition is a flexible microcircuit that might perform a variety of functional tasks, it does not play a role in determining whether the principal neuron will fire a spike or not. This is because feedback inhibition needs at least one spike to be activated in contrast to feed-forward inhibitory microcircuits. The most basic feed-forward inhibitory microcircuit consists of a principal neuron that receives excitatory input. The excitatory input also activates inhibitory interneurons that inhibit the principal neuron. Therefore, feed-forward inhibition (FFI) is driven by the input in contrast to feedback inhibition, which is driven by the output of the principal neuron. In the neocortex and many other brain areas most cells receive feed-forward and feedback inhibition (Shepherd, 2004). Some inhibitory neurons, like cerebellar Golgi cells, even mediate both feed-forward and feedback inhibition at the same time (Eccles *et al.*, 1967; Marr, 1969).

In the hippocampus, FFI strongly influences timing of spikes in response to excitatory inputs (Pouille & Scanziani, 2001). FFI only allows excitatory inputs occurring within 3 ms of each other to summate compared to a summation window of several tens of milliseconds in the absence of inhibition. Furthermore, without FFI an input triggers spikes within a time window of 10 ms

after the input. In contrast FFI forces spikes into a 2 ms time window, illustrating the role of FFI in increasing temporal spike precision.

The feed-forward inhibitory circuit of the cerebellar molecular layer formed by parallel fibres, Purkinje cells and interneurons is characterised in chapter 3, the circuit's potential role in forming the somatotopic cerebellar map is investigated in chapter 4 and functional consequences of synaptic modifications are the subject of chapter 5.

1.2 Cerebellum

Cerebellum literally means "little brain", a term inspired by its gross morphology: it has a different appearance from the rest of the brain due to the folia on its surface, it is a large structure occupying about 13% of the total brain volume (Clark *et al.*, 2001) and it is clearly separated from the rest of the brain located at the posterior surface of the brainstem only connected by three pairs of fibre bundles, the cerebellar peduncles. At first glance three lobes can be separated by vertical fissures, the hemispheres on both sides and the vermis placed between them. The flocculonodular lobe is more hidden between brainstem and the other lobes (Ramón y Cajal, 1904; Eccles *et al.*, 1967; Nolte, 1999).

The cerebellum consists of the deep cerebellar nuclei (DCN), white matter carrying all the fibre tracts and the cortex. The principal input of the cerebellum is provided by the mossy fibres. The majority of them are axons of the pontine nuclei neurons, which relay input from neocortical areas although some fibres enter the cerebellum directly from the spinal cord and the vestibular system. Mossy fibres travel through the inferior and middle cerebellar peduncle, enter the cerebellum and travel through the white matter to the cerebellar cortex. While passing through the white matter of the medullary center of the cerebellum, mossy fibres give of collaterals exciting the DCN neurons located there.

The cerebellum receives a second kind of input, the climbing fibres (CFs). Stemming from the inferior olive they take the same path as the mossy fibres and like them innervate the DCN with collaterals on their way to the cerebellar cortex.

The output of the cerebellar cortex, the Purkinje cell (PC) axons, do not leave the cerebellum but travel through the white matter to terminate in the DCN neurons which they inhibit. Therefore the cerebellar cortex together with the

cerebellar afferents can be seen as a feed-forward inhibitory circuit providing input to the neurons of the DCN (fig 1.1 A).

In addition to the excitatory input from mossy fibres, CFs, inhibition from PCs and local connections, DCN neurons spike spontaneously due to intrinsic currents (Raman *et al.*, 2000). A subset of DCN neurons makes inhibitory connections to the inferior olive (de Zeeuw *et al.*, 1989; Fredette & Mugnaini, 1991) whereas most neurones of the DCN make excitatory connections with several, often motor-related nuclei in the brainstem, such as the red nucleus, ventral thalamic nuclei, nuclei in pons and medulla. Some fibres also travel without relay through the cervical spinal cord (Shepherd, 2004).

The cerebellar cortex is usually divided into three layers. The granule cell layer is named after the tightly packed granule cells (GCs) making up most of its volume. The superficial surface of the GC layer is covered by the PC layer, which consists of a single sheet of PC somata. The dendrites of PCs together with the GC axons make up the bulk of the molecular layer which is covered by the pia mater (fig1.1 B).

1.2.1 The Granule Cell Layer

The first comprehensive investigation of the cerebellar anatomy describing all major cell types as well as the connections between them was published more than a hundred years ago by Santiago Ramon y Cajal (Ramón y Cajal, 1904). In contrast to the neocortex and other brain areas, the cerebellar cortex has a remarkably regular, almost crystalline structure that is conserved across the whole cerebellum and remarkably invariant across all vertebrates. A composite drawing of Golgi stained cells of a parasagittal cut (perpendicular to the folium) taken and modified from Ramon y Cajal is shown in figure 1.1 B.

The white matter in the center is carrying mossy fibres that enter the GC layer and provide the only excitatory input to that layer. A mossy fibre can spread fairly widely within and across different folia (chapter 4.3.3). GCs are by far the most common neuron of the brain constituting more than half of the total number of neurons in the brain. Mossy fibres form synapses with GC dendrites

at axon terminals or swellings that give these fibres the appearance of a string of beads. Each of these swellings is studded with up to 50 GC dendrites (Hamori & Somogyi, 1983) forming a structure called "glomerulus". Each mossy fibre collateral that enters the GC layer shows 20 – 30 synaptic varicosities (Palay & Chan-Palay, 1974) and each mossy fibre can have as many as 30 collaterals (Wu *et al.*, 1999). That means that there is a huge divergence and a single mossy fibre can excite up to 45,000 GCs. In contrast to this huge figure, GCs only receive input from 4 mossy fibres on average. GCs are small, with a soma between 5 – 8 μm and 4 or five dendrites less than 30 μm long with which they receive input from different mossy fibres. Due to their size they are electrically compact and have a high input resistance (about 1GΩ), which leads to large EPSPs in response to unitary inputs. GCs do not fire spontaneously but two or three inputs are sufficient to cross threshold and trigger a spike even in the presence of tonic inhibition (Chadderton *et al.*, 2004). GCs in juvenile animals need fewer inputs to reach threshold compared to adult animals where resting potential and input resistance are decreased and single quanta are not sufficient to activate NMDA receptors (Cathala *et al.*, 2003).

Mossy fibres also excite Golgi cells whose inhibitory axons terminate on GC dendrites in the glomeruli. Axons of GCs also terminate on Golgi cell dendrites located in the molecular layer and therefore Golgi cells provide feed-forward as well as feed-back inhibition to GCs which is thought to control GC layer activity (Eccles *et al.*, 1966; Maex & De Schutter, 2005).

The close proximity of excitatory and inhibitory pre- and postsynaptic elements in the glomerulus was recently shown to be important for synaptic transmission in the glomerulus. Neurotransmitter released at active zones in the glomerulus diffuses to receptors located on the opposing postsynaptic membrane. Some transmitter diffuses out of the synaptic cleft and can activate extrasynaptic receptors at pre- and postsynaptic membranes or receptors of neighbouring synapses. Such "spillover" is important for regulation of presynaptic release by presynaptic $GABA_B$ (Dittman & Regehr, 1997) and metabotropic glutamate receptors (Mitchell & Silver, 2000). Glutamate spillover onto neighbouring synapses has a large effect on EPSCs carrying a significant fraction of the total charge (DiGregorio *et al.*, 2002). Similarly, GABA spillover contributes most of

the charge transferred by IPSCs in GCs following Golgi cell activation (Rossi & Hamann, 1998). High affinity $GABA_A$ receptors are activated by basal levels of GABA in the glomerulus, giving rise to a tonic inhibitory conductance which can be regulated by hormones in a process that might determine activity levels in the GC layer (Brickley *et al.*, 1996; Stell *et al.*, 2003).

1.2.2 The Molecular Layer

Axons from GCs ascend through the PC layer to bifurcate in a T-junction in the molecular layer giving rise to the parallel fibres (PFs) that run horizontal for 2 to 2.5 mm to either side (Pichitpornchai *et al.*, 1994). PFs transect the flat planes of PC dendritic trees that are oriented perpendicular to the direction of the PFs. PCs possess one of the most highly branched and elaborate dendritic trees found in the nervous system (fig 1 B). The structure of the PC gives the best example for a space filling dendrite found in the nervous system (Stuart *et al.*, 1999) and seems to be designed to sample as many PFs as possible. Indeed, electron-microscopic studies indicate that PCs make one or two synaptic contacts with every second or third PF that passes through its dendrite. Not only the PF part of the GC axon but also the ascending segment of the GC axon makes synaptic contacts with PCs. Together, PFs and the ascending segment make between 150,000 to 200,000 synapses onto PCs (Palay & Chan-Palay, 1974; Napper & Harvey, 1988), a convergence unparalleled in the nervous system. Although much shorter than the PF portion, the ascending segment was found to make up 20% of the total GC synapses onto PCs (Gundappa-Sulur *et al.*, 1999). Unitary PF EPSCs in PCs have an amplitude of only 10 pA and the connection probability for GCs via the ascending segment is much higher (50%) than for PF synapses (7% ; Barbour, 1993; Isope & Barbour, 2002) which is complemented by some differences in synaptic properties (Isope & Barbour, 2002; Sims & Hartell, 2005). The discrepancy between the small functionally observed connection probability and the high connection probability found with electron microscopy led to the hypothesis that a large fraction of PF synapses are silent (Brunel *et al.*, 2004). Instead of being useless leftovers from previous motor learning that led over consecutive LTD

inductions to an eventual loss of function these dormant "silent" synapses might be important for reliable recognition of inputs and allow the PC to work as a perceptron (Brunel *et al.*, 2004).

Not only PFs but also CFs provide input to the molecular layer. These axons wrap around proximal parts of PCs making hundreds of synaptic contacts with proximal parts of the PC dendrite which receives only one CF. However, each CF contacts on average 10 different PCs in different folia and lobules of the cerebellar cortex (Sugihara *et al.*, 2001).

PCs are complex cells, not only their morphology but also their repertoire of ion channels endows them with several interesting properties. Due to their size, PCs have a low input resistance (tens of megaohms) responsible for small potentials in response to current injection. The large membrane surface area together with the low input resistance cause synaptic potentials to be filtered by the time they reach the soma (Roth & Häusser, 2001). *In vivo* PCs spike continuously with frequencies between 10 and 100 Hz (Granit & Phillips, 1956; Eccles *et al.*, 1967; Thach, 1968; Bell & Grimm, 1969; Armstrong & Rawson, 1979a; Nitz & Tononi, 2002) similar to frequencies of the regular firing observed *in vitro* (Llinas & Sugimori, 1980; Smith & Otis, 2003). In slice preparations excitatory inputs to PCs hardly contribute to the observed firing frequencies (Häusser & Clark, 1997). Instead, intrinsic currents, predominantly the resurgent sodium current but also voltage-dependent calcium currents, are responsible for inward currents between spikes but spike frequency also depends on currents contributing to the afterhyperpolarisation (Raman & Bean, 1997, 1999). Bistability, where regular spiking and hyperpolarised periods are interleaved (Williams *et al.*, 2002; Loewenstein *et al.*, 2005) or trimodal firing patterns, where in addition to regular spiking and quiescent states periods of burst firing occurs (Womack & Khodakhah, 2002; Womack & Khodakhah, 2004) were suggested to be the normal operational mode of PCs. Two conductances favour regular spiking: the hyperpolarisation activated current (I_h) and calcium activated potassium currents (K_{Ca}). CF or strong PF input leads to strong PC depolarisation (chapter 6). Calcium influx through voltage gated channels then leads to activation of K_{Ca} compensating the depolarisation, which prevents burst firing. If this mechanism overcompensates the depolarisation or if PCs get

strong inhibitory input I_h is activated by the hyperpolarisation and depolarises the cell thus preventing quiescent hyperpolarised states (Williams *et al.*, 2002). Whether bistability or trimodal firing is a physiological behaviour is controversial (Loewenstein *et al.*, 2005; Schonewille *et al.*, 2006).

The molecular layer also contains inhibitory interneurons. These interneurons have quite diverse morphologies (Ramón y Cajal, 1904; Palay & Chan-Palay, 1974) and were separated into two classes by Cajal: basket cells with somatas in the lower molecular layer and stellate cells located in the upper molecular layer. While their morphologies are quite different, there is a smooth gradient between them and there is little evidence that they are two distinct cell types (Sultan & Bower, 1998). Interneurons receive excitatory input from PFs and their GABAergic axons synapse with PCs and other interneurons. This arrangement was thought to regulate activity in the molecular layer and provide a kind of gain control similar to the function of Golgi cells in the GC layer (Marr, 1969; Albus, 1971). Like PCs interneurons spike spontaneously. *In vivo* spike rates are only 3 Hz (Jorntell & Ekerot, 2003) whereas in slice interneurons fire around 13 Hz in the absence of synaptic transmission (Midtgaard, 1992; Häusser & Clark, 1997; Carter & Regehr, 2002; Molineux *et al.*, 2005). Input resistance in these neurons is high (up to 1 GΩ) and membrane time constants are fast leading to large sharply rising EPSPs in response to release of single vesicles, which might even be sufficient to trigger a spike (Carter & Regehr, 2002).

A more detailed description of interneuron morphology is given in chapter 3.1.1.

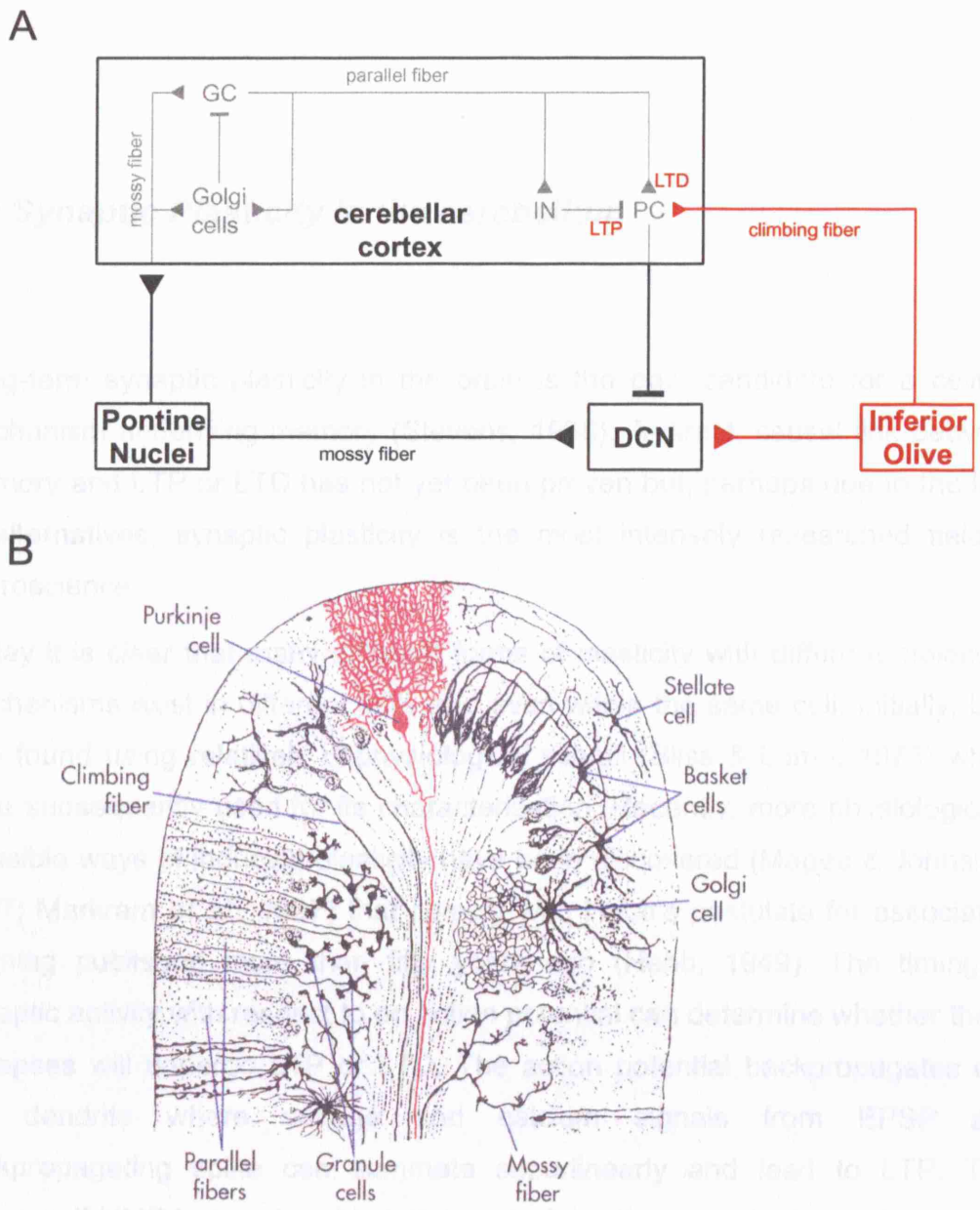

Figure 1.1

The **cerebellum**
A Schematic of the circuitry of the cerebellum. The mossy fiber circuit can be seen as a feed-forward inhibitory circuit. The mossy fibers from the pontine nuclei directly excite the DCN. They also provide excitatory input to the cerebellar cortex whose inhibitory output inhibits the DCN. Within the cortex two feed-forward inhibitory circuits exist, the mossy fiber → GC, mossy fiber → Golgi cell → GC circuit and the PF → PC, PF → interneuron → PC circuit. Golgi cells also receive input from PFs and provide feedback inhibition to GCs. CFs also form a feed forward inhibitory circuit exciting the DCN and PCs which inhibit the DCN. CF action leads to LTD of PF synapses and LTP of inhibitory synapses. **B** Composite drawing of Golgi-stained cerebellar neurons from sagittal sections. PFs are cut and travel orthogonal to the plain of the paper. Note the dense mesh of basket cell axons surrounding PC somas. Modified from Ramón y Cajal (1909) by Nolte (1999).

1.3 Synaptic Plasticity in the cerebellum

Long-term synaptic plasticity in the brain is the best candidate for a cellular mechanism underlying memory (Stevens, 1998). A direct, causal link between memory and LTP or LTD has not yet been proven but, perhaps due to the lack of alternatives, synaptic plasticity is the most intensely researched field in neuroscience.

Today it is clear that many different forms of plasticity with different molecular mechanisms exist in different cells and even within the same cell. Initially, LTP was found using relatively unphysiological stimuli (Bliss & Lomo, 1973) which were subsequently used for its characterisation. Recently, more physiologically plausible ways of inducing plasticity have been discovered (Magee & Johnston, 1997; Markram *et al.*, 1997) that comply with Hebb's postulate for associative learning published more than fifty years ago (Hebb, 1949). The timing of synaptic activity with respect to an action potential can determine whether these synapses will undergo LTP or LTD. The action potential backpropagates into the dendrite where voltage and calcium signals from EPSP and backpropagating spike can summate superlinearly and lead to LTP. This happens if NMDA receptors bind glutamate from the synaptic transmission and the magnesium block is relieved by the depolarisation provided by the backpropagating spike (Sjostrom *et al.*, 2001; Kampa *et al.*, 2004). If the action potential occurs before the EPSP the magnesium block prevents opening of NMDA receptors, calcium levels stay too low for LTP and the EPSP undergoes LTD (Sjostrom *et al.*, 2003).

PCs do not express any functional NMDA receptors (Crepel *et al.*, 1982) and backpropagation of action potentials into the dendrite is poor (Stuart & Häusser, 1994). However, PF → PC synapses express both LTP and LTD, but this is mechanistically distinct from plasticity seen in other cell types.

1.3.1 LTD of synapses between parallel fibre and Purkinje cell

PF LTD was first postulated to exist (Marr, 1969; Blomfield & Marr, 1970; Albus, 1971) on theoretical grounds. Consistent with this theory, pairing the powerful CF input with PF activation produced LTD of the PF synapses (Ito *et al.*, 1982). Today, a lot is known about this process although some controversial issues remain.

Synaptic transmission at CF synapses is mediated by AMPA receptors (Audinat *et al.*, 1990) and is associated with a huge EPSP triggering significant calcium transients in the dendrite due to activation of voltage gated P/Q type calcium channels (Miyakawa *et al.*, 1992; Watanabe *et al.*, 1998).

Both CF and PF synaptic transmission is mediated by AMPA receptors (Konnerth *et al.*, 1990) but PFs also activate metabotropic glutamate receptors (mGluR ; Baude *et al.*, 1993; Tempia *et al.*, 1998). LTD is expressed postsynaptically as it can be detected with exogenous pulses of glutamate (Ito & Kano, 1982; Ito *et al.*, 1982) and is mediated by a reduction of AMPA receptor number by clathrin-mediated endocytosis (Matsuda *et al.*, 2000; Wang & Linden, 2000). Phosphorylation of a serine residue of the AMPA receptor is a tag for endocytosis. This phosphorylation is catalyzed by protein kinase C (PKC ; Oancea & Meyer, 1998) and can be cleaved by protein phosphatase 1 and 2A (PP ; Launey *et al.*, 2004). Activity of PKC and phosphatases thus control endocytosis and LTD (fig 1.2).

The pathway leading to activation of PKC requires activation of mGluRs by glutamate (Aiba *et al.*, 1994; Conquet *et al.*, 1994) released from PFs. Phospholipase C (PLC) is activated by mGluR coupled G-protein (Miyata *et al.*, 2001). PLC hydrolyses 4,5-bisphosphate (PIP_2) to inositol-1-3-5 triphosphate (IP_3) and diacylglycerol (DAG ; Finch & Augustine, 1998; Takechi *et al.*, 1998). If PF activity coincides or was preceded by CF activity, intracellular calcium levels are high and calcium and IP_3 together activate IP_3 receptors located at the ER membrane leading to calcium-induced calcium release from the endoplasmatic reticulum (ER ; Wang *et al.*, 2000). This superlinear rise in calcium concentration together with DAG leads to activation of PKC (Oancea &

Meyer, 1998) and to phosphorylation of the AMPA receptor (Leitges *et al.*, 2004).

Phosphorylation of the AMPA receptors is cleaved by PP (Launey *et al.*, 2004) and inhibition of PP is thought to be required for effective LTD induction because blockade of parts of the pathway leading to inhibition of PP prevents LTD induction (Daniel *et al.*, 1993; Boxall & Garthwaite, 1996; Hartell, 1996a). The first step of this pathway is activation of nitric oxide synthase (NOS). NOS is expressed in GCs but not PCs (Southam *et al.*, 1992) and activation of PFs leads to glutamate binding to presynaptic NMDA receptors with subsequent spikes releasing the magnesium block leading to calcium influx and NOS activation (Casado *et al.*, 2002). NO is membrane permeable and diffuses to PCs where it activates soluble guanylate cyclase (sGC) leading to increases in cGMP (Garthwaite *et al.*, 1988). Protein kinase G (PKG) is activated by cGMP (Hartell, 1994) and might play a direct part in the phosphorylation of AMPA receptors and so facilitates LTD directly (Nakazawa *et al.*, 1995). But the main action of PKG is phosphorylation of G-substrate, a powerful inhibitor of PP (Endo *et al.*, 1999). Inhibition of PP leads to more phosphorylated AMPA receptors, which then get internalised and so produce LTD.

1.3.2 Synapse specificity of parallel fibre LTD

PF LTD was thought to be specific to PFs active during CF activation. Specificity was tested by activating two independent inputs but submitting only one of them (the test input) to an LTD induction protocol. *In vivo* only the test input but not the control input showed LTD (Ekerot & Kano, 1985; Kano & Kato, 1987). This finding was confirmed in slice and culture (Chen & Thompson, 1995; Linden & Ahn, 1999).

Recently, work performed by Nicholas Hartell induced PF LTD with strong PF stimulation alone, without activation of the CF. This form of plasticity was not synapse specific and spread to the control input (Hartell, 1996b; Reynolds & Hartell, 2000). By strong stimulation of PFs, the necessity of CF activation was

overcome because PF EPSPs were large enough to trigger calcium influx through voltage-gated channels at synapses of the test pathway. However, LTD also spread to the control input, which was blocked by inhibiting NOS, sGC or PKG whereas LTD of the test input was unaffected (Hartell, 2001).

One interpretation of these results is that PF LTD can be induced through different signalling pathways. Strong stimulation of PFs can result in a strong activation of the NO dependent pathway at synapses of the control input leading to inhibition of AMPA receptor dephosphorylation. Although not independent of mGluR or PKC activation (Hartell, 2001) it is likely that little activity of the PKC pathway was required for induction of LTD in synapses of the control input because significant calcium rises were confined to synapses of the test pathway. Thus combinations of different grades of activity in distinct pathways operating in parallel might lead to the same result, PF LTD (Hartell, 2002). If this interpretation is correct, it may account form some controversies in the field. Other, yet not understood pathways might lead to LTD or modulate the mGluR / PKC and NO / PKG pathway. This is consistent with many other signalling molecules that have been linked to LTD such as protein tyrosine kinases LTD (Boxall *et al.*, 1996) or a pathway involving arachidonic acid (AA), phospholipase A2 (Linden, 1995) and maybe mitogen activated protein kinase (MAPK ; Lin *et al.*, 1993). Furthermore, involvement of receptors for the corticotropin-releasing factor and the insulin-like growth factor (IGF) receptor as well as the δ_2 glutamate receptor have been shown but remain unclear (Ito, 2001).

Another interesting new molecular player in LTD induction is the type 1 endocannabinoid receptor (CB1), which has been established to underlie short-term depression of excitation and inhibition (Llano *et al.*, 1991; Kreitzer & Regehr, 2001). Activation of CB1 by 2-arachidonyl glycerol (2-AG) was found to be necessary for induction of LTD (Safo & Regehr, 2005). This finding complicates further the picture of the signalling processes underlying PF LTD. In addition to neurotransmitters, anterograde signalling by NO and complicated intracellular signalling cascades the involvement of endocannabinoids now adds retrograde signalling and links short and long term plasticity to a common molecular signal.

1.3.3 LTD of synapses from the granule cell ascending segment

As mentioned above, up to 20% of GC → PC synapses are formed by the ascending segment of the GC axon (Gundappa-Sulur *et al.*, 1999). At the electron microscopic level these synapses differ from PF synapses in that they have a higher density of vesicles (Gundappa-Sulur *et al.*, 1999) although PF synapses display a range of synaptic structures themselves: the size of the presynaptic varicosity and the length of the postsynaptic density are highest close to the bifurcation point and decrease towards the end of the PF (Pichitpornchai *et al.*, 1994). Although rise and decay of EPSCs from PF and ascending segment are similar (Isope *et al.*, 2004; Sims & Hartell, 2005), paired pulse facilitation of PFs is higher indicating a lower release probability. The quantal amplitude of ascending segment synapses was also larger than for PF synapses, giving the picture of a stronger more reliable transmission for ascending segment synapses compared to PFs (Sims & Hartell, 2005).

LTD of PF synapses did not spread to synapses of the ascending segment and it was not possible to induce LTD at synapses of the ascending segment (Sims & Hartell, 2005). While these experiments suggest two different groups of GC → PC synapses it is unclear whether synapses of the ascending segment are incapable of LTD or whether stronger induction protocols are needed.

1.3.4 LTP of synapses between parallel fibre and Purkinje cell

The synapses between GC and PC can also undergo LTP. LTP was found not long after the discovery of LTD (Sakurai, 1987) but did not receive much attention and was characterised only a decade later (fig 1.3 A ; Salin *et al.*, 1996). Repetitive stimulation of PFs at 4 to 8 Hz induces LTP that does not require activation of AMPA receptors, is not abolished by buffering postsynaptic calcium with BAPTA but requires rises in presynaptic calcium during induction (Salin *et al.*, 1996). Calcium can activate adenylate cyclase (AC) and

subsequent rises in cAMP are necessary and sufficient to induce LTP (Salin *et al.*, 1996; Lev-Ram *et al.*, 2002). Protein kinase A (PKA) is activated by cAMP and inhibition of PKA prevents LTP (Salin *et al.*, 1996; Linden & Ahn, 1999). Activation of PKA leads to increases in release probability and thus LTP is expressed presynaptically (Jacoby *et al.*, 2001).

LTP is necessary for balancing the action of LTD to prevent saturation and allow extinction of LTD-dependent motor learning (Medina *et al.*, 2000; Boyden *et al.*, 2004). Because this form of LTP is presynaptically expressed and LTD is postsynaptic it is a poor candidate for reversing LTD. Recently, a pharmacologically separate form of LTP has been described that is postsynaptically expressed (fig 1.3 B ; Lev-Ram *et al.*, 2002). This form of LTP is independent of cAMP or PKA activity and NO is necessary and sufficient for induction of LTP (Lev-Ram *et al.*, 2002). As opposed to the presynaptic cAMP-dependent form of LTP the NO-dependent postsynaptic form of LTP could reverse LTD (Lev-Ram *et al.*, 2003; Coesmans *et al.*, 2004). Curiously, induction of the two forms of LTP is very similar, presynaptic cAMP – mediated LTP is induced by 4 Hz PF stimulation for 120 times whereas postsynaptic NO – dependent LTP is evoked by 1 Hz stimulation for 300 times. Not much is known about the mechanism of postsynaptic NO – dependent LTP, but it is independent of sGC and cGMP (Lev-Ram *et al.*, 2002) as well as CaM-KII (Kakegawa & Yuzaki, 2005). The final effect seems to be delivery of GluR2 to the synaptic membrane by activation of N-ethylmaleimide-sensitive factor (NSF ; Kakegawa & Yuzaki, 2005).

The induction of postsynaptic NO – dependent LTP is similar to the induction for LTD, only CF activation is lacking. The postsynaptic calcium level can therefore act as a switch between LTD and LTP (Coesmans *et al.*, 2004). This is reminiscent of the Bienenstock – Cooper – Moonroe (BCM) model (Bienenstock *et al.*, 1982) for induction of LTD / LTP only the polarity is reversed: cerebellar LTD but not LTP requires a high calcium level unlike pyramidal cells in the neocortex where LTP but not LTD requires high calcium levels (Sjostrom *et al.*, 2001, 2003).

1.3.5 Plasticity of inhibitory Purkinje cell inputs

Not just excitatory GC synapses, but also inhibitory input to PCs provided by basket and stellate cells undergo LTP. Spontaneous IPSCs recorded in PCs show LTP after PC depolarisation or activation of the CF (Kano *et al.*, 1992). This phenomenon was termed "rebound potentiation" (RP) because in the course of a whole-cell recording spontaneous IPSCs get progressively smaller ("run-down") and LTP of IPSCs is counteracting this. RP is expressed postsynaptically and requires elevated postsynaptic calcium as it is blocked by BAPTA (Kano *et al.*, 1992). Elevated calcium levels lead to activation of the Ca^{2+}/ calmoduline – dependent protein kinase II (CaM-KII) which is necessary for RP (Kano *et al.*, 1996; Kawaguchi & Hirano, 2000; Kawaguchi & Hirano, 2002). CaM-KII phosphorylates $GABA_A$ receptors directly leading to an increase in $GABA_A$ receptor sensitivity (Kano *et al.*, 1992; McDonald & Moss, 1994). Figure 1.4 shows this pathway schematically.

RP is an interesting form of plasticity because inhibitory inputs have a strong effect on spiking in PCs (Häusser & Clark, 1997; Jaeger & Bower, 1999). However, RP is not input specific and leads to potentiation of all inhibitory inputs to a PC, regardless of their own activity. RP is induced by only 5 -10 complex spikes at 1 Hz (Kano *et al.*, 1992). PCs recorded *in vivo* show complex spikes occurring with frequencies around 1 Hz (Armstrong & Rawson, 1979a) making it difficult to speculate about the physiological role of RP. Recent findings might shed light on this issue: co-activation of inhibitory input and depolarisation in the PC does not lead to RP of that input but potentiates other inputs that were inactive during the induction (Kawaguchi & Hirano, 2000) thus generating synapse specific suppression of non-specific LTP. Suppression of RP requires postsynaptic $GABA_B$ receptors which activate G_i/G_0 proteins that inhibit adenylyl cyclase (AC) activity (Kaupmann *et al.*, 1997). The resulting decrease in cAMP concentration inhibits activity of PKA and PKA inhibition is necessary for suppression of RP (Kawaguchi & Hirano, 2000).

Protein phosphatase 1 (PP-1) acts as an inhibitor of CaM-KII (Strack *et al.*, 1997) and this inhibition is required for suppression of RP (Kawaguchi & Hirano,

2002). PCs express DARPP-32, which in its phosphorylated form inhibits PP1. The phosphorylation of DARPP-32 is controlled via two pathways.

1. Calcium activates calcineurin (also called protein phosphatase 2B), which dephosphorylates DARPP-32 and therefore releases PP-1 from inhibition so that PP-1 can inhibit CaM-KII. Because CaM-KII is also activated by calcium this pathway is a negative feed-back to check CaM-KII activity (Kawaguchi & Hirano, 2002).
2. PKA phosphorylates DARPP-32 which leads to inhibition of PP-1 which therefore cannot check CaM-KII activity anymore (Kawaguchi & Hirano, 2002).

Kawaguchi and Hirano (2002) suggest that during PC depolarisation and high calcium levels the first pathway leads to activation of CaM-KII leading to RP. Calcineurin inhibits this process via dephosphorylation of DARPP-32 but looses against PKA that phosphorylates DARPP-32. If depolarisation coincides with $GABA_B$ receptor activation falling cAMP levels reduce PKA activity. Lack of PKA activity tips the balance of DARPP-32 phosphorylation towards the dephosphorylated state leading to inhibition of CaM-KII and suppression of RP.

While this pathway provides a plausible mechanism for suppression of RP it has not yet been shown to reverse RP or to induce depression. Similar to the case of PF LTD, a reversal of previously established LTP is necessary to prevent convergence of synaptic strength towards a maximum value and saturation. The mechanism of this reversal could be static resulting in a non-specific activity-independent run – down as has been previously observed (Kano *et al.*, 1992). Alternatively reversal could be activity dependent as indicated by data presented in chapter 5.

There are other forms of synaptic plasticity in the cerebellum that are not specifically mentioned here because they are not directly connected to the work presented in this thesis. For review see (Hansel *et al.*, 2001).

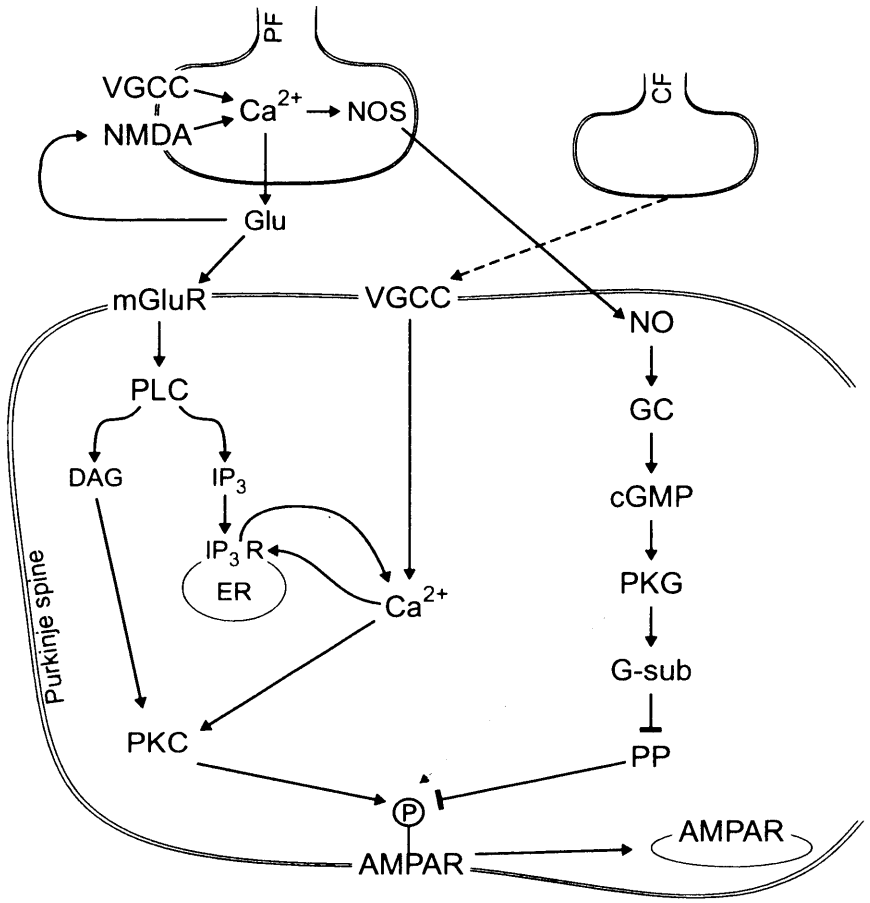

Figure 1.2

Biochemical pathways leading to **PF LTD**
Internalisation of phosphorylated AMPARs causes LTD. Calcium influx triggered by CF activity leads to calcium-induced calcium release. Prerequisite for this is IP_3 stemming from activation of mGluRs by the PFs. Activation of mGluRs also leads to a rise in DAG which together with calcium activates PKC which posphorylates AMPARs. The NO – GC pathway leads to inhibition of the dephosphorylation of AMPARs.

CF	climbing fiber	mGluR	metabotropic Glu receptor
cGMP	cyclic GMP	NOS	nitric oxide synthase
DAG	diacylglycerol	PF	parallel fiber
ER	endoplasmatic reticulum	PKC	protein kinase C
GC	guanylate cyclase	PKG	protein kinase G
G-sub	G-substrate	PLC	phospholipase C
IP_3	inositol-1-3-5 triphosphate	PP	protein phospatase 1 / 2A
IP_3R	IP_3 receptors	VGCC	voltage gated Ca^{2+} channel

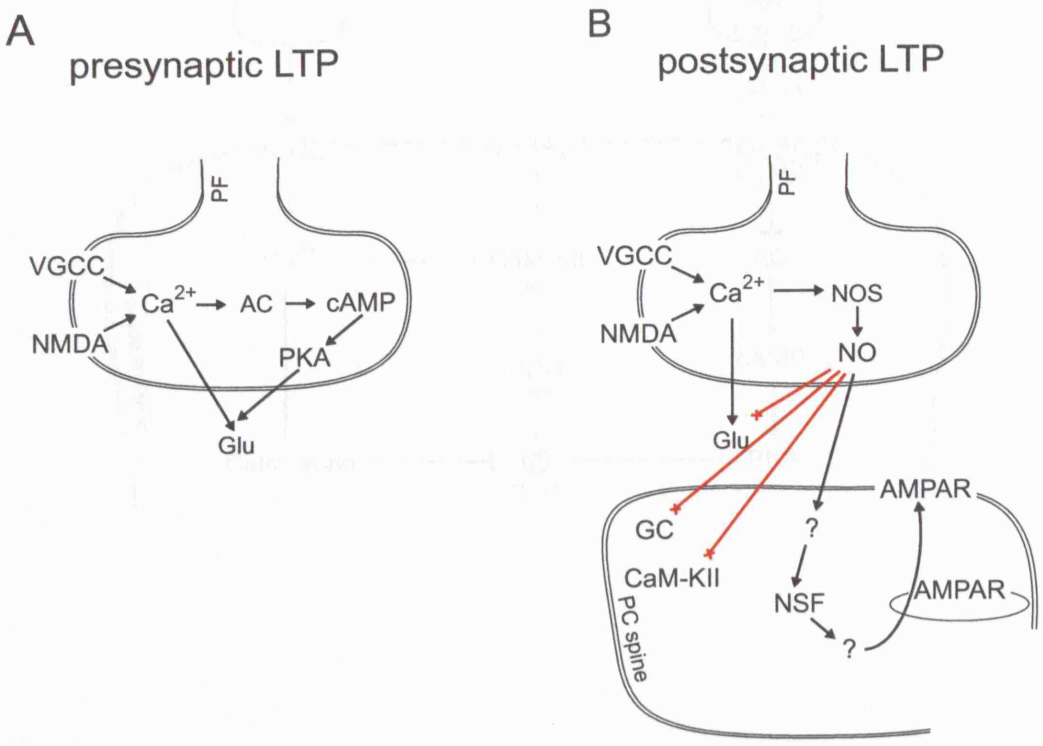

Figure 1.3

Two distinct forms of **LTP** of the PF to PC synapses
A 4 Hz cAMP-dependent presynaptic LTP leads to an increase in release through the action of PKA. **B** 1 Hz NO-dependent LTP is postsynaptic and leads to insertion of AMPARs. NO is necessary and sufficient for LTP induction. The mechanism by which NO leads to LTP is poorly understood. NO does not affect release, and activation of GC or CaM-KII is not necessary.

AC	adenylate cyclase
cAMP	cyclic AMP
CaM-KII	Ca^{2+}/calmodulin-dependent protein kinase
GC	guanylate cyclase
NOS	nitric oxide synthase
NSF	N-ethylmaleimide-sensitive factor
PF	parallel fiber
PKA	protein kinase A
VGCC	voltage gated Ca^{2+} channel

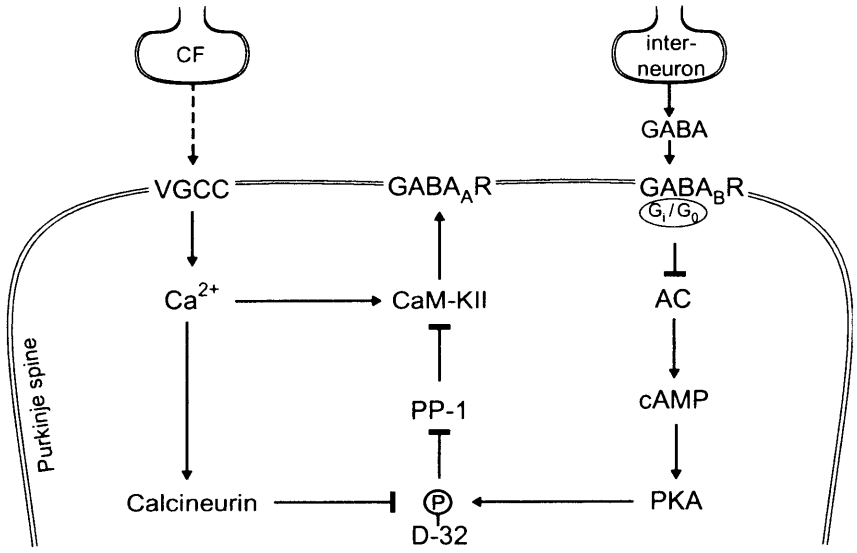

Figure 1.4

Rebound potentiation of inhibitory inputs to Purkinje cells and the block of rebound potentiation
RP is induced by calcium influx from VGCC following depolarization by the CF. Calcium activates CaM-KII which directly phosphorylates $GABA_A$Rs leading to LTP by increasing sensitivity. Although calcium activates CaM-KII it also inhibits CaM-KII by activating calcineurin. Calcineurin dephosphorylates DARP-32, thus inactivating the inhibition of PP-1. The disinhibited PP-1 now inhibits CaM-KII. Calcium entry has a net activating effect on CaM-KII because PKA counteracts calcineurin and phosphorylates DARP-32. Baseline levels of cAMP are necessary for this action of PKA but when $GABA_B$Rs are activated AC is inhibited and the resulting low concentration of cAMP leads to reduced activity of PKA. Therefore, simultaneous calcium influx and $GABA_B$R activation does not lead to RP. Taken and modified from (Kawaguchi & Hirano, 2002).

AC	adenylate cyclase
cAMP	cyclic AMP
CaM-KII	Ca^{2+}/calmodulin-dependent protein kinase
CF	climbing fiber
D-32	DARPP-32
PP-1	protein phosphatase I
VGCC	voltage gated Ca^{2+} channel

1.4 Outline of thesis

The aim of this thesis was to examine the influence of inhibition on the computations performed by the cerebellar cortex. It is divided into four experimental chapters preceded by a chapter describing materials and methods (chapter 2).

In chapter 3 I describe the circuit that ensures that excitation is followed by feed-forward inhibition. FFI temporally limits excitation from the PFs resulting in short excitatory potentials which forces spikes to fall into a narrow time window. The implications of this finding for summation of synaptic inputs are also considered.

Chapter 4 shows how FFI could explain a long-standing conundrum in cerebellar research, the missing PF beams. Evidence that PCs lack activity along the course of their afferent PFs has been accumulating. I investigate whether differences in PF conduction velocity, spatial or temporal spread of PF activity can lead to cancellation of PF excitation by FFI and thus can explain this puzzling finding.

Chapter 5 is concerned with the learning – induced changes in the feed – forward circuit and the resulting consequences for the spike output of the cerebellar cortex. I show that inhibition undergoes LTD to an extent similar to the excitation from the PFs. This balanced plasticity can lead to increases in spike output in response to CF-induced plasticity, contrary to classical theories of cerebellar motor learning.

Chapter 6 shows experimental evidence that strong PF input can be followed by a pause in spontaneous spiking. This pause reflects the strength of the input and therefore could be used to distinguish between novel inputs and inputs depressed by motor learning. The experiments are consistent with theoretical work of my collaborators.

The thesis concludes with a general discussion (chapter 7).

2 Materials and Methods

2.1 Introduction

The data presented in this thesis were obtained from PCs and interneurons of the rat cerebellar vermis using an acute slice preparation. Intracellular electrophysiological recordings were made using the patch clamp technique developed by Neher & Sakman (Neher & Sakmann, 1992). Recordings were performed in whole-cell voltage clamp or current clamp mode, or using dynamic clamp (Robinson & Kawai, 1993). The experimental procedures and techniques used in this thesis have been established previously and are briefly outlined in this chapter.

2.2 Slice preparation

Acute slices were prepared from 18 – 25 days old Sprague – Dawley rats. For chapter 4, 14 – 15 days old animals were used to allow better space clamp in more compact PCs (Roth & Häusser, 2001) and controls with 56 – 60 days old rats were made for chapter 3. All procedures conformed with the UK Animals (Scientific Procedures) Act 1986. Rats were deeply anaesthetized via isoflurane inhalation and decapitated. The head was briefly cooled and rinsed in a dish with ice-cold artificial cerebrospinal fluid (ACSF). The scalp was removed to reveal the skull, which was cut open along both sides in a caudo – rostral

direction with scissors. The brain was scooped out of the skull into a Petri dish containing ice-cold ACSF. The brain was kept in this solution which was bubbled with 95% O_2 and 5% CO_2 for oxygenation and pH buffering for the remainder of the procedure. The brain was secured via two pins inserted through the neocortex, and the pia mater covering the vermis of the cerebellum was removed with a pair of fine watchmaker's forceps (Dumont No. 5). For sagittal slices a rostro – caudal cut was made through the vermis about 1/3 in from the border of the hemisphere. The other hemisphere was cut off directly on the border to the vermis. The vermis was fixed onto the more medial side in the mount of a vibratome (Leica VT 1000S, Nussloch, Germany) with cyanoacrylate glue (RS, Corby, UK). Slices of 200 – 300 μm thickness were cut and transferred into a chamber containing ACSF warmed to 33 °C with a wide pipette. Slice were incubated at that temperature for 30 – 50 minutes and then maintained at room temperature until transferred to the recording set-up. For coronal slices both hemispheres were cut off at the border to the vermis, which was then glued to the rostral surface of the cerebellum. The vermis was oriented so that the folia were parallel to the blade.

2.3 Electrophysiology

Slices were visualised with an upright microscope (Axioskop, Zeiss) and viewed with infrared differential interference contrast optics (Stuart *et al.*, 1993). An unambiguous visual identification of PCs and interneurons was possible because of the distinct PC morphology whereas interneurons are the only neurons with cell bodies in the molecular layer. A Multiclamp 700A amplifier (Axon Instruments, Foster City, CA) was used for all recordings and pCLAMP 9 (Axon Instruments) was used as acquisition software. Data was low-pass filtered at 3 – 10 kHz by the amplifier with an 8-pole Bessel filter and sampled at 20 kHz. All experiments were performed at near physiological temperatures (34 ± 0.1 °C) and the flow rate was set to 4 ml/min for a 2 ml recording chamber.

2.3.1 Whole-cell current clamp

Recording electrodes were pulled from "thin" (1.5 mm outer, 1.17 mm inner diameter) borosilicate capillaries (Harvard Apparatus, Edenbridge, UK) with a two-stage vertical puller (PC-10, Narashige, Japan). Electrodes were pulled to resistances of about 4 MΩ.

Recording pipettes containing internal solution were brought down to the cell with minimal positive pressure (about 20 mbar). The electrode was pushed into the cell and immediately after formation of a clear "halo" or "dimple" around the pipette tip positive pressure was released and gentle suction (about – 10 mbar) was applied to facilitate seal formation. The cell was patched in voltage clamp mode and the command potential was set to -70 mV during sealing, which helped to increase seal resistance. Only seals larger than 1 GΩ were accepted and the typical seal resistance was about 5 GΩ. After observation of spontaneous spikes in PCs, the whole-cell configuration was established with a brief suction pulse applied to the pipette to break the patch membrane and establish a continuum between the pipette and the cell interior. Following break-in I switched to current clamp mode, hyperpolarised the cell to avoid spiking and adjusted bridge balance and capacitance compensation guided by a square current injection of 0.2 nA at 100 Hz.

For experiments relating synaptic input and spike output, synaptic input was recorded while the cell was hyperpolarized (-70 to -65 mV for EPSPs and -65 to -60 mV for IPSPs). These hyperpolarized sweeps were interleaved with sweeps of the freely spiking cell.

In the course of long plasticity recordings the access resistance often changed. To avoid frequent interruptions to the acquisition, I adjusted the bridge balance guided by the relaxation of the voltage after current injection during the hyperpolarized sweeps, whereas capacitance compensation was typically not adjusted.

2.3.2 Whole-cell voltage clamp

For voltage clamp experiments recording electrodes with lower resistance (between 2 and 3 MΩ) were used resulting in access resistances of 4 to 15 MΩ. After break-in, the cell was held at – 70 mV and fast (pipette) capacitance compensation (0.5 – 1.8 μs, 8 – 12 pF), slow (whole-cell) capacitance (15 – 50 pF) and access resistance (4 – 15 MΩ) were manually adjusted guided by a -10 mV step. Series resistance compensation of 70 – 90% was employed.

2.3.3 Dynamic clamp

Dynamic clamp (Robinson & Kawai, 1993; Sharp *et al.*, 1993) was used to mimic inhibition. This technique resembles synaptic input because instead of a fixed current a conductance command is used. The current that is actually injected into the cell therefore depends on the membrane voltage, similar to the situation for real synapses.

Here, I used a custom-built analogue multiplication circuit (Harsch & Robinson, 2000) to generate a conductance input. In current clamp a command waveform determined by the acquisition software is transformed into a current that is injected into the cell. For dynamic clamp, the amplifier is set to current clamp but the command waveform represents a conductance due to the dynamic clamp circuitry. This circuitry continuously calculates the product of driving force and conductance and injects the resulting current into the cell. The driving force is given by the difference of the measured voltage and the reversal potential:

$$(V_M - E_{rev}) \cdot g_{Command} = I_{inject} \qquad \text{Equation 2.1}$$

The reversal potential of inhibitory conductances was set to -88 mV matching the reversal potential measured for evoked inhibitory inputs with the internal solution used here (-88.4 ± 1.9 mV ; n = 4), which is similar to the values of

physiological reversal potentials published previously (Carter & Regehr, 2002; Chavas & Marty, 2003).

In experiments using evoked synaptic inputs imperfect bridge balance did not change sub- or superthreshold responses because synaptic potentials were recorded only in the absence of current injection or during DC current injection. However, when using dynamic clamp, bridge balance errors would not only result in deviations of the measured potentials from the potential inside the cell but would also lead changes in the injected current. To avoid such errors I injected all currents with one electrode and monitored voltage with a second independent electrode. First, both electrodes were placed far enough above the cell to avoid spillage of internal solution onto the cell. After establishing whole-cell voltage clamp with one electrode, the cell was patched with the second electrode on the opposite side of the soma.

2.3.4 Extracellular recordings

For extracellular recordings patch electrodes with resistances between 2 and 4 MΩ filled with ACSF were used. Either electrodes were placed close to the cell body usually around the axon hillock or loose cell-attached recordings with resistances of 10 to 100 MΩ were made (Forsythe & Clements, 1990; Barbour, 1993). For these recordings electrodes were gently pushed against the cell and without any pressure. When spikes were visible small negative pressure (around 10 mbar) was applied. This resulted in an increase in spike amplitude and a decrease in noise. Loose cell-attached recordings were mechanically more stable and fewer recordings were lost due to mechanical drift compared with extracellular recordings where electrodes did not touch the cell.

2.3.5 Extracellular stimulation of synaptic inputs

For stimulation of synaptic inputs patch electrodes of 2 – 6 MΩ filled with ACSF were used. In experiments where strong PF inputs were used (chapter 6) or

where PFs were activated far from the patched PC (chapter 4) electrode tips were broken to decrease resistance (> 1MΩ). The ACSF in the electrode was in contact with a platinum wire, which was connected to an isolated stimulator (DS2, Digitimer Ltd.).

In sagittal slices PF stimulation electrodes were buried in the molecular layer beneath the recorded PC. The electrode was brought down to the surface of the slice about 50 μm from the side of the PC and then advanced into the tissue with an angle of about 35°. When using high stimulation intensities (typical intensities were 30 to 60 V for 0.2 ms but high stimulation intensities of up to 100 V for 0.5 ms were used in chapter 7) the resulting separation between PC dendrite and stimulus electrode was not always sufficient to prevent activation of the CF. For these experiments electrodes were buried up to 100 μm deep in the tissue. CFs were activated with a separate electrode placed in the GC layer. Usually the electrode was located close to the recorded cell (about 20 μm). Inhibitory inputs were activated by placing an electrode lateral to the recorded PC. In sagittal slices PFs run perpendicular to the surface of the slice. To avoid activation of PFs that terminate on the recorded PC stimulus locations were at least 50 μm distant from the outermost visible dendrite.

In coronal slices the plane of PC dendrites is oriented perpendicular to the surface of the slice. To stimulate PFs and FFI, two independent stimulating electrodes were placed around 100 and 600 – 1600 μm lateral to the cell along the course of the PFs.

2.4 Analysis

Data was analyzed offline using Igor Pro (Wavemetrics, Lake Oswego, OR). Custom written procedures used for data analysis were written by myself or by Dr. Jason Rothman (NeuroMatic 1.2, http://www.wavemetrics.com). Pooled data are expressed as mean ± S.E.M. and statistical significance was

determined using Student's paired *t*-test (unless otherwise indicated). Traces in figures are averages from 15 to 60 trials unless otherwise indicated.

2.4.1 Subthreshold data

EPSP integrals (fig 3.4) were calculated from stimulus artifact until the voltage stably relaxed to baseline. Undershooting phases contributed negative integrals and reduced the total integral. For determining changes in EPSP integral, SEM and statistical significance was calculated from the absolute changes of individual cells normalized by the population average. For quantification of EPSP summation experiments (fig 3.7) I measured the residual amplitude of EPSP 1 contributing to EPSP 2 by subtracting the amplitude of EPSP 2 alone from the combined amplitude and dividing by the amplitude of the EPSP 1. Inputs were considered to be stimulated independently at an interval > 600 ms.

2.4.2 Superthreshold data

Cell-attached and intracellularly recorded spikes were detected using a threshold-crossing algorithm. Temporal dispersion in first spike latencies (spike jitter, fig 3.6) was determined by fitting a latency histogram with a Gaussian of the form:

$$f(x) = A \cdot e^{-\left(\frac{x - x_0}{\text{width}}\right)^2} \qquad \text{Equation 2.2}$$

The width is the product of the standard deviation and the square root of 2 and was used as a measure of spike jitter.

Synaptic inputs (EPSPs and IPSPs) led to spikes that were surplus or short of the number of spikes expected from spontaneous spiking (fig 3.5, 5.1, 5.4, 5.5, 5.6). To determine this spike output in response to synaptic input, peri-stimulus time histograms (PSTH) were computed and integrated (Fetz & Gustafsson, 1983). A linear fit to the baseline range of the integral (>100 ms) was

extrapolated over the entire trial duration and subtracted from the integral to yield the 'corrected cumulative spike count'. Averaging over a 100 – 200 ms period following stimulation gives the number of spikes evoked (or prevented) by the input. This measure of the input evoked spike response is called 'net spike output'. For IPSPs the net spike output is negative.

Spike shifts were used to determine the effect of an input on the timing of the first spike after the input (fig 5.1, 5.4, 5.5, 5.6). Spike shifts were calculated by dividing the average time from stimulus to the first spike with half the inter spike interval of baseline spiking. (Half the inter spike interval is the average time between a random point in time and the next spike.) Because EPSPs speed up the occurrence of spontaneous spikes, the spike shift for EPSPs is between one and close to zero. Conversely, IPSPs delay the occurrence of spontaneous spikes resulting in spike shifts larger than 1.

2.5 Solutions

Internal solutions:

Internal	**Current Clamp**	**Voltage Clamp 1**	**Voltage Clamp 2**	**Extra-cellular**
Used in:	all chapters	chapter 3	chapter 4	chapter 3, 6
Comment:			= Current Clamp	= ACSF
Compound				
Methanesulfonic acid	130	115	130	
HEPES	10	10	10	
KCl	7	1	7	
EGTA	0.05		0.05	
Na_2 ATP	2	2	2	
Mg ATP	2	2	2	
Na_2 GTP	0.4	0.3	0.4	
Biocytin	0.4%	-	0.4%	
Cs_4 BAPTA	-	10	-	
QX-314	-	5	-	
$CaCl_2$		0.5		
KOH	to pH 7.3		to pH 7.3	
CsOH		to pH 7.3		

Concentrations in mM (unless otherwise stated). All chemicals were from Sigma unless indicated otherwise (see below). Internal solutions were calibrated to a pH of 7.3 with a hydroxide solution of the principal cation. Since the principal anion (methanesolfonate) was added as acid and the triphosphates are strongly acidic, the principal cation had a concentration of about 143 mM. The osmolarity of the solutions was between 281 and 287 mOsm.

Artificial cerebrospinal fluid (ACSF):

Compound	ACSF
NaCl	125
$NaHCO_3$	25
Glucose	25
KCl	2.5
$CaCl_2$	2
$MgCl_2$	2
NaH_2PO_4	1.25

This solution was continuously bubbled with 95% O_2 / 5% CO_2 for at least 5 minutes before it came in contact with brain tissue.

Full names of chemicals:

Abbreviation	Full Name
Cs_4 BAPTA	1,2,-bis(2-aminophenoxy)ethane-N,N,N',N'-tetraacetic acid tetracesium salt (from Molecular Probes)
CsOH	Cesium Hydroxide
EGTA	Ethylene glycol-bis(2-aminoethylether)-N,N,N',N'-tetraacetic acid (from Fluka)
Glucose	D-glucose
SR	SR95531 or 2-(3-Carboxypropyl)-3-amion-6-(4 methoxyphenyl) pyridazinium bromide
HEPES	4-(2-Hydroxyethyl)piperazine-1-ethanesulphonic acid
KCl	Potassium Chloride
Mg ATP	Magnesium adenosine triphosphate
$MgCl_2$	Magensium Chloride
NaCl	Sodium Chloride
$NaHCO_3$	Sodium bicarbonate
NaH_2PO_4	Sodium dihydrogen phosphate
Na_2 GTP	Disodium guanosine triphosphate
NBQX	1,2,3,4-Tetrahydro-6-nitro-2,3-dioxo-benzo[f]quinoxaline-7-sulfonamide (from Sigma or Tocris)
QX-314	Lidocaine N-ethyl bromide

Frequently used abbreviations:

Abbreviation	Full Name
CF	climbing fibre
DCN	deep cerebellar nuclei
EPSC	excitatory postsynaptic current
EPSP	excitatory postsynaptic potential
FFI	feed-forward inhibition
GC	granule cell
GABA	γ-aminobutyric acid
$GABA_AR$	ionotropic γ-aminobutyric acid receptor
I / E ratio	IPSP amplitude divided by EPSP amplitude at -65 mV
IPSC	postsynaptic inhibitory current
IPSP	postsynaptic inhibitory potential
LTD	long-term depression
LTP	long-term potentiation
PC	Purkinje cell
PF	parallel fibre
PSTH	post stimulus time histogram

This table is also printed on the last page of this thesis.

3 Characterisation of feed-forward inhibition

3.1 Introduction

The cerebellum is important for the correct timing of movements indicating that it is capable of implementing timing information on the timescale of milliseconds to seconds (Ivry, 1997; Spencer *et al.*, 2003). Most theories about the cerebellum require the output of the cortex to be precisely timed for the cerebellum to achieve its timing tasks (Braitenberg & Atwood, 1958; Welsh & Llinas, 1997; Vos *et al.*, 1999).

In this chapter I characterise the currents generated by the molecular layer feed-forward inhibitory circuit and how they lead to brief subthreshold potentials. The resulting consequences for spike timing and implications for sub- and super-threshold summation of inputs are considered. The results suggest that FFI has important consequences for cerebellar processing and is likely be a mechanism underlying the precisely timed output of the cerebellar cortex.

3.1.1 Anatomical basis for feed-forward inhibition

Ramón y Cajal's outstanding work had described all the cellular components of a feed-forward inhibitory circuit in the cerebellar molecular layer by the beginning of the last century (Ramón y Cajal, 1904). The morphology of PCs and interneurons, which Cajal divided into stellate and basket cells, were accurately characterised with Golgi stains and light microscopy. Furthermore, after his discovery of PFs (Ramón y Cajal, 1888) and formulation of the 'law of

dynamic polarisation' in 1891 (published in Ramón y Cajal, 1894), Cajal realised amazingly early, that PCs (and maybe also interneurons) receive information from PFs. Palay and Chan-Palay added the electron – microscopic level with their comprehensive microscopic study and showed the existence of all synapses required for the circuit (Palay & Chan-Palay, 1974). PCs receive PF synapses on dendritic spines (called thorns) at all depths of the molecular layer. This is also the case for basket cells. Basket cell somata are located in the lower third of the molecular layer sending their dendrites up until they reach the pia mater. There they curve back or can run parallel to the pial surface for several tens of micrometers. Thus they sample PF activity from all depths of the molecular layer. This is not the case for stellate cells, especially superficial ones, whose dendrites are confined to the upper regions of the molecular layer and only sample PF activity there.

The axons of basket cells cross many PC somata (7-20 ; Palay & Chan-Palay, 1974; Shepherd, 2004) in the sagittal plane perpendicular to the PFs. Collaterals descend to the PC layer and form a characteristic plexus (pinceau) around the PC initial segments where a fine mesh of axons and terminals make synapses with the initial segment. The basket cell can therefore sample activity throughout the entire depth of the molecular layer and inhibit the initial segment of PCs. Through sparse ascending axons they can also inhibit dendrites of PCs, stellate and other basket cells.

As opposed to the quite widespread basket cell axon, which is capable of inhibiting 50 – 70 PCs, stellate cell axons, like their dendrites, are much more locally confined. Although rare descending collaterals make synapses with PC dendrites down to the PC layer, the majority of the synapses are located in the immediate vicinity of the stellate cell body. However, stellate cells located more proximal can have long axons (as long as 450 μm) running in the sagittal plane like basket cell axons. Both stellate and basket cells synapse on dendrite and somas of other stellate and basket cells at all levels of the molecular layer. Whilst stellate cells do not show any inhibitory synapses on the dendrite, 8% of somatic synapses are from basket or stellate cells. In basket cells this value is 11% and interneuron synapses also make up 6% of basket cell dendritic synapses.

3.1.2 Inhibition exerts a powerful influence on spike timing in Purkinje cells

Theoretical and experimental studies have shown that inhibition can have a powerful influence on spike timing in PCs. In a biophysically realistic model of a PC (Jaeger & Bower, 1999), random, uncorrelated PF and interneuron input resulted in spike trains similar to those observed *in vivo* (Jaeger & Bower, 1994). The characteristic long pauses as well as spike timing were strongly correlated with the inhibitory but not the excitatory input. These results were confirmed with simulation of synaptic inputs with dynamic clamp in an *in vitro* preparation. However, the model is flawed in that spiking is achieved by excitatory input and not like in real PCs through intrinsic currents (Raman & Bean, 1999).

With paired recordings Häusser and Clark (Häusser & Clark, 1997) showed directly that activity in only a single presynaptic interneuron can strongly influence spike timing and delay the occurrence of a spontaneous spike by tens of milliseconds. The spontaneous spiking of PCs (1 – 148 Hz, average 39 ± 2 Hz ; Häusser & Clark, 1997) allows them to 'read out' inhibitory input independently of excitatory input. This has special physiological relevance because interneurons also spike spontaneously without excitatory input (3 – 12 Hz ; Häusser & Clark, 1997; Jorntell & Ekerot, 2003; Molineux *et al.*, 2005). PC spike timing will be strongly influenced by spontaneous activity in the population of presynaptic interneurons in a situation of small or no PF activity. However, the activity levels of PFs in a physiological situation is unclear and even under anaesthesia mild sensory stimulation leads to bursts of spikes in GCs (Chadderton *et al.*, 2004). Interneurons have a low rate of spontaneous firing but their input resistance is high and they fire a spike in response to single inputs (Carter & Regehr, 2002). This makes it unlikely that spontaneous interneuron firing controls spike timing in PCs in physiological situations. It is also unknown whether PC output is in any way meaningful to the animal during states of sleep or inactivity in which sufficiently low PF activity might be possible.

For higher levels of PF activity interneurons will be driven by PF input in a feed-forward manner leading through sharply rising EPSPs to a precise control of spike timing (Carter & Regehr, 2002). The temporal correlation and the relative strength of PF and inhibitory input to PCs, and the influence on subthreshold and superthreshold responses remain unclear.

3.1.3 Previous evidence and characterisation

Since the classical work of Eccles and colleagues in the sixties (Eccles *et al.*, 1967) it was known that stimulation of PFs leads to excitatory currents rapidly followed by inhibition, consistent with FFI. In this work sharp electrodes were used to record from PCs. "On-beam" PCs displayed biphasic currents while those PCs to either side of the stimulated PF beam received inhibition but no excitation ("off-beam" or lateral inhibition). For biphasic currents they found the peak of the inhibitory current delayed by 2 ms with respect to the peak of the EPSC. In a more recent study it was shown that the inhibitory component is sensitive to blockers of AMPA receptors (Delaney & Jahr, 2002).

Off-beam as well as on-beam inhibition were also detected when imaging neural activity with voltage sensitive dyes in isolated guinea pig cerebella (Cohen & Yarom, 2000). Although the signals are fast, the recording locations consistent with the type of inhibition observed and the resulting signal reflective of the voltage, the subthreshold and superthreshold PC or interneuron responses remain unknown for three reasons: 1) the dye picks up signals of all membranes, PCs, interneuron, PFs and glia, 2) the signal contribution from different depth of the molecular layer is an unknown complicated function of the intensity dependence of excitation and emission light on depth in the molecular layer and 3) the signal is filtered by the kinetics of the dye.

Ebner and colleagues showed excitatory and inhibitory signals with pH sensitive dyes and autofluorescence imaging (Chen *et al.*, 1996; Ebner *et al.*, 2005; Gao *et al.*, 2005), but the signals are slow and even more difficult to relate to the voltage in PCs and interneurons than voltage sensitive dyes.

Although there is good evidence for the existence of FFI, it is poorly characterised and an understanding of the contribution of this hard-wired circuit to information processing in the cerebellar cortex is lacking. In this chapter, FFI in both PCs and interneurons is characterised, and the effect on subthreshold potentials and PC spike output is investigated.

The work for this chapter was done in collaboration with Dr. Ursula Koch and published in the Journal of Physiology (Mittmann *et al.*, 2005). Dr. Koch collected most of the data presented in figure 3.5, 3.6 and 3.8. I collected all other data and devised and performed analysis of all, including Dr. Koch's data independently.

3.2 Results

3.2.1 Feed-forward inhibitory synaptic currents activated by parallel fibres

To investigate FFI in the cerebellar cortex I used coronal cerebellar slices to preserve PFs and to allow stimulation of PFs at distances outside the dendritic tree of the recorded cell. PF stimulation evoked a sequence of inward current followed by outward current in PCs (fig 3.1 A, C ; Delaney & Jahr, 2002) and molecular layer interneurons (fig 3.1 B, D) when the cell was voltage clamped at potential between the IPSC and EPSC reversal potentials. The outward current was reversibly blocked by the selective $GABA_A$ receptor antagonist SR95531 ('SR', 10 µM ; Hamann *et al.*, 1988) in both cell types (fig 3.1 A, B ; n = 4). The AMPA-type glutamate receptor antagonist NBQX (6 µM) reversibly blocked both the inward current and the outward current in PCs (n = 10) and interneurons (n = 8). These results confirm that the inhibitory component represents FFI, and rule out direct stimulation of interneurons. The resulting microcircuit is shown in figure 3.1 E, illustrating the direct activation of PCs and interneurons by the PFs, as well as the indirect, disynaptic pathway for activation of FFI.

3.2.2 Timing and kinetics of feed-forward IPSCs

In order to precisely determine the relative timing of excitatory and inhibitory inputs, EPSCs and feed-forward IPSCs were separated by voltage-clamping at their respective reversal potentials. PF stimulation strength was adjusted so that only relatively small EPSCs/IPSCs were recruited (Purkinje: EPSC –89 ± 16 pA; IPSC 356 ± 50 pA; interneuron: EPSC –150 ± 33 pA; IPSC 115 ± 21 pA), corresponding to only a few unitary synaptic inputs (Pouzat & Hestrin, 1997; Carter & Regehr, 2002; Isope & Barbour, 2002). I fitted EPSCs and feed-forward IPSCs with double exponential functions (fig 3.2). EPSCs rose and

decayed rapidly in both cell types (Purkinje EPSC : τ_{rise} = 0.79 ± 0.19 ms, 10 to 90% risetime = 1.07 ± 0.14 ; τ_{decay} = 5.4 ± 1.8 ms ; Interneuron EPSC: τ_{rise} = 0.30 ± 0.04 ms , risetime = 0.48 ± 0.05 ms ; τ_{decay} = 0.92 ± 0.10 ms; n = 9) whereas IPSCs decayed more slowly (Purkinje IPSC: τ_{rise} = 2.49 ± 0.34 ms , risetime = 2.23 ± 0.27 ; τ_{decay} = 11.41 ± 0.94 ms; Interneuron IPSC τ_{rise} = 0.42 ± 0.06 ms risetime = 1.01 ± 0.20 ms; τ_{decay} = 12.4 ± 2.0 ms ; n = 9).

I used the 10% risetime points to determine the EPSC-IPSC delay, which was 1.4 ± 0.2 ms (range 0.69 to 2.50 ms, n = 11) for PCs (fig 3.3 A, B) and 1.4 ± 0.1 ms (range 1.0 to 1.76 ms, n = 11, $p > 0.4$) for interneurons (fig 3.3 C, D). To test whether the delay in PCs is similar in older animals, I performed control experiments in PCs in slices from P56 to P60 rats. The delay between EPSC and IPSC was indistinguishable from the delay in younger animals (1.4 ± 0.1 ms, n = 3; $p > 0.5$).

3.2.3 Feed-forward inhibition shapes subthreshold synaptic potentials

The rapid onset of FFI suggests that it will significantly influence the timecourse of EPSPs triggered by PF activation. I investigated the effect of FFI on PF EPSP timecourse with current clamp recordings from PCs. I injected hyperpolarising current to avoid spontaneous spiking, holding the cells at membrane potentials between –60 to –65 mV. PF stimulation evoked brief EPSPs (halfwidth: 13 ± 2.6 ms) that were often followed by a pronounced hyperpolarisation (fig 3.4 A and 3.7 A). Blocking inhibition with SR more than doubled EPSP amplitude (from 1.4 ± 0.2 mV to 3.2 ± 0.6 mV in SR; $p < 0.01$, n = 26), led to a substantial increase in EPSP half-width (from 13.1 ± 2.6 ms to 43.7 ± 3.1 ms in SR; $p < 0.01$, n = 26) and increased the EPSP integral by an order of magnitude (from 15 ± 8 mV*ms to 141 ± 33 mV*ms; $p < 0.01$, n = 26). The effect of SR on EPSP amplitude and timecourse was much larger for evoked EPSPs than for EPSPs simulated by somatic injection of currents shaped like EPSCs in the same cells (change in evoked EPSP amplitude 1.9 ± 0.7, halfwidth 3.4 ± 1.7; integral 6.4 ± 4.0 times greater than for injected EPSPs;

n = 3). This indicates that the effect of SR on evoked PF EPSPs in these experiments is mediated primarily via block of FFI rather than through an effect on "tonic" background inhibition (Häusser & Clark, 1997).

Similar experiments were performed on interneurons, which showed consistent but smaller changes to those observed in PCs (fig 3.4 C). EPSP amplitude (4.6 ± 0.9 mV to 6.1 ± 1 mV), halfwidth (10.5 ± 2.2 ms to 13 ± 2.1 ms) and integral (68 ± 22 mV*ms to 120 ± 36 mV*ms, fig 3.4 D) all increased significantly ($p < 0.01$, n = 15) in the presence of SR. These changes were significantly smaller in interneurons than in PCs (fig 3.4 E ; $p < 0.05$).

3.2.4 Feed-forward inhibition regulates the level and precision of spike output

Because FFI dramatically shortens PF EPSPs in PCs, I expected that this would be reflected in the timing of action potentials evoked by PF stimulation. I tested this hypothesis using non-invasive cell-attached recordings. PCs generated spontaneous spikes and thus PF stimulation led to a brief increase in spike probability on top of the baseline firing rate (fig 3.5 A, B). To measure the net spike output in response to the PF input I integrated the resulting PSTH to yield the cumulative spike probability (Fetz & Gustafsson, 1983) which I then corrected for the spontaneous spike rate (see Methods; fig 3.5 C). Blocking inhibition with SR strongly increased the spike output as evident in raw traces, the PSTH and the corrected cumulative spike output (fig 3.5 A, B, C, right panels). On average, the number of additional spikes evoked in control conditions nearly tripled when inhibition was blocked (from 0.38 ± 0.09 spikes to 0.99 ± 0.18 spikes; $p < 0.01$, n = 21).

The shortening of EPSPs by FFI (fig 3.4) suggests that spikes triggered by these inputs will fall into a narrow time window defined by FFI. In cell-attached recordings from PCs, this could indeed be observed in control conditions, but not when inhibition was blocked (fig 3.6 A). I fitted a Gaussian to the spike latency distribution to provide a measure for the latency of the spike response

(location of peak) and for the temporal dispersion (halfwidth) of the spike response. In the example cell shown in figure 3.6, blocking inhibition with SR only modestly increased the mean latency from 3.6 to 4 ms, but almost doubled the half-width of the Gaussian fit from 0.7 to 1.4 ms. On average, latency increased from 3.4 ± 0.1 to 3.7 ± 0.2 ms ($p < 0.01$, $n = 21$) whereas spike jitter almost doubled, going from 0.96 ± 0.1 ms to 1.6 ± 0.3 ms (fig 3.6 D; $p < 0.01$, $n = 21$) when inhibition was blocked.

3.2.5 Feed-forward inhibition shortens the time window for synaptic integration

In the behaving animal neurons are thought to receive a constant barrage of synaptic inputs (Destexhe *et al.*, 2003). Since FFI curtails PF EPSPs (fig 3.4) I investigated how this changes summation of EPSPs with strong FFI. I stimulated two PF inputs with separate stimulation electrodes and tested independence of both excitatory inputs by checking for cross-facilitation (40 to 80 ms interval; Perkel *et al.*, 1990). Inputs that showed such cross-facilitation were excluded. In half of the cells tested the decay of the second potential was slower when activated shortly after the first (fig 3.7 A, see also figure 4 in Brunel *et al.*, 2004). This could reflect a partial overlap between the populations of interneurons mediating FFI activated by the two inputs, or it could be a consequence of FFI in the inhibitory network.

In the cell shown in figure 3.7, synchronous activation of both inputs led to an amplitude that equalled the linear sum of the individual amplitudes. When introducing a brief delay between the two stimuli, the EPSPs failed to summate and the second potential was reduced compared to its size when activated alone. This reduction tracked the time course of the undershooting inhibitory component of the first input and lasted for about 30 ms. When FFI was blocked with SR, the second EPSP summated with the first, following its time course over a window of about 50 ms (fig 3.7 B). On average, effective EPSP summation in control conditions only took place when both inputs were activated in a narrow window of about 1 – 2 ms. With delays of 5 ms or longer

no summation of EPSPs was observed (fig 3.7 C). This was significantly different to the very effective EPSP summation when inhibition was blocked ($p < 0.05$, $n = 6$; fig 3.7 C).

3.2.6 Feed-forward inhibition reduces spike generation by asynchronous inputs

I tested whether the efficacy of a PF input in triggering spike output can be reduced by FFI engaged by previously active PFs. To assess this issue, I used cell-attached recordings and two separate stimulation electrodes to activate independent PF inputs. Input size was adjusted such that a mean maximum spike probability of 28 ± 6% (bin = 1 ms; n = 5) was achieved. After collection of cell-attached spike data the recording pipette was removed and the cell was re-patched in whole-cell mode to confirm the independence of the two inputs (see above). The spike generation efficacy of a PF input was strongly reduced if it was preceded by an independent PF input (fig 3.8 A). The suppression of the spike response to the second input lasted ~50 ms, similar to the time course of the inhibitory component of the EPSP-IPSP sequence (fig 3.4, 3.7). When FFI was blocked with SR, little or no inhibition of the second input was observed (fig 3.8 B). I compared across cells by calculating the average spike probability within a 10 ms window after each stimulus. The spike responses for delays up to 30 ms were significantly smaller when inhibition was intact ($p < 0.05$, $n = 5$; fig 3.8 C). These results show that FFI evoked by a PF input can penalise subsequent PF inputs in terms of their efficacy to generate PC output.

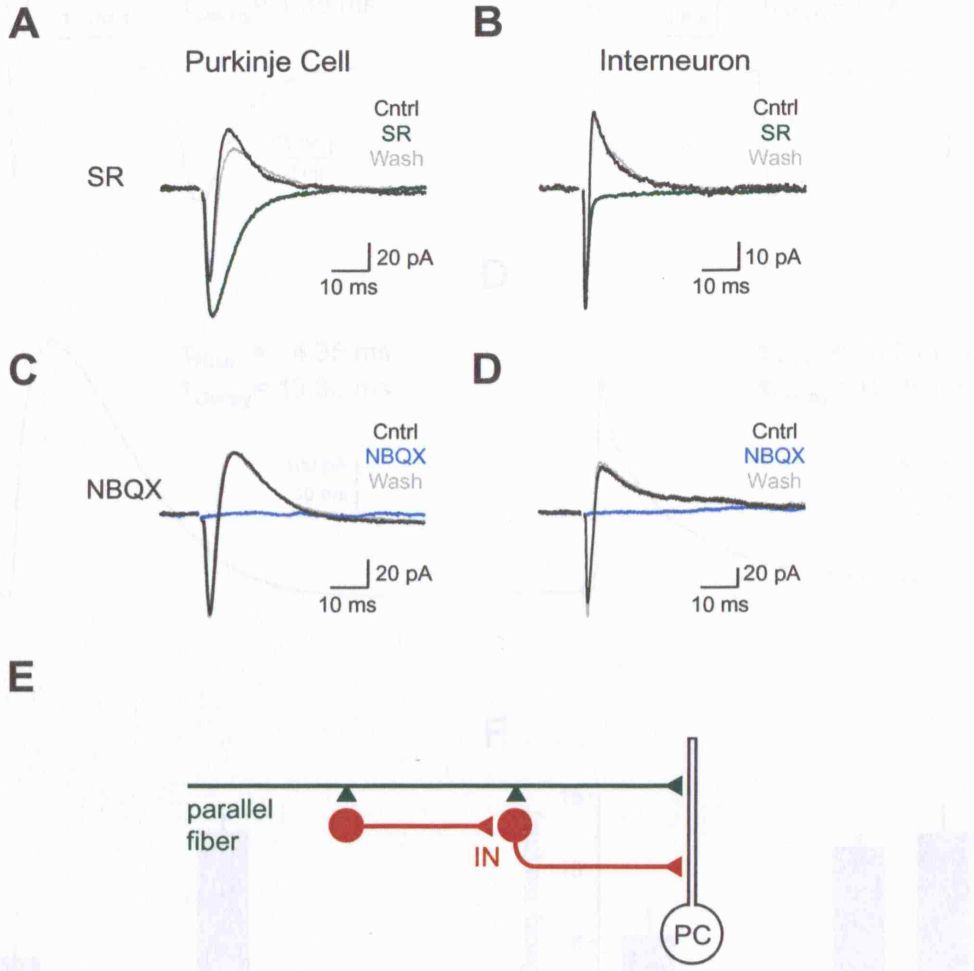

Figure 3.1

Feed-forward inhibition onto Purkinje cells and interneurons
Purkinje cells and interneurons show sequences of inward – outward currents in response to PF stimulation. Traces in this and subsequent figures are averages of 15 to 60 trials unless stated otherwise. **A, B** The $GABA_A$ receptor antagonist SR 95531 (10 µM) reversibly blocks the outward current in Purkinje cells and interneurons. **C, D** The AMPA-type glutamate receptor antagonist NBQX (6 µM) reversibly blocks both inward and outward currents. **E** Schematic drawing of the microcircuit underlying FFI.

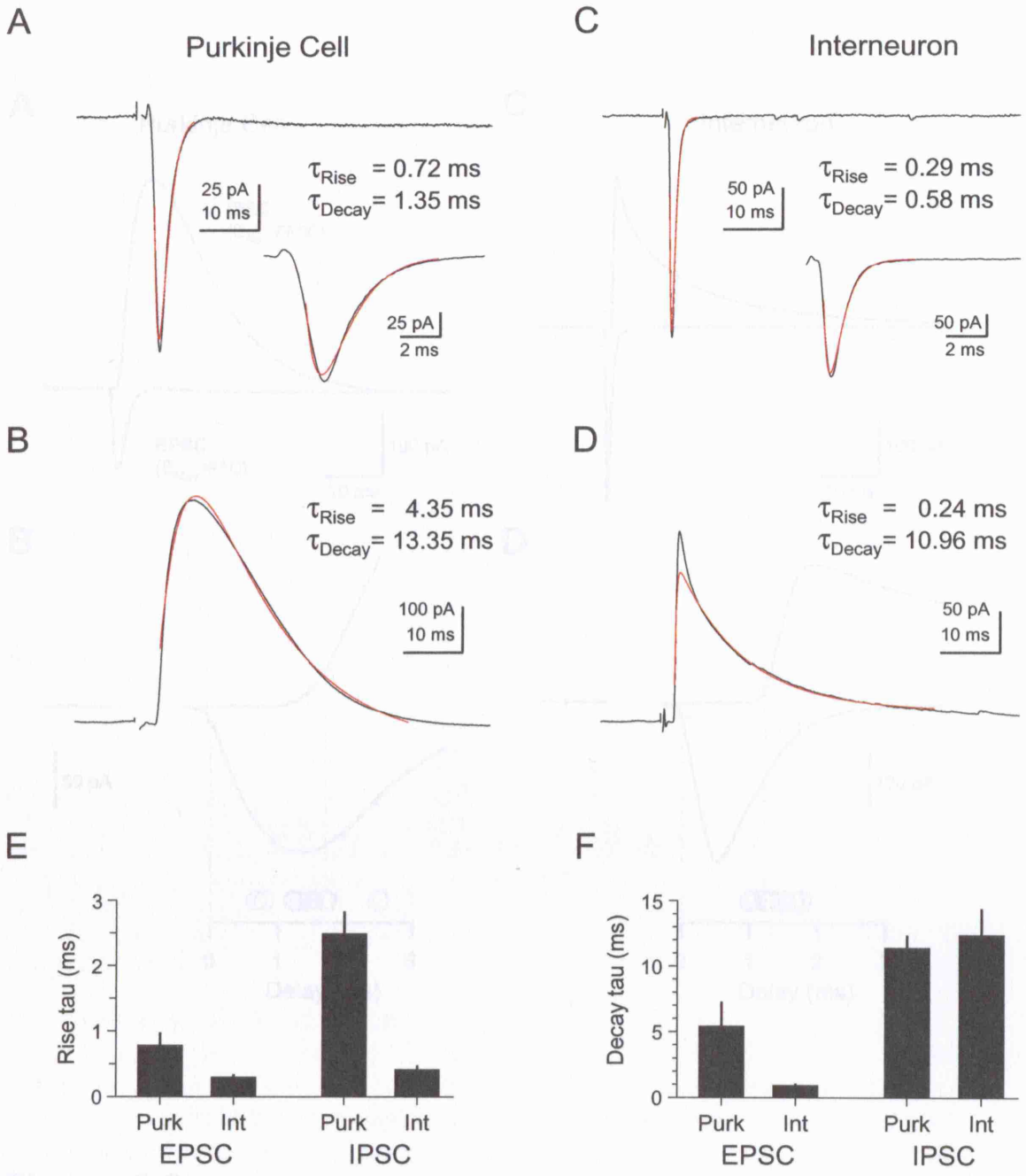

Figure 3.2

Kinetics of the biphasic currents
Currents are separated by holding potential. **A** An EPSC in a PC with its double exponential fit is shown. **B** Feed-forward IPSC of the same input recorded at 0 mV. Rise and decay of the IPSC are slower than the EPSC. **C, D** Same for interneurons. Kinetics of the EPSC are very fast whereas the IPSC has a fast rise followed by a slow decay. **E** Summary data of rise of EPSC and IPSC. **F** Summary data of the decay at a different scale. Note that although the rise of IPSCs (**E**) is much faster in interneurons than PCs, the decay is similar.

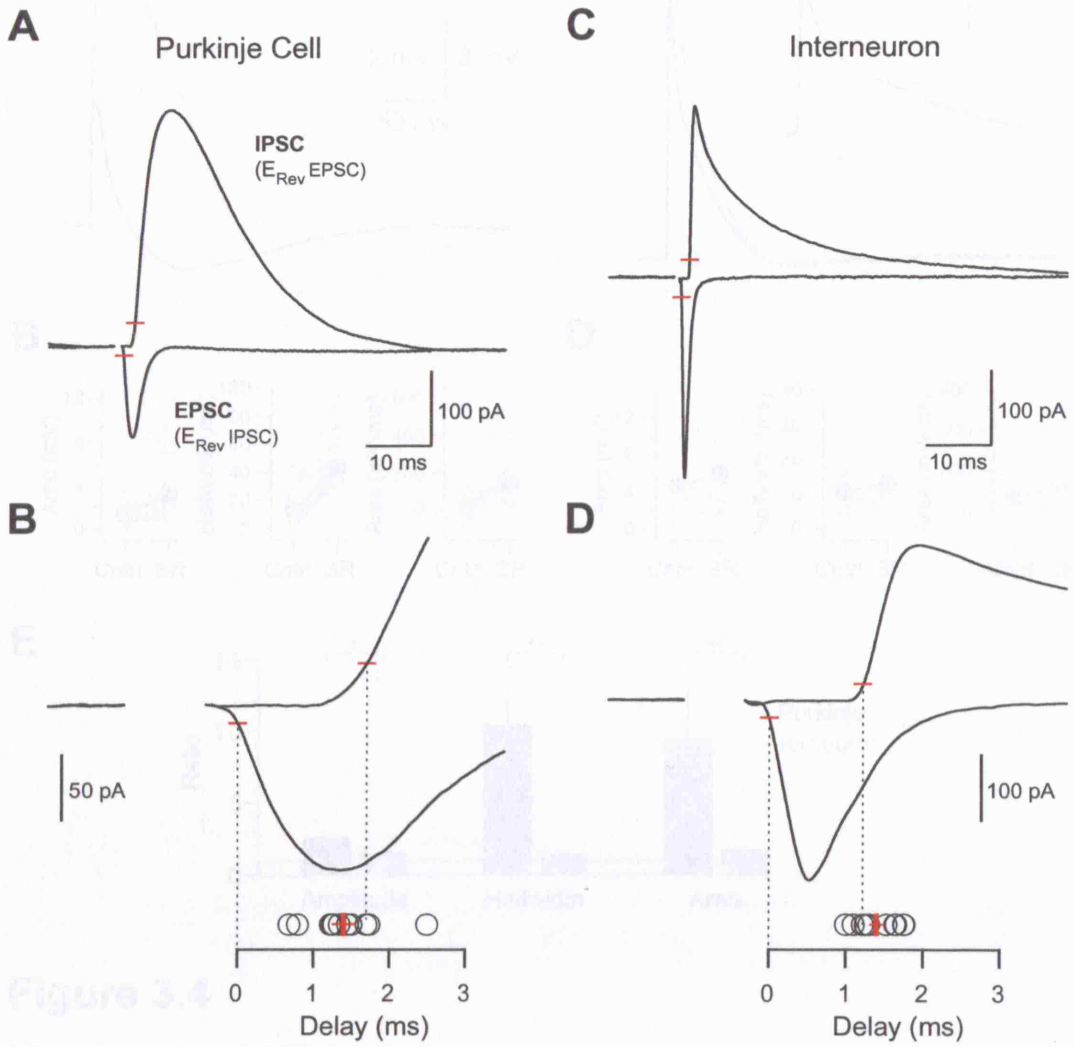

Figure 3.3

Timing of feed-forward inhibition

A, C Inhibitory and excitatory synaptic currents were separated by voltage-clamping the cell to the reversal potential of the IPSC (Purkinje cell: -60 ± 2 mV, interneuron: -60 ± 1 mV) or EPSC (Purkinje cell: 6 ± 2 mV, interneuron: 4 ± 1 mV). The peak of the averaged currents was measured and the 10% level was detected (red lines). **B, D** Currents are shown on an expanded timescale. The mean delay between the 10% risetime point of the EPSC and feed-forward IPSC was 1.4 ± 0.2 ms for Purkinje cells and 1.4 ± 0.1 ms for interneurons (red symbols); individual data points from different cells are shown as open circles. Note that the 10% percent level more accurately reflected the delay of the onset of currents than the peak since it minimizes the contribution of differences in EPSC and IPSC risetimes.

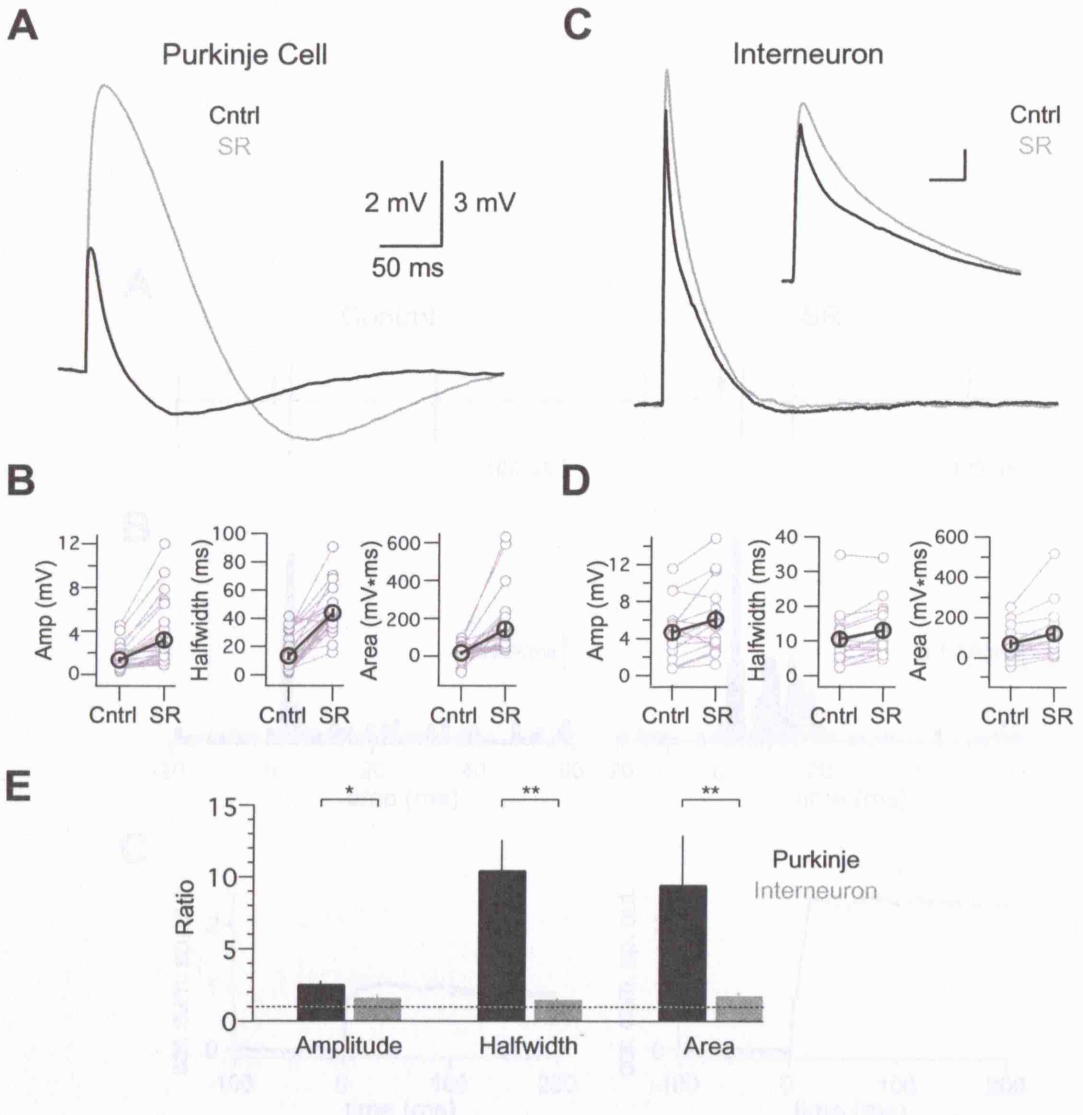

Figure 3.4

FFI determines **EPSP kinetics**
Cells were hyperpolarised to -60 to -65 mV to avoid spontaneous spikes and subthreshold voltage responses to parallel fiber stimulation were recorded. **A** Purkinje cells often displayed very brief depolarisations in response to PF stimulation in control conditions. In this example, blocking inhibition with SR increased the amplitude (2.9 to 6.7 mV), halfwidth (13.2 to 67.7 ms) and integral (-88 to 235 mV*ms) of the PF EPSP. **B** Changes in EPSP amplitude, halfwidth and integral following block of inhibition (all changes significant; $p < 0.01$). Individual cells are shown in grey, average values in black. **C** Interneuron EPSPs were more rapid and blocking inhibition led to smaller changes. In this cell, blocking inhibition increased EPSP amplitude from 9.2 to 11.6 mV, halfwidth from 13.8 to 18.5 ms and integral from 197 to 294 mV*ms. Inset shows the same traces on an expanded timescale (scale bar 2 mV, 10 ms). **D** Increases in EPSP amplitude, halfwidth and integral in all cells following block of inhibition (all changes significant; $p < 0.01$). (E) Summary of changes in EPSP properties caused by blocking inhibition in Purkinje cells and interneurons. The dotted line indicates no change; * $p < 0.05$; ** $p < 0.01$, unpaired t-test.

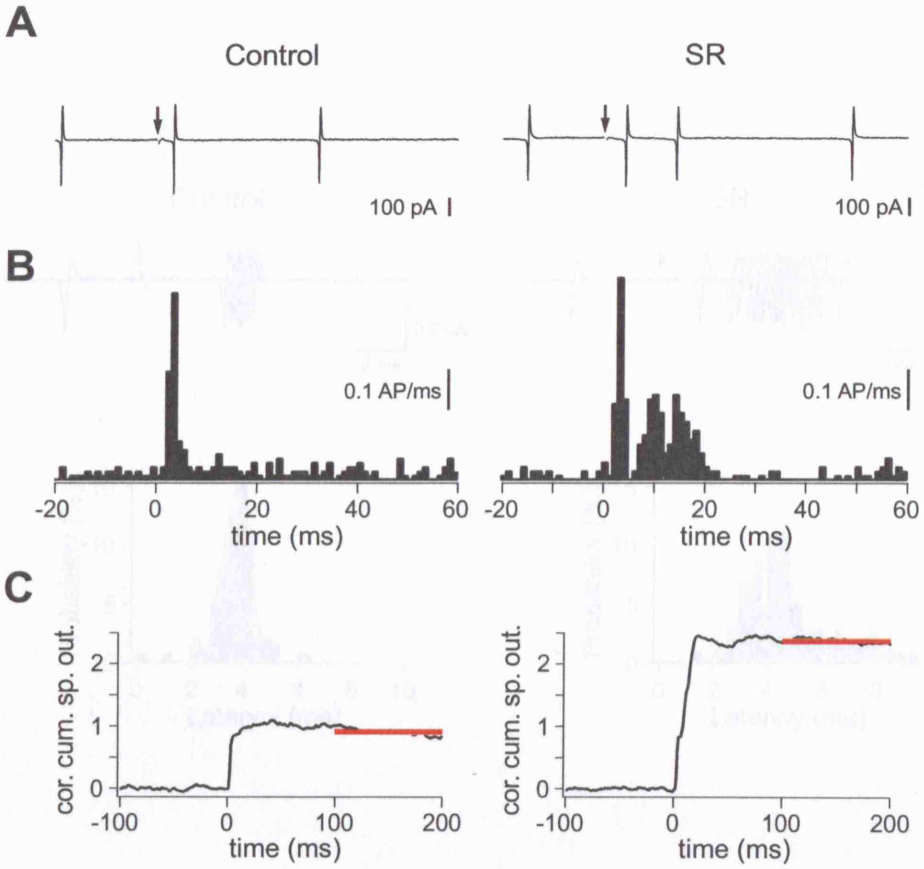

Figure 3.5

FFI regulates **spike output**
A Single trials from a cell-attached Purkinje cell recording showing spontaneous spikes and the short-latency spikes observed in response to parallel fiber stimulation. The number of spikes observed shortly after stimulation increased when SR was applied (right panel). **B** Probabilities calculated from 200 trials in control (left) and SR (right). **C** To measure the number of spikes evoked by the stimulation we calculated the corrected cumulative spike output. To estimate the additional evoked spikes, we averaged over a 100 ms window (red line) starting 100 ms after stimulation. In the cell shown parallel fiber stimulation evoked 0.9 extra spikes over baseline, increasing to 2.5 spikes when inhibition was blocked. Note the different time scale in B and C.

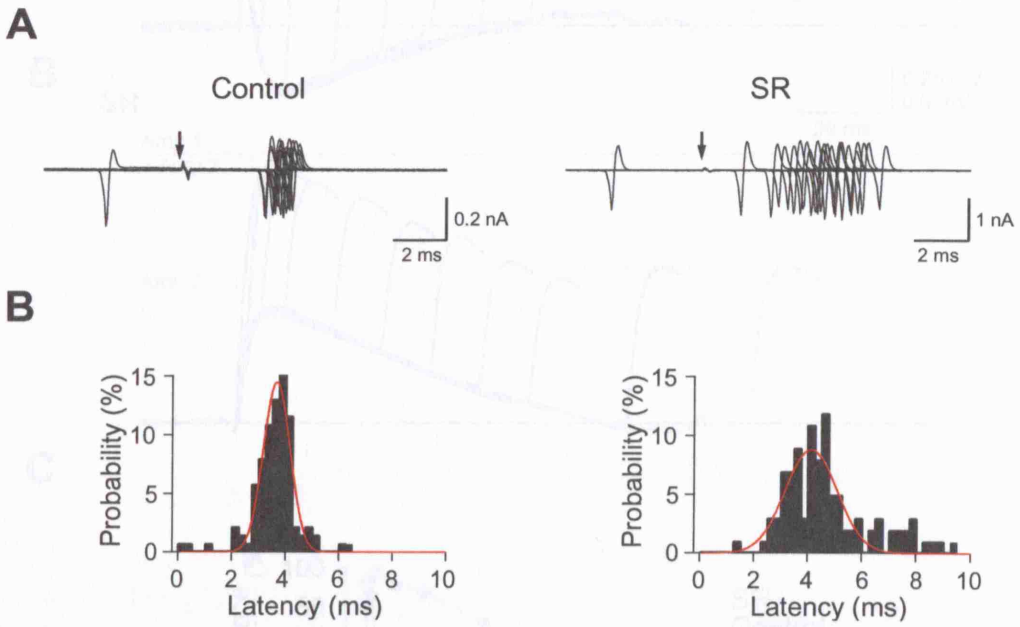

Figure 3.6

FFI increases the **temporal precision** of spikes

A Cell-attached recording (twenty superimposed trials) from a spontaneously firing Purkinje cell showing the response to parallel fiber stimulation. Evoked spikes occurred with a short latency (3.37 ± 0.08 ms) in a narrow time window after the stimulation (left panel). Blocking inhibition widened the window in which evoked spikes occurred (right panel). **B** A Gaussian was fit to the latency histogram and the width was taken as a measure of spike jitter. Blocking inhibition widened the latency distribution from 0.7 to 1.4 ms in the example shown.

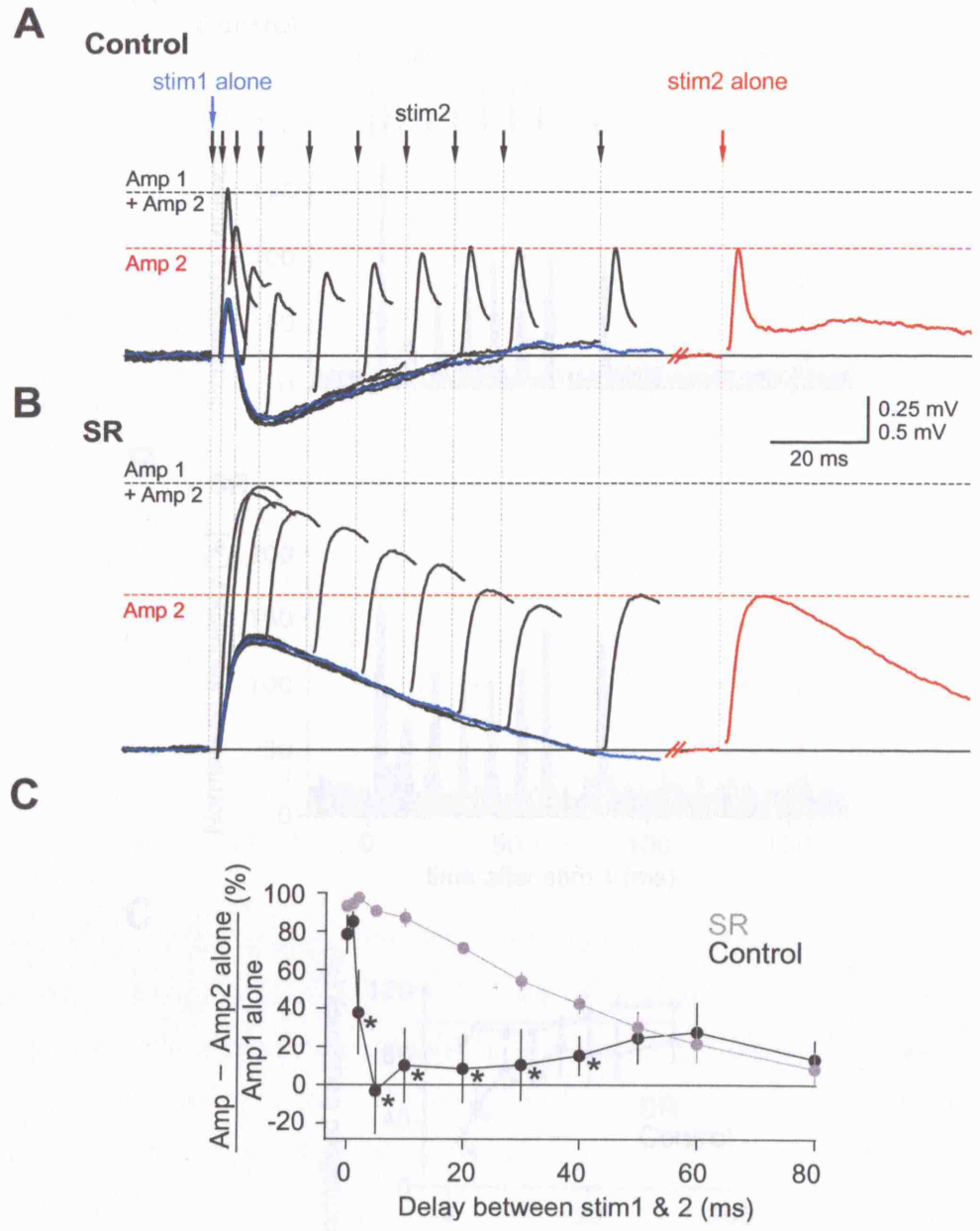

Figure 3.7

FFI limits the time window for **EPSP summation**

A Two independent parallel fiber inputs with strong feed-forward inhibitory components were activated separately (input 1, blue trace; input 2, red trace) or with delays of 0, 1, 2, 5, 10, 20, 30, 40, 50, 60 or 80 ms (black traces). Stimulus artefacts and the 1 ms delay traces were omitted for visual clarity. Traces were truncated 5 ms after stimulus 2. The amplitude of the potential resulting from input 1 and the sum of both amplitudes are indicated (red and black dotted lines, respectively). Note that the second input only exceeds its own amplitude when stimulated with a delay of 0 or 2 ms. **B** Blocking inhibition strongly lengthened this narrow window for EPSP summation due to the prolonged time course of the EPSPs. **C** EPSPs are not increased by preceding potentials unless they fall within a 2 ms window. Blocking inhibition widens that window to about 40 ms. Asterisks indicate significance (* $p < 0.05$, $n = 6$).

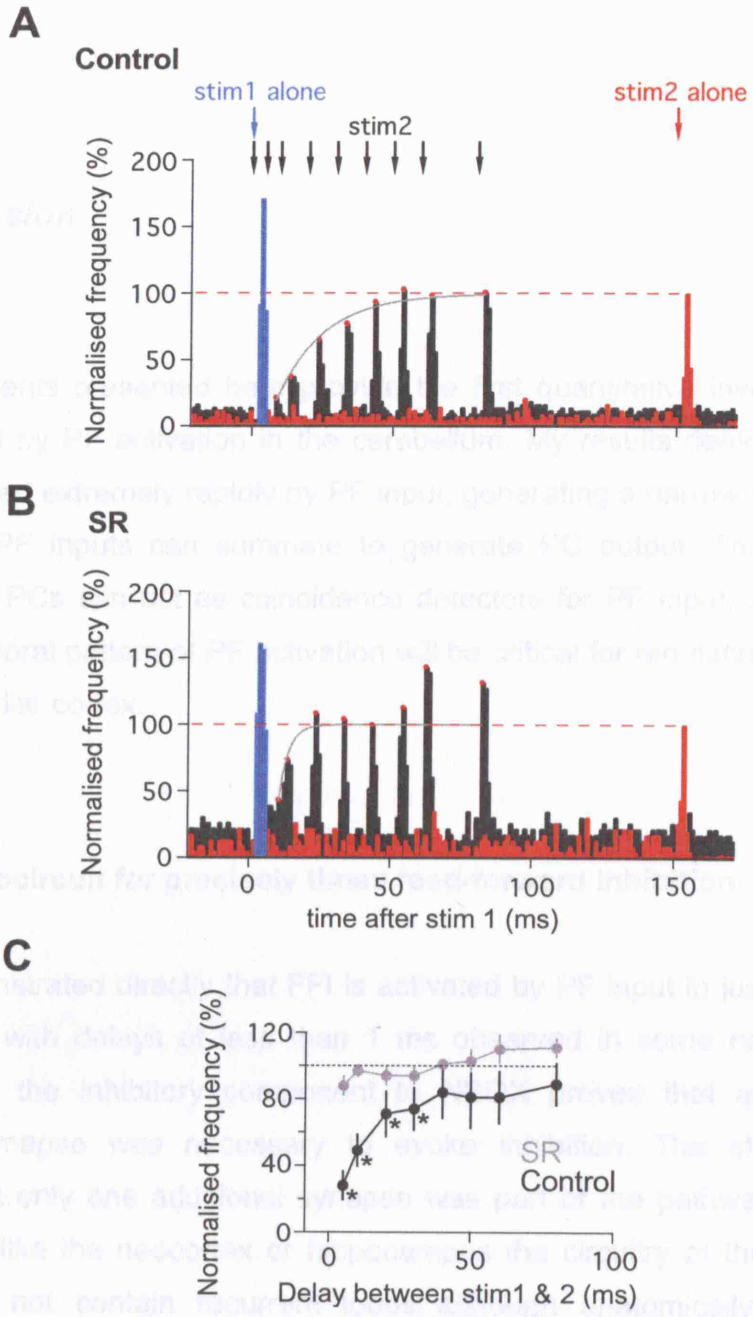

Figure 3.8

FFI limits **superthreshold summation** and suppresses spike responses to asynchronous inputs

A The spike probability for two independent parallel fiber inputs is shown (response to stimulus 1, blue bins; response to stimulus 2, red bins) when stimulated separately. Probabilities for delays of 5 to 80 ms between the stimuli are overlaid (black traces). Note that the probability following stimulus 2 is suppressed for delays up to 50 ms. Probabilities are normalised to response 2 alone (red dotted line). An exponential (grey trace) is fit to the maximum probabilities and restricted to 100%. **B** Blocking inhibition leads to a faster recovery. **C** Average spike probability over 10 ms after stimulus 2 is significantly smaller for delays up to 40 ms if inhibition is intact ($p < 0.05$, $n = 5$).

3.3 Discussion

The experiments presented here provide the first quantitative investigation of FFI triggered by PF activation in the cerebellum. My results demonstrate that FFI is triggered extremely rapidly by PF input, generating a narrow time window over which PF inputs can summate to generate PC output. These findings indicate that PCs can act as coincidence detectors for PF input, and suggest that the temporal pattern of PF activation will be critical for regulating the output of the cerebellar cortex.

3.3.1 A microcircuit for precisely timed feed-forward inhibition

I have demonstrated directly that FFI is activated by PF input in just over 1 ms on average, with delays of less than 1 ms observed in some neurons. The sensitivity of the inhibitory component to NBQX proves that at least one excitatory synapse was necessary to evoke inhibition. The short latency indicates that only one additional synapse was part of the pathway activating inhibition. Unlike the neocortex or hippocampus the circuitry of the cerebellar cortex does not contain recurrent loops although anatomically many PC collaterals curve back to enter the molecular layer (Palay & Chan-Palay, 1974). Feed-forward inhibitory currents observed here are unlikely to stem from these collaterals because no physiological evidence for functional connections between PC collaterals and cells of the molecular layer has yet been found leaving only interneurons as possible source of FFI.

PCs and interneurons receive two excitatory inputs, PFs and CFs. CFs as the source of the observed excitatory currents can be ruled out because CF responses are far bigger than the currents observed here (Silver *et al.*, 1998). This leaves PFs as the only source for the excitatory currents and the

schematic pathway in figure 3.1 E as the only possible one consistent with the data.

In PCs the rise of the IPSC was slow compared to interneurons (fig 3.2). This is not surprising because interneurons are smaller, more compact cells. However, the decay of the IPSC in both cell types was similarly slow, which at least for the interneuron is surprising as the decay of the EPSC was more than ten times faster. Deactivation of $GABA_AR$s has previously been shown to be prolonged at depolarising voltages (Mellor & Randall, 1998), which is likely to be the reason for the slow IPSC decay observed here for interneurons and maybe also for PCs.

The brief delay of inhibition was measured by comparing the times of the 10% rise time points. Since IPSCs rise slower this should induce and error in the delay measurement. Simplifying the exponential rise as a line (which would overestimate the error because the exponential function would rise steeper than a line between 0 and 10%) using the 10 – 90% risetimes extrapolated to 100% gives an upper estimate of the error (E). This is given by

$$E = 10\%\frac{\tau_{IPSC}}{80\%} - 10\%\frac{\tau_{EPSC}}{80\%} \qquad \text{Equation 3.1}$$

For PCs with risetimes of 1.07 ms and 2.23 ms for EPSCs and IPSCs respectively, this gives 0.145 ms. For interneurons with risetimes of 0.48 and 1.01 ms for EPSCs and IPSCs this gives 0.04 ms. These errors would shorten the delay slightly but as the cell to cell variability is much larger it can be ignored.

Compared to a feed-forward circuit of the hippocampus consisting of Schaeffer collaterals activating inhibition onto pyramidal cells with a delay of 1.9 ± 0.2 ms (Pouille & Scanziani, 2001) the delay measured here is briefer but comparable. The FFI delay was indistinguishable for interneurons and PCs, indicating that it arises from a hard-wired microcircuit common to both cell types (fig 3.1 E). In order to be activated so rapidly, the elements of this microcircuit must be optimized for speed. Thus, PF EPSC kinetics in molecular layer interneurons

are extremely rapid (fig 3.2 A ; Llano & Gerschenfeld, 1993; Carter *et al.*, 2002; Clark & Cull-Candy, 2002), and single PF inputs can reliably trigger spike outputs in interneurons (Barbour, 1993; Carter & Regehr, 2002) with sub-millisecond delays (Carter & Regehr, 2002; Suter & Jaeger, 2004). Interneurons have rapid membrane time constants (Häusser & Clark, 1997) and brief EPSPs (fig 3.4 ; Carter & Regehr, 2002) which are normally not prolonged by postsynaptic NMDA receptor activation (Clark & Cull-Candy, 2002). The short interneuron axon collaterals making contacts with neighbouring PCs and interneurons (Palay & Chan-Palay, 1974) help to minimize axonal delay associated with FFI activation. Finally, the rapid rise of IPSCs in PCs (fig 3.2 B ; Vincent *et al.*, 1992) will help to ensure a rapid onset of FFI. Taken together, these considerations indicate that both the anatomical and physiological properties of the FFI microcircuit are tuned for maximum speed.

3.3.2 Feed-forward inhibition regulates spike output of Purkinje cells

The rapid onset of FFI curtails the PF EPSP in PCs to a fraction of its original duration. I have shown directly that the shape of the resulting biphasic EPSP-IPSP waveform, originally reported by Eccles and colleagues *in vivo* (Eccles *et al.*, 1967) and also observed with voltage-sensitive dye signals from the molecular layer of isolated cerebellum (Cohen & Yarom, 1998), can be explained by the kinetics and latencies of the underlying EPSC and feed-forward IPSCs. The shortening of EPSP timecourse by FFI has several important consequences. First, it enforces precisely timed output spikes in response to synchronous inputs (fig 3.6). My results show that FFI allows PC output in response to PF stimulation to be timed to a precision of less than a millisecond, similar to the effect of FFI in hippocampal pyramidal cells (Pouille & Scanziani, 2001). Second, it limits the time window for summation of multiple asynchronous inputs to only a few ms (see also Brunel *et al.*, 2004). Furthermore, inputs falling outside this time window are penalized, and have a lower-than-normal efficacy of spike generation. This provides a mechanism to further enhance the signal-to-noise of precisely timed inputs at the expense of inaccurately or asynchronously timed ones.

In contrast to pyramidal cells, cerebellar PCs show spontaneous activity. As a consequence, both excitation and FFI are superimposed on a background of activity, and can act not only by initiating individual spikes, but also by accelerating or delaying spontaneous spikes. The proximity to threshold also means that even small inputs can influence spike output (chapter 5 ; Häusser & Clark, 1997; Carter & Regehr, 2002; Suter & Jaeger, 2004). I have measured the suppressive effect of FFI on subsequent spike generation to be on the order of 30 ms. Therefore, even small PF inputs which do not on their own trigger spikes can influence the spike output by reducing the efficacy of subsequent inputs or by preventing spontaneous spikes. In a situation where the PC receives hundreds or thousands of PF inputs FFI could mediate 'gain control' of asynchronous 'tonic' excitation (Marr, 1969) whereas synchronous inputs could overcome FFI and result in fast-rising EPSPs that trigger spikes with high temporal precision due to subsequent FFI.

3.3.3 Mutual feed-forward inhibition in the inhibitory network

Molecular layer interneurons are highly interconnected (Häusser & Clark, 1997; Kondo & Marty, 1998), and single spikes in presynaptic interneurons can powerfully regulate spike timing in postsynaptic interneurons (Häusser & Clark, 1997; Carter & Regehr, 2002). I have demonstrated that molecular layer interneurons, in addition to generating FFI onto PCs, also receive FFI from each other. Interestingly, the level and effect of FFI in interneurons seems much weaker than that observed in PCs in measures of both the apparent underlying inhibitory conductance relative to the excitatory conductance and the effect of FFI on the EPSP waveform. This could either reflect differences in the ratios of unitary PF and inhibitory conductances in PCs and interneurons, or alternatively PFs could activate fewer feed-forward interneurons onto interneurons than onto PCs.

What is the functional role of this FFI onto interneurons? One reason may be to ensure the brevity of FFI onto PCs by shortening the excitation of interneurons. The timecourse of the FFI IPSC in PCs (fig 3.2 A) is comparable to that of

IPSCs evoked by direct electrical stimulation (Vincent *et al.*, 1992), suggesting that activation of interneurons contributing to the FFI is rapidly terminated. This could occur via a combination of FFI onto interneurons themselves and the prominent reset caused by the AHP following single interneuron spikes (Carter & Regehr, 2002). The fact that PF synapses onto both interneurons and PCs facilitate (Perkel *et al.*, 1990; Clark & Cull-Candy, 2002) suggests that FFI can keep pace with PF activation even during bursts of activity (Chadderton *et al.*, 2004).

3.3.4 Functional implications for cerebellar processing

Several lines of evidence have converged to support the idea that the cerebellum is involved in representation of precise temporal information (Ivry & Spencer, 2004). I have now identified FFI as a key cellular mechanism that can help to preserve timing of cerebellar simple spike output to within millisecond precision. These properties may help PCs act as coincidence detectors responding only to well-timed PF inputs. Furthermore, the rapid onset of FFI may have special relevance for the functional architecture of the molecular layer. There has been considerable controversy regarding the role of PF 'beams' in cerebellar processing, with little direct evidence available for beam-like activation of PCs in the intact cerebellar cortex (chapter 4 ; Cohen & Yarom, 1998; Jaeger, 2003). An existing hypothesis of how FFI can explain the discrepancy between the beam-like input to PCs and the lack of beam-like activation of PCs is considered in chapter 4 and two alternative hypotheses are proposed.

4 Distance dependence of feed-forward inhibition

4.1 Introduction

In the previous chapter I showed that FFI onto PCs has a strong effect on spiking. The delay of FFI allows for a narrow window of excitation in which the cell is likely to fire a spike. The spatial pattern in which PCs are activated in behaving animals has been controversial for more than 30 years. It has been shown that activation of PFs through sensory stimulation does not lead to a beam of excited PCs as expected from the anatomy. Instead, PC activity is confined to small patches of cerebellar cortex (Eccles *et al.*, 1972a). Patches of PC activity seem to require activity in the underlying GC layer (Bower & Woolston, 1983).

PF excitation of PCs could be cancelled by a reduction in the delay of FFI. If excitation and inhibition arrive synchronously, the inhibition could cancel the excitation. Asynchrony of action potential propagation in the PFs has been proposed as a mechanism for the reduction of the delay of FFI (Bower, 2002). The data presented in this chapter do not support this mechanism and theoretical considerations show that this mechanism is unlikely to result in small active PC patches as observed *in vivo*. I suggest two alternative hypotheses, one of which consistent with small patch dimensions.

4.1.1 Fractured somatotopic maps but no beams

The cerebellar architecture suggests that GC activity results in PC activation along the course of GC axons (Braitenberg & Atwood, 1958). Activation of a

patch of GCs or PFs should therefore evoke a beam of PCs activated by the excitatory PFs (this is henceforth called "PC beam" and the active PF tract is called "PF beam"). In their classic work on the cerebellum (Eccles *et al.*, 1967), Eccles and Ito tested this prediction with 'local' electrical stimulation of PFs and indeed found PC beams leading to the idea of the beam as "the basic unit of operation of a mossy fibre input into the cerebellum" (page 114). Several imaging studies confirmed that direct stimulation of PFs leads to PC beams (Cohen & Yarom, 1998; Coutinho *et al.*, 2004; Dunbar *et al.*, 2004; Gao *et al.*, 2005).

However, when electrical stimulation of afferent nerves or sensory stimulation was used, PC beams were not detected, rather the PC response was found to be patchy and mosaic-like (Eccles *et al.*, 1971; Eccles *et al.*, 1972a, b); fig 4.1 B). This has since been confirmed with different techniques (Allen *et al.*, 1974; Bower & Woolston, 1983; Kolb *et al.*, 1997; Cohen & Yarom, 1998; Jaeger, 2003) and seems to be true even in an isolated cerebellum (Cohen & Yarom, 1998). Following this surprising finding investigators focussed on the PC afferents and, again, found that sensory stimulation also leads to non-continuous patches of activity in the GC layer (Joseph *et al.*, 1978; Shambes *et al.*, 1978a; Shambes *et al.*, 1978b). While adjacent patches received inputs from non-adjacent body parts, the organization within a patch was found to be somatotopic leading to the term "fractured somatotopic map" (Welker, 1987). This discontinuity stands in contrast with the more or less continuous body-representation of cerebral S1 (Welker, 1971). Subsequent research characterised mossy fibres and mossy fibre afferents projecting to the cerebellum and found the afferent projection pattern to be the basis for the map (Kassel, 1980; Bower *et al.*, 1981; Woolston *et al.*, 1981). In these studies activity in the cerebellum and elsewhere was measured with extracellular microelectrodes recording multi-unit field potentials. Space was resolved by many closely spaced recordings, a technique called micro-mapping. The spatial resolution can be as high as 50 μm, but most mappings were done with lower resolution. The fractured somatotopic map of the cerebellar hemisphere with crus I and II as well as neighbouring folia is shown in figure 4.1 A (taken from Bower *et al.*, 1981). Many areas of the rat's face are represented in small

patches, usually in more than one folium (e.g. upper lip and vibrissae are represented in all folia) and often one area is represented in disjoined patches within the same folium (e.g. lower incisor in crus II A, B and hand in paramedial lobule). Patch sizes in the direction of the PFs (parallel to the long sides of the folia) vary between 0.1 to 1.5 mm.

Similarities between GC and PC somatotopic maps led to speculation that the same map exists in both layers. Indeed, Bower and Woolston showed in a now famous paper that active PCs were always directly above activity in the GC layer and activity in the GC layer was always mirrored by activity of the overlying PCs (Bower & Woolston, 1983). After recording PC single unit activity they advanced the recording electrode into the GC layer to record multi-unit activity. Activation of the spontaneously active PCs was assessed by changes in spike probability. Patches of activated PCs range from 0.1 mm to > 1 mm. An example of a small patch is shown in figure 4.1 B (from Bower & Woolston, 1983). These active patches are often surrounded by areas in which spike probability was reduced by the sensory stimulation. Explanation of these findings focussed on the ascending segment of GCs providing input only to overlying PCs (Bower & Woolston, 1983; Jaeger & Bower, 1994; Gundappa-Sulur *et al.*, 1999; Bower, 2002; Santamaria *et al.*, 2002). To date, several studies using electrophysiology (Allen *et al.*, 1974; Kolb *et al.*, 1997; Bower, 2002), imaging with voltage sensitive dyes (Cohen & Yarom, 1998) and cross correlation techniques (Jaeger, 2003) have failed to find PC beams, and the lack of sensory-evoked PC beams is generally accepted. But even taking synapses of the ascending segment into account it remains unclear why PFs do not activate PCs. Failure of action potential propagation in the PFs or at the T-junction of the ascending segment and the PF is unlikely because electrical stimulation of GCs leads to normal EPSPs in PCs (Sims & Hartell, 2005) and stimulation of mossy fibres leads to beam-like metabolic activity (Coutinho *et al.*, 2004), indicating that metabolically costly synaptic transmission takes place along the PF axons. However, even with an isolated cerebellar preparation, stimulation of the mossy fibres does not result in beams but in patches similar to the ones described *in vivo* (Cohen & Yarom, 1998).

4.1.2 Temporal dispersion of spikes in parallel fibres as mechanism

The only theory explaining why PFs do not excite PCs along their path has been published by Bower (Bower, 2002). According to this theory (fig 4.2 C), PFs have a different action potential conduction velocities. Synchronous activity in one spot (top panel) leads to a gradual lead of the spikes travelling in the faster fibres of the lower molecular layer (middle panel). PFs excite PCs along their path (red PC soma and dendrites) but due to fast FFI the initial excitation is quickly followed by inhibition (blue soma / dendrite). If the lead of the lower PFs gets larger than the monosynaptic delay between excitation and FFI (bottom panel) then PCs first receive very little excitation by the early spikes followed by inhibition that is present at the time of arrival of the majority of the spikes and cancels their effect. This elegant theory is consistent with the properties of the participating cells and synapses: PF synapses onto PCs are weak, giving rise to an EPSP of approximately 0.07 mV (Isope & Barbour, 2002). Therefore, a small number of fast PFs would exert little effect on the spiking of PCs. The opposite is true for PF → interneuron synapses, where minis are large (-127 pA ; Carter & Regehr, 2002) and can trigger spikes in these cells due to their high input resistance (Carter & Regehr, 2002). Compared to PF synapses, unitary inhibitory inputs to PCs are large (1.8 nA with high internal chloride ; Diana & Marty, 2003). Therefore, it is likely that few early arriving spikes can trigger a powerful inhibition that cancels the bulk of the later arriving excitation.

The assumption that some PFs are faster is also supported by some experimental data. PFs in the lower molecular layer were reported to be about 10% faster, which was age dependent (fig 4.2 A from Vranesic *et al.*, 1994). Several electron-microscopic studies examined PF diameters because the diameter of unmyelinated fibres is correlated to their conduction velocity. The PF diameter was found to depend on the location in the molecular layer with larger diameters close to the PC layer (Palay & Chan-Palay, 1974; Wyatt *et al.*, 2005). Wyatt et al estimated conduction velocity from PF diameters

(Hoffmeister *et al.*, 1991) and calculated the time a spike needs to travel the entire length of the PF, using 4.5 mm PF length for the rat (Pichitpornchai *et al.*, 1994). This gives a range of conduction velocities of about 20 – 32 cm/s, an even wider range than measured by Vranesic et al (1994 ; fig 4.2 A from Wyatt *et al.*, 2005).

Although the Bower theory is capable of explaining the lack of beams and is consistent with the available data, it currently lacks direct experimental support. However, the theory gains some indirect support from a recent, to date still unpublished, experiment by the Bower lab. They mapped the area of the GC layer of crus IIa activated by stimulation of the upper lip or frontal bold patch in anaesthetised rats. A recording from a PC located along the direction of the PFs but outside the active patch did not show any activity, which was also true for the underlying GC layer. Interestingly when they washed in the $GABA_A$ antagonist bicuculline, the responses in the GC layer did not change, indicating that Golgi cell inhibition was not required for suppressing GC activity in these circumstances. However, the presence of bicuculline unmasked a high firing probability in the recorded PC similar to the ones seen in the active patch (Bower, J.M. personal communication). These experiments clearly show that PCs outside the patches of PC activity receive excitatory input from PFs which is cancelled by inhibition.

In this chapter I tested Bower's theory with experiments in cerebellar slices. I looked at the distance-dependence of the kinetics of EPSCs, feed-forward IPSCs and the delay between them and I present a quantitative formulation of Bower's theory. Neither experiments nor theoretical considerations were found to support Bower's theory. However, two alternative theories are proposed at the end of the chapter, which can explain the lack of PC beams.

4.2 Results

4.2.1 Parallel fibre conduction velocity

In order to test whether temporal dispersion within the PFs could be a mechanism to cancel PF excitation I recorded currents evoked at different distances from the recorded PC and measured PF conduction velocity, kinetics of excitatory and inhibitory currents and the delay between them. I used coronal cerebellar slices where PFs run in the plane of the surface of the slice allowing stimulation at different distances to the recorded PC. Depending on the exact cutting angle and the position of the slice within the curved vermis, stimulation of PFs at distances of up to 1.6 mm from the recorded PC still resulted in excitatory currents followed by FFI (fig 4.3 B). These currents were similar to currents evoked in alternating trials at closer distances (105 ± 3 µm ; n = 14) to the PC with a second stimulation electrode (fig 4.3 A). Biphasic currents were recorded at membrane potentials in between the EPSC and IPSC reversal potential (-45 ± 0.2 mV ; range -60 to -38 mV n = 26). The membrane potential was adjusted to clearly resolve excitatory and inhibitory components of both stimulus locations. After recording biphasic currents the FFI component was blocked by washing in SR. The IPSC was calculated by subtracting the EPSC recorded in SR from the biphasic current (fig 4.3). On average EPSCs were -176 ± 30 pA (n = 24) and IPSCs 226 ± 28 pA (n = 22).

The latency of the EPSC was measured as delay between stimulus artefact and excitatory current and was larger for the far stimulus location, reflecting the longer distance the action potentials have to travel to reach the PC (fig 4.4 A). Assuming a constant conduction velocity along the length of the PF, the conduction velocity was calculated by fitting a line to the graph plotting the distance between stimulus electrode and recorded PC as a function of the EPSC latency (fig 4.4 B). The slope corresponds to a conduction velocity of 23.8 ± 1.3 cm/s. The extrapolation of the line fit to zero gives the value of the

synaptic delay between PF → PC synapses. This delay of 0.85 ms is contaminated by the 0 to 10% risetime of the EPSC. Correcting for the EPSC risetime of 0.15 ± 0.01 ms gives a delay of 0.7 to 0.8 ms (see equation 3.1 in chapter 3.3.1). The synaptic delay should be slightly shorter due to measuring the EPSC latency from the beginning of the stimulus artefact the PF spike latency is contained in the measurement.

An alternative method of calculating the conduction speed was plotting the difference of the EPSC latencies from the two stimulus locations as a function of the distance between them (fig 4.4 C). The average PF conduction velocity was then calculated by fitting a regression line constrained to go through zero giving a value of 24.6 ± 1.5 cm/s. This method should be independent of the synaptic delay and the PF spike latency assuming that both stimulus locations can be treated identically. Because of this independence it is also possible to determine the conduction velocity in single experiments. This gives a range of 18.0 to 52.8 cm/s although the experiment with 52.8 cm/s could be treated as outlier because this velocity was more than five standard deviations faster than the mean. The second fastest measurement was only 29.0 cm/s. These conduction speeds compare well to a velocity of 24.1 ± 0.2 cm/s measured by Vranesic et al (1994, fig 4.2), 20 – 32 cm/s calculated by Wyatt et al (2005) or about 30 cm/s shown by Heck (1993, peak in fig 4 A). For unknown reasons measurements of conduction velocity with extracellular field potentials give faster values of around 45 cm/s (Eccles, 1973; Garwicz & Andersson, 1992).

4.2.2 Kinetics of the excitatory and inhibitory components

If temporal dispersion is a mechanism to reduce the delay of FFI one would expect significantly slower kinetics of the EPSC evoked far from the cell. Specifically the rise should reflect the asynchrony of arrival times of spikes travelling in the PFs. EPSCs could be fitted with double exponential functions (fig 4.5 A, B). In all 10 cells with good fits the rise time constants were larger at greater distance (fig 4.5 C). This increase between stimulation close to the recorded PC (105 ± 3 µm) and stimulation far from the cell (1029 ± 25 µm) was

statistically significant (0.80 ± 0.02 ms to 1.29 ± 0.04 ms ; n = 10 ; $p < 0.01$) and similar to the increase in the 10 – 90% risetimes (1.13 ± 0.04 ms to 1.79 ± 0.06 ms ; n = 10; $p < 0.01$). The decay time constant was independent of distance (fig 4.5 D ; 7.2 ± 0.2 ms to 7.5 ± 0.2 ms ; n = 10 ; $p > 0.4$).

If some early arriving fibres trigger inhibition early the rise of the IPSC should also be slower at long distances. Double exponential functions provided good fits for feed-forward IPSCs but occasionally the peak differed from an otherwise good fit (fig 4.6 A, B). Rise time constants of IPSCs were larger than for EPSCs and also increased with distance from 1.17 ± 0.4 ms to 1.47 ± 0.05 ms (n = 8; $p < 0.05$; fig 4.6 C). Similarly, 10 – 90% risetimes increased from 1.67 ± 0.07 ms to 2.08 ± 0.04 ms (n = 10 ; $p < 0.05$). The decay time constant of stimulation close to the cell was with 9.9 ± 0.5 ms similar to 9.8 ± 0.3 ms of the far stimulation (n = 8 ; $p > 0.4$).

4.2.3 Temporal dispersion of parallel fibres cannot account for the lack of beams

The Bower theory states that the temporal dispersion of PFs leads to fast fibres triggering inhibition early to cancel the bulk of the later arriving PF excitation. In this case it is expected that the delay between excitatory current and feed-forward IPSC decreases as the distance to the stimulation site increases. Eventually the excitatory current and FFI arrive simultaneously and cancel each other. To test this I measured the dependence of the delay between excitatory current and feed-forward IPSC on the distance from the stimulation site. The delay between 10% of the rise of EPSC and IPSC was independent of the distance from the stimulation site (fig 4.7 A). At greater distances the IPSC never occurred earlier or at the same time as the EPSC but always lagged by more than 1.2 ms (fig 4.7 B). On average, the delay for the stimulation close to the PC was 1.51 ± 0.04 ms and was statistically indistinguishable from 1.67 ± 0.03 ms, the delay of the far stimulation ($p > 0.4$; n = 9).

The length of many PC receptive fields in the direction of the PFs is short. (The spread of receptive fields into the other dimension of the plane of the GC layer

orthogonal to the direction of the PFs is not considered here because I tried to find the basis for the missing spread of PC activity in direction of the PFs.) An example of a receptive field smaller than 0.2 mm is shown in fig 4.1. If Bower's theory is correct, the fast fibres must reach the border of the PC patch and produce FFI in the same time it takes the average fibres to reach the border. Therefore, the difference in velocity between the fastest fibres (v_{Max}) and the average fibres (v_{Ave}) determines the PC receptive field size. The time spikes need to cross the length of the receptive field (L) when travelling in fibres with average conduction velocity is given by the length of the field divided by the velocity. The fast fibres have to gain a lead equal or larger than the delay between EPSC and IPSC (d). This means that fast fibres have to cross the receptive field in the time it takes the average fibres to cross it minus the delay. The velocity of the fastest fibres is given by

Equation 4.1

$$v_{Max}(L_{PC}) = \frac{L_{PC}}{\frac{L_{PC}}{v_{Ave}} - d}$$

v_{Max} , v_{Ave}	maximum, average PF velocity
L_{PC}	PC receptive field size
d	EPSC / IPSC delay

Since GC axons bifurcate and run in opposite directions of the molecular layer, a PC receptive field limited by Bower's mechanism would extend to both sides of the activated GCs. Therefore, the fast fibres have to gain the lead of one EPSC / IPSC delay within half of the length of the receptive field:

$$v_{Max}(L_{PC}) = \frac{L_{PC}/2}{\frac{L_{PC}/2}{v_{Ave}} - d} = \frac{L_{PC}}{\frac{L_{PC}}{v_{Ave}} - 2d}$$

Equation 4.2

This function is plotted in figure 4.8 with an average PF velocity of 25 cm/s and three different delays. For conduction velocities in the range of the ones measured above or published previously, the minimum receptive field sizes that could be generated by the Bower mechanism are too large. Furthermore, the Bower theory assumes activation of a point in the GC layer with no lateral extent. Using more realistic spatially extended GC patch sizes has two consequences: 1) The PC receptive field calculated so far would be increased

by the size of the GC layer patch giving even larger receptive fields. 2) PC activity would not be confined to locations directly overlying the active GC layer as Bower and Woolston emphasized in their paper (1983). Since the receptive field sizes calculated in figure 4.8 are a lot larger than GC layer patches (fig 4.1) active PCs would only rarely have active GC layer underneath them.

4.2.4 Spatially distributed sensory activation of granule cells can kill the beam

Instead of relying on temporal dispersion within PFs, the spatial arrangement of GCs activated by sensory stimulation might act to ensure that PF excitation is cancelled by inhibition. For simplicity I have assumed that a stimulus simultaneously activates GCs in a 1 mm patch with even probability (fig 4.9 A). The action potential in a GC on the border of the patch (red cell in fig 4.9 A) will travel in both directions and trigger inhibition with a delay of 1.4 ms (fig 3.3). A PC just outside the patch will receive excitation via the PFs from this GC. However, the PC will not be excited by all GCs in the patch because spikes in GCs further away reach the PC after the onset of FFI. Consequently, all PCs outside the patch will receive some excitation before FFI cancels the present and subsequently arriving excitation. The distance from the border of the patch in which GC spikes reach PCs before FFI is determined by the average velocity (v_{Ave}) and the delay of FFI (d). With the experimental values this gives

$$v_{Ave} \cdot d = 25\frac{cm}{s} \cdot 1.4\ ms = 0.35\ mm \qquad \text{Equation 4.3}$$

Summing GC spikes reaching the PC before the onset of FFI gives an arbitrarily scaled measure of PF excitation received by PCs. In figure 4.9 B the red function, scaled to a maximum of 1.0, shows the steady level of this PF excitation to both sides of the black step function of activity in the GC layer.

FFI also leads to some excitation inside the patch arriving after inhibition. Only neighbouring GCs closer than 0.35 mm will reach a given PC in time. This leads to a reduction of the activity received by PCs in the center of the patch because action potentials in GCs outside the central 0.7 mm arrive after onset of inhibition. In addition to this, a further decrease occurs at the margin of the patch: the closer to the border, the fewer active GCs to that side of the PC until all PF excitation is received from the other side and is identical to the excitation received by PCs outside the patch (see red curve figure 4.9 B).

The spatial extent of the GC layer patch automatically leads to cancellation of a part of the PF activity. How much excitation will "escape" from inhibition? I defined this escape as the number of GC spikes reaching PCs before FFI divided by the total number of GC spikes. This fraction (f) depends on the size of the patch because the total number of GCs increases with the patch size. Therefore, for a step function the required GC layer patch size for a given fraction is:

$$L_{GC}(f) = \frac{v_{Ave} \cdot d}{f} \qquad \text{Equation 4.4}$$

The function is plotted in figure 4.9 D. For fractions of 10 to 20% the resulting receptive field sizes are larger than the ones observed experimentally (fig 4.1). However, sensory stimulation is unlikely to result in a step function of activation in the GC layer. Field potentials in the GC layer measured by Bower & Woolston (1983) show a gradual decrease in amplitude towards the borders of the field. This is probably a consequence of the considerable spread of mossy fibre axons within and across folia (Palay & Chan-Palay, 1974; Wu *et al.*, 1999), although spike probability of GCs as a function of location in the GC patch is unknown. In this spatial spread model the fraction of escaped excitation and total excitation depends on the function of GC spike probability. Because only spikes in GCs within 0.35 mm from the border of the patch arrive before inhibition, this fraction is:

$$f = \frac{\int_{0}^{0.35\,mm} gc(x)dx}{\int_{0}^{\infty} gc(x)dx}$$

f fraction of E before I

$gc(x)$ GC spike probability

Equation 4.5

The excitation PCs receive outside the patch along the entire PF beam is

$$pc(x) = \int_{0}^{0.35\,mm} gc(x)dx$$

Equation 4.6

Inside the patch PCs receive excitation from both sides. This is given by

$$pc(x) = \int_{x-0.35mm}^{x+0.35\,mm} gc(x)dx$$

$pc(x)$ PC excitation

Equation 4.7

In figure 4.9. C a Gaussian is used to demonstrate that for GC spike probability functions with smaller probabilities on the margins compared to the center, the fraction of escaped excitation gets smaller. The area of the Gaussian within the dotted lines occupies a smaller fraction of the total area than is the case for the step function. In figure 4.9 D I plotted the length of the receptive field, defined as the distance of the 1% limits of the Gaussians, as a function of the fraction of escaped over total excitation (equation 4.5). It is clear that for smaller escape fractions Gaussian functions of spike probability in the GC layer can result in much smaller PC receptive fields than step functions.

PC receptive fields can be dramatically reduced when GC probability functions that are slimmer than Gaussians are used. The more of the total area under the curve is confined to the center, the smaller the resulting PC receptive fields will be. However, there is a minimum for the PC receptive field size generated by this spatial spread theory: at 0.7 mm, the fixed 0.35 mm stretch of "escaping" GCs will include the high probability of the center and lead to an escape of 50%. This is independent of the GC activity function used as long as it is symmetric around the center. This effect will lead to minimum PC receptive field sizes converging to 0.7 mm for GC activity functions that are progressively slim

and steep in the center. While this minimum cannot be changed by progressively slimmer GC activity functions, the amount of escaping excitation will converge to zero even for fields close to 0.7 mm. This 0.7 mm minimum of PC receptive field sizes is bigger than fields measured experimentally (Bower & Woolston, 1983) but it is likely to be consistent with the data which is discussed in chapter 4.3.1.

A different problem is more troubling for the spatial spread theory: so far the rationale for estimating the minimum receptive field size was based on what percentage of escaping excitation is tolerable without leading to a PC beam. The major flaw of the model is that irrespective of the GC spike probability function FFI needs 1.4 ms to kick in. Consequently, PC receptive field sizes will be at least 0.7 mm regardless of the underlying GC activity function.

Finally it should be mentioned that in this theory I focussed on the question why PFs do not lead to beams of excited PCs and ignored excitation provided by synapses of the ascending segment. One can account for this by adding a constant multiplied by the GC activity function to the PC excitation function. This will further increase the contrast of the strong excitation of the center compared to the tails. The value for that constant reflects the relative amount of excitation provided by the ascending segment versus the PF and has been suggested to be quite high (Gundappa-Sulur *et al.*, 1999; Santamaria *et al.*, 2002).

4.2.5 Non-simultaneous sensory activation of granule cells can kill the beam

In chapter 4.2.4 the spatial spread of active GCs led to inhibition occurring earlier than excitation and therefore prevented PC beams. Instead of a spatial spread, a temporal spread of GC activity could have a similar effect. A few early GCs could trigger inhibition spreading along the PFs ahead of the bulk of GC activity and thus cancel the effect of PFs.

Like in the previous model I assumed that very few GCs can trigger inhibition and this inhibition is sufficient to cancel PF excitation. The feasibility of this

assumption is discussed later (chapter 4.3.4). This simplification is necessary as it allows reduction of the specific temporal distribution of GC activity to a single parameter, the time from the first GC spikes to the average GC spike time (Δt).

Spikes in a few active GCs that occur ahead of most GCs activated by a sensory stimulus can trigger FFI. This inhibition then has to be overcome by excitation. This is metabolically more costly because more excitation for a given sensory induced activity of PCs is necessary than if inhibition were absent. Because inhibition has to be sufficiently strong to cancel PF excitation an extra source of excitation is necessary to provide net excitation inside the PC receptive fields. This could be provided by the ascending segment of the GC axon, which in the spatial spread model was not required for excitation inside the active PC patch. What fraction of GC excitation stems from the ascending segment is unknown. Fractions towards the extremes (0 or 100%) are unlikely: the ascending segment cannot be too weak, because if inhibition and PF excitation cancel each other's effect, the ascending segment on its own has to provide sufficient excitation for a robust activation of the active PC patch. Conversely, PFs cannot be too weak either, because blocking inhibition unmasked PF mediated excitation outside the active patch with magnitudes similar to the ones seen inside the patch before the block of inhibition (Bower, personal correspondence, chapter 4.1.2). Therefore, PF excitation and FFI have to be of similar magnitude and opposite sign and PF and ascending segment excitation also have to be similar and were all assigned the same value.

For a GC patch that has a Gaussian spike probability I assumed that early spikes occur in GCs near the center of the patch where spike probability is highest. This is the simplest assumption because there is no reason to assume a different probability distribution for early GC spikes than for all GC spikes (but see below). After the delay between EPSC and IPSC, inhibition starts to spread from the location of the early GCs towards the edges of the patch (fig 4.10 A, red box in B – D). Three cases are considered in which the early spikes lead by 1) the synaptic delay (fig 4.10 B), 2) the synaptic delay plus the time FFI takes to travel to the margins of the patch (fig 4.10 C) and 3) leads greater than that

(fig 4.10 D). The level of PC input (sum of excitation or inhibition) for the lead equal to the FFI delay (d) is shown for a 0.2 mm and 0.6 mm GC patch (fig 4.10 B left and right panel, respectivey). After d (1.4 ms) the overlying PCs receive excitation from the ascending segment directly proportional to the GC spike probability function (fig 4.10 B left, thick top trace). Briefly after (bottom trace), inhibition starts to spread in the center together with PF excitation that starts to spread outside and within the patch. This tips the balance of FFI and ascending segment excitation in the center of the patch towards excitation. The time (t) after which all PFs reached the center is given by

$$t = \frac{L}{2\, v_{PF}} \qquad \text{Equation 4.8}$$

After this time (0.4 ms or 1.2 ms for the 0.2 mm or 0.6 mm patch, respectively) the central region reached its peak. The inhibition by then reached the borders of the patch. FFI at the borders is only fully compensated after twice that time after the arrival of PFs from the far end of the patch. Because the PFs in the entire patch start at the same time as the FFI starts in the center, half of the excitation escapes to both sides (middle to upper traces). The escaping excitation has half-maximal amplitude and lasts for the time given in equation 4.8. It is followed by inhibition resembling the half-Gaussian of the excitation only point mirrored at the intersection with zero (fig 4.10 B upper traces).

Another case is considered where early spikes lead by

$$\Delta t = d + \frac{L}{2\, v_{PF}} \qquad \text{Equation 4.9}$$

Inhibition already arrived in all PCs overlying the patch at the time when the excitation of the ascending segment arrives (fig 4.10 C bottom trace). In this scenario the PC receptive field overlying active GC layer is initially inhibited for times given in equation 4.8 in the center to twice that at the margins of the patch. The ascending segment excitation compensates the inhibition in the center and PF excitation quickly leads to maximal excitation in the center and

later of the rest of the patch, as described for smaller delays above. Because spikes in PFs started leaving the patch with or after inhibition, inhibition is transmitted ahead of excitation with maximal amplitude. This results in PC inhibition outside the GC patch for twice the time given in equation 4.8 because inhibition is only fully compensated after the arrival of the PFs from the far end of the patch. From the excited PC patch a stretch of inhibited PCs equal in size to the patch will travel down the PFs.

If the early spikes are ahead by even longer times, the scenario inside the patch will be identical after arrival of the ascending segment excitation (fig 4.10 D). But the time PCs inside or outside the patch stay inhibited before excitation cancels inhibition will increase.

As mentioned above, early spikes were assumed to occur at the places of the highest GC spike probabilities (usually the center), resting on the assumption that no special mechanism for early spikes exists. However, because I assumed that very few active GCs are capable of triggering inhibition sufficient to cancel PF excitation, it becomes unlikely that early spikes will be confined to the center during strong activity in the GC layer. For increasingly high GC spike probabilities outside the center in the tails of the Gaussian, early GC spikes there become increasingly likely. For the extreme case where all GCs within the patch will fire, early spikes will happen throughout. Therefore inhibition, instead of spreading from the center will be present throughout the patch. For a lead of early GC spikes equal to the delay of FFI pictured in figure 4.10 B, inhibition will have spread further like in figure 4.10 C. Generally, a situation where early spikes are distributed over the entire patch can be treated identically to the situation with early spikes in the center if travel time of PFs through the patch is added:

$$\Delta t_{distr.} = \Delta t_{center.} + \frac{L}{2\, v_{PF}} \qquad \text{Equation 4.9}$$

Early activity confined to the center or distributed over the entire patch are two extremes of a range and the location depends on the abundance of activated cells and on the GC spike probability distribution.

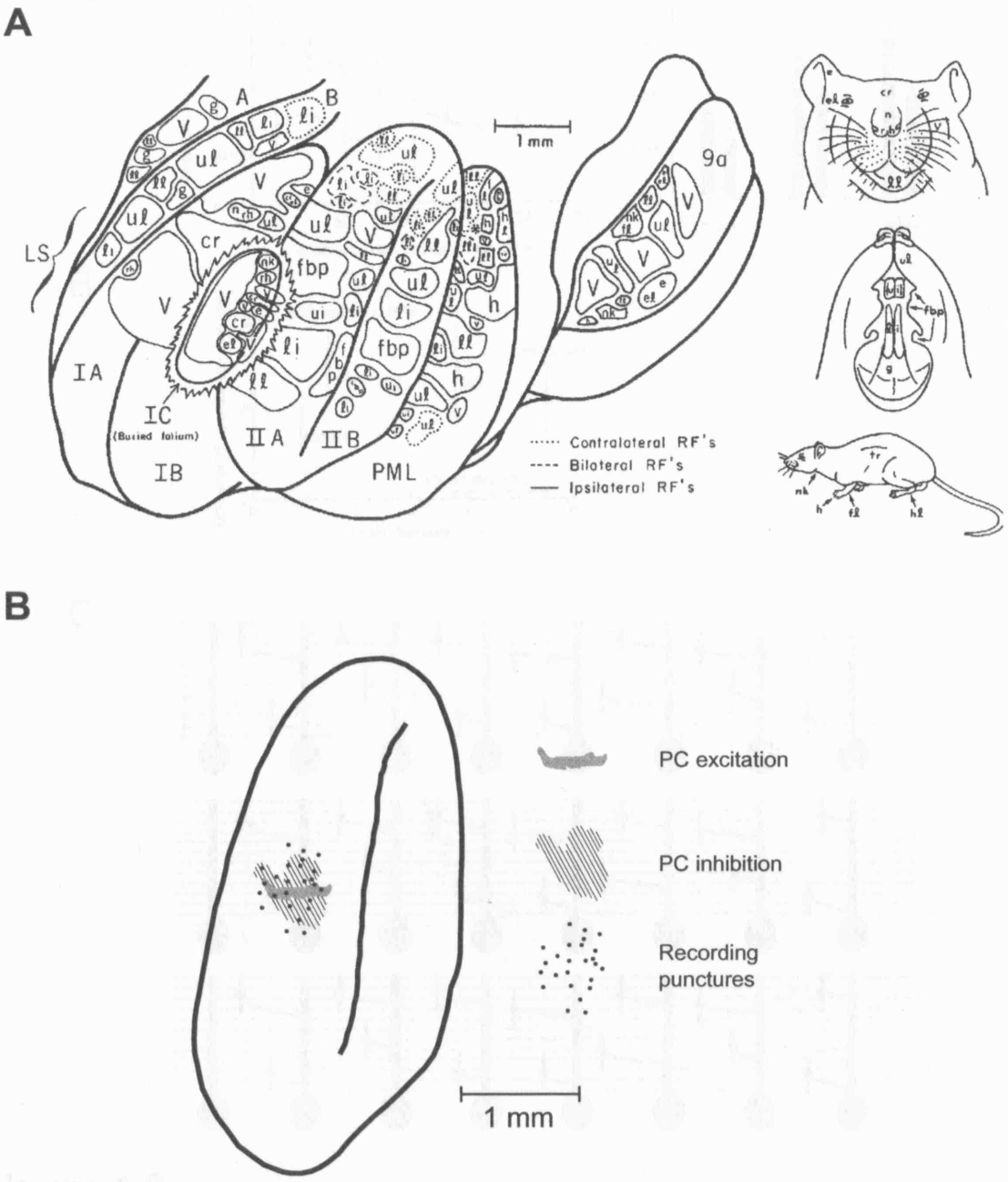

Figure 4.1

Fractured somatotopy and PC patches
A The GC layer somatotopic map of Crus I and II and neighbouring folia. Parts of the body are represented in several folia. Many areas are represented more than once within the same folium in disjoined patches. Relevant legend: h : hand, li : lower incisor, ul : upper lip, v : vibrissae. Taken from (Bower, 2002).
B An example of a small PC receptive field or "patch". PCs in the grey area show excitatory, in the hatched area inhibitory spike responses to mechanical sensory stimulation of the upper lip. Dots represent the recording locations. The density of recordings limits the spatial resolution. The length of the excitatory patch in PF direction varies between 0.1 and 0.2 mm. Taken from Bower & Woolston (1983).

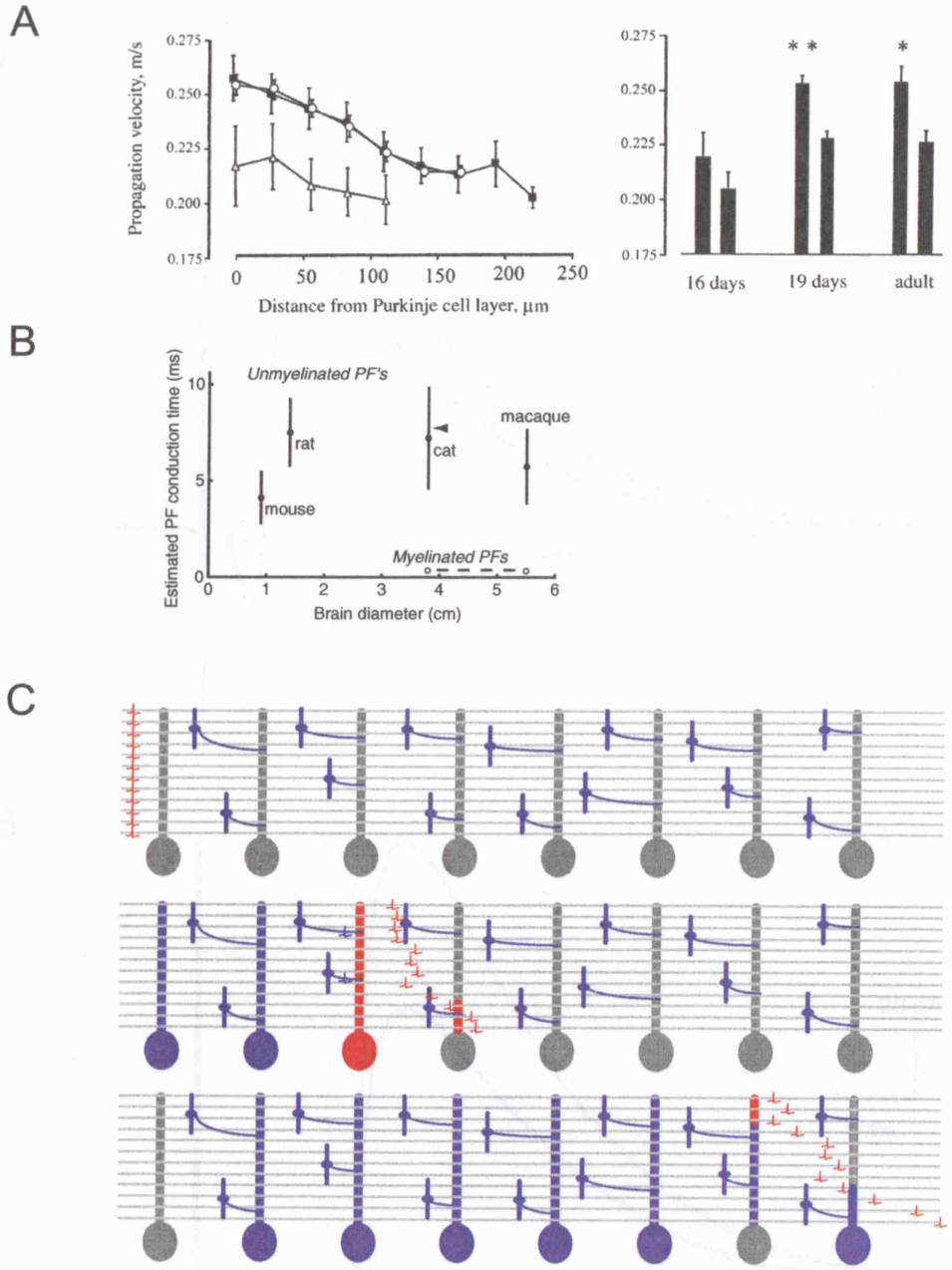

Figure 4.2

Bower's theory and spread of PF conduction velocities
A Voltage imaging in rat cerebellar slices reveals a linear gradient of PF conduction velocities depending on the position in the molecular layer. The fastest PFs are located close to the PC layer, the slowest close to the pia mater. This effect is age dependent. Open triangles : P16, open circles : P19, solid squares : adult. Taken from Vranesic *et al.* (1994). **B** Estimated conduction time for the entire length of the PF based on electron microscopic measurements of PF diameter. No myelination was found in mouse or rat. From Wyatt *et al.* (2005). **C** Coincident activity of PFs (upper panel) excites PCs (red) followed by inhibition from interneurons (blue). Because PFs close to the PC layer conduct faster they gradually gain a lead (middle and bottom). Eventually the lead of the fast fibers is greater than the synaptic delay and by the time most of the PF excite the PC FFI is already present (bottom).

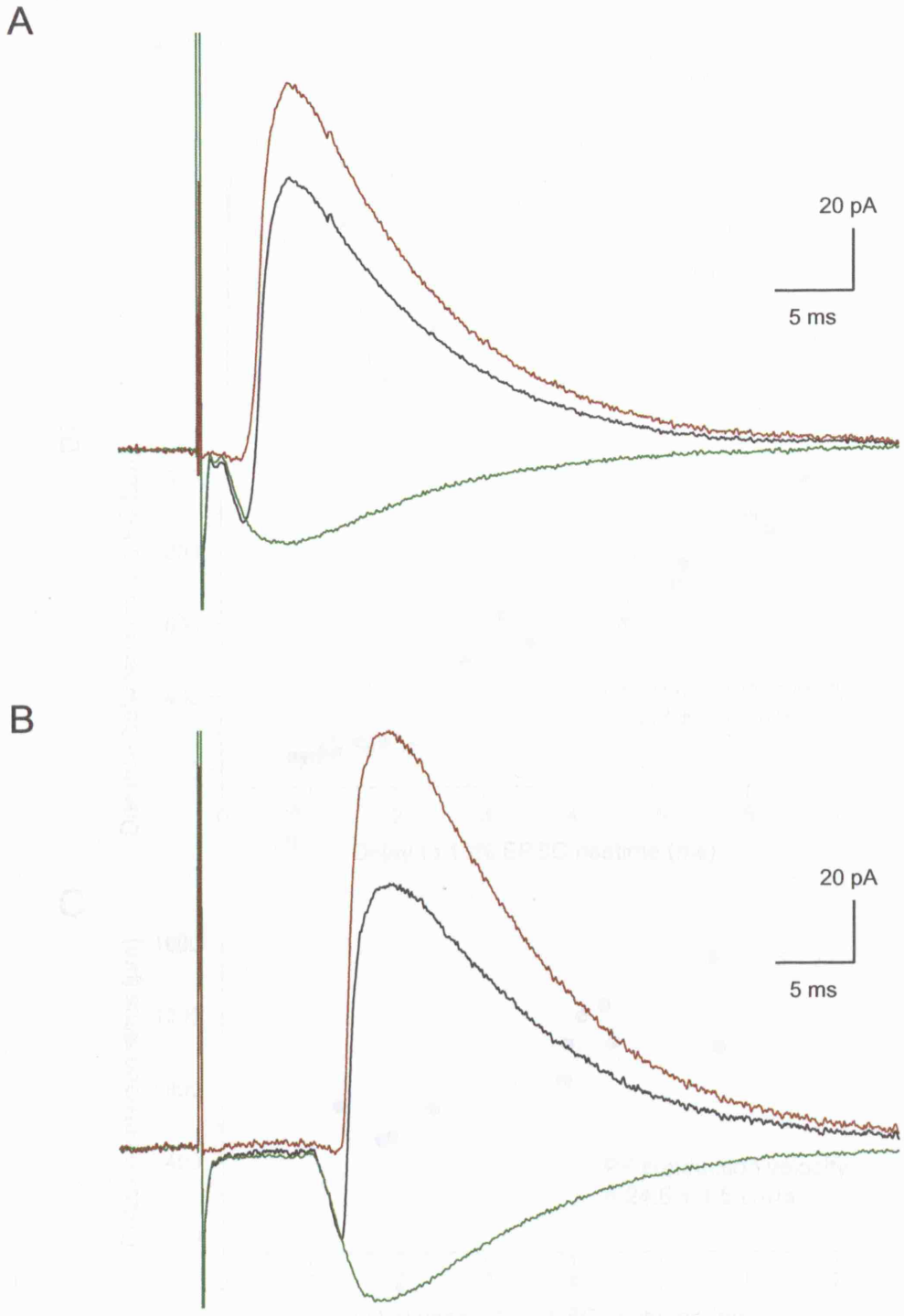

Figure 4.3

FFI at **different distances**
Typical experiment showing biphasic currents in control condition (black), EPSCs after blocking bath application of SR (green) and IPSCs calculated by subtraction of responses in SR from control (brown). Stimulation was alternated between the site close (**A**) and far (**B**) from the recorded PC. The cell was voltage clamped to -45 mV.

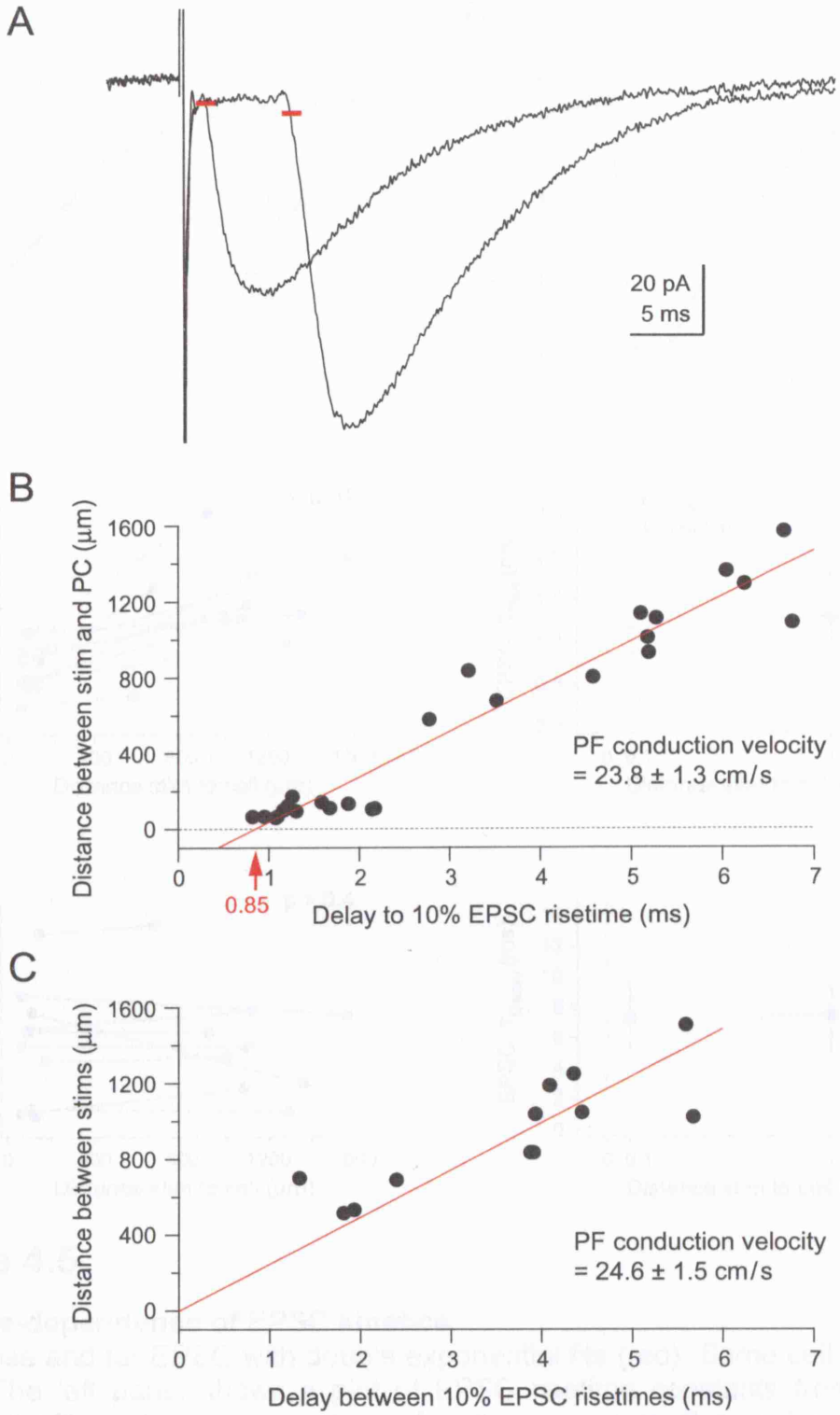

Figure 4.4

PF conduction velocity

A EPSCs from both stimulus locations. Note the increased latency of the EPSC from the far stimulus location reflecting the conduction time. Latency was measured between stimulus onset and 10% rise of the current. Same cell as in figure 4.3. **B** Calculation of PF conduction velocity using the PC – stimulation electrode distance and the delay of the onsets of EPSCs. This gave a synaptic delay of 0.85 ms. **C** PF conduction velocity calculated by using the distance between stimulation electrodes and differences between EPSC latencies.

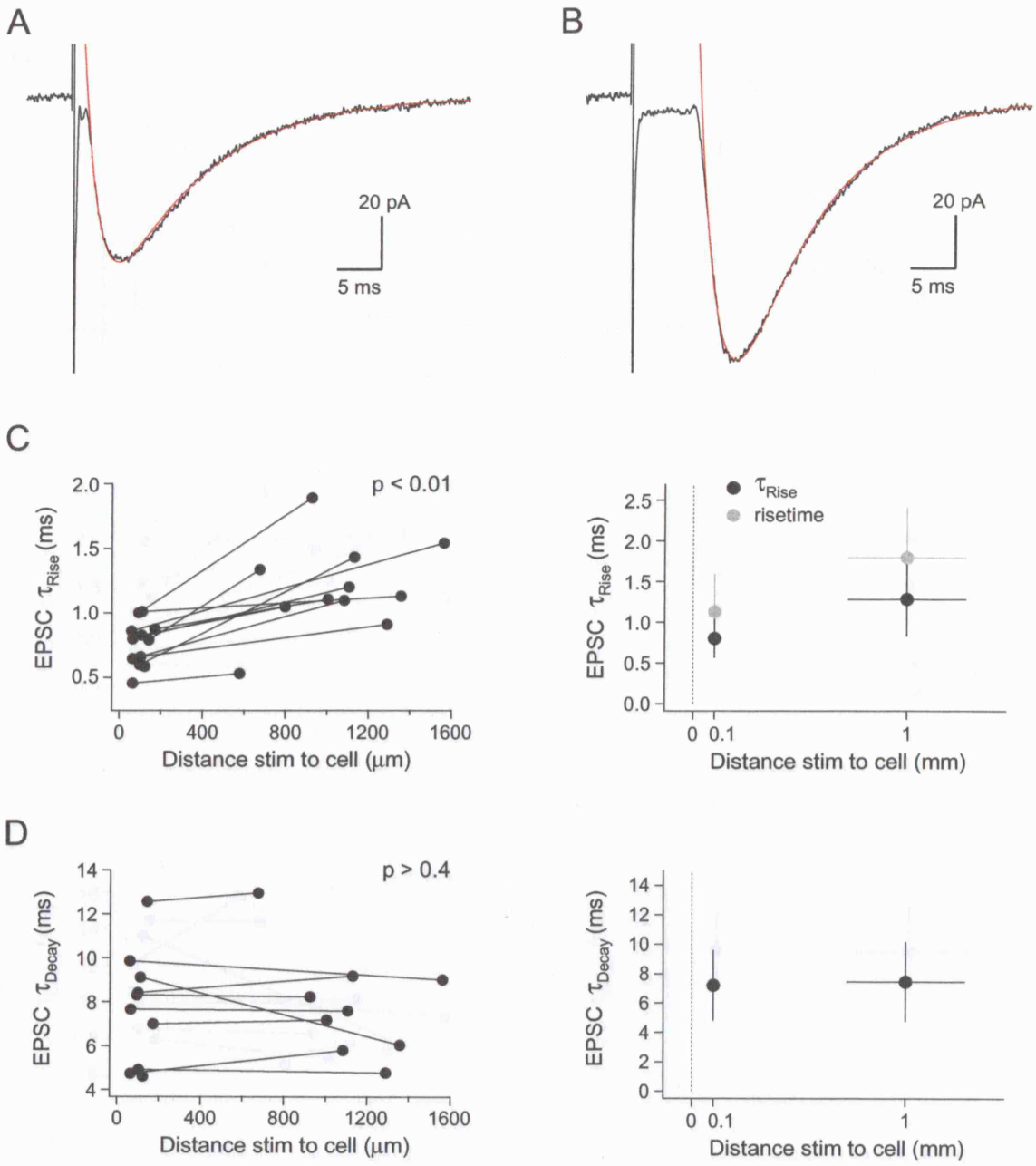

Figure 4.5

Distance-dependence of EPSC kinetics

A, B Close and far EPSC with double exponential fits (red). Same cell as figure 4.3. **C** The left panel shows a plot of EPSC risetime constants from double exponential fits as function of distance for all experiments. Data points from two different stimulus locations recorded in a single PC are connected and were used for statistical tests (p-values are indicated). Single unconnected points are from experiments with only a single successful stimulation. Unpaired Student's *t*-tests including these points did not change the significance levels (not shown). The rise of EPSCs from far stimulations was always slower than for close stimulations. The right panel shows the average risetime constants from double exponential fits as well as the 10 - 90% risetimes over the average distance of stimulation. **D** Same as C for decay time constants. The EPSC decay was independent of stimulation distance.

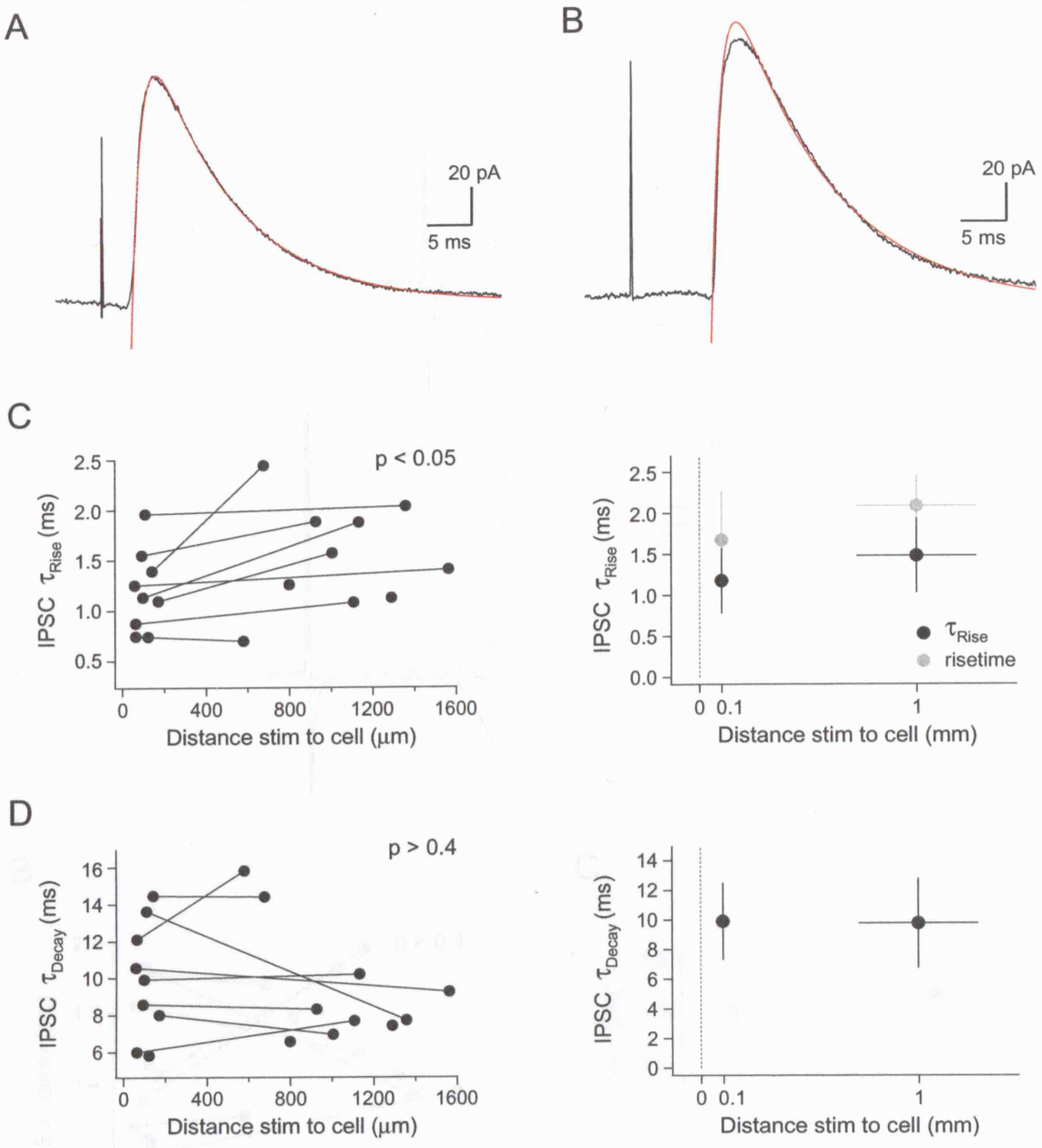

Figure 4.6

Distance dependence of IPSC kinetics
Same as figure 4.5 but for feed-forward IPSCs. **A,B** IPSCs from close and far stimulations with double exponential fits, same cell as figure 4.3. **C** IPSC risetime constants from double exponential fits as function of distance for all experiments. Data points from two different stimulus locations recorded in a single PC are connected and were used for statistical tests (p-values are indicated). Single unconnected points are from experiments with only a single successful stimulation. Unpaired Student's *t*-tests including these points did not change the significance levels (not shown). The rise of IPSCs from far stimulations was slower than for close stimulations, similar to the situation for EPSCs. The right panel shows average risetime constants and the 10 – 90% risetimes. **D** Distance had no effect on the decay of IPSCs.

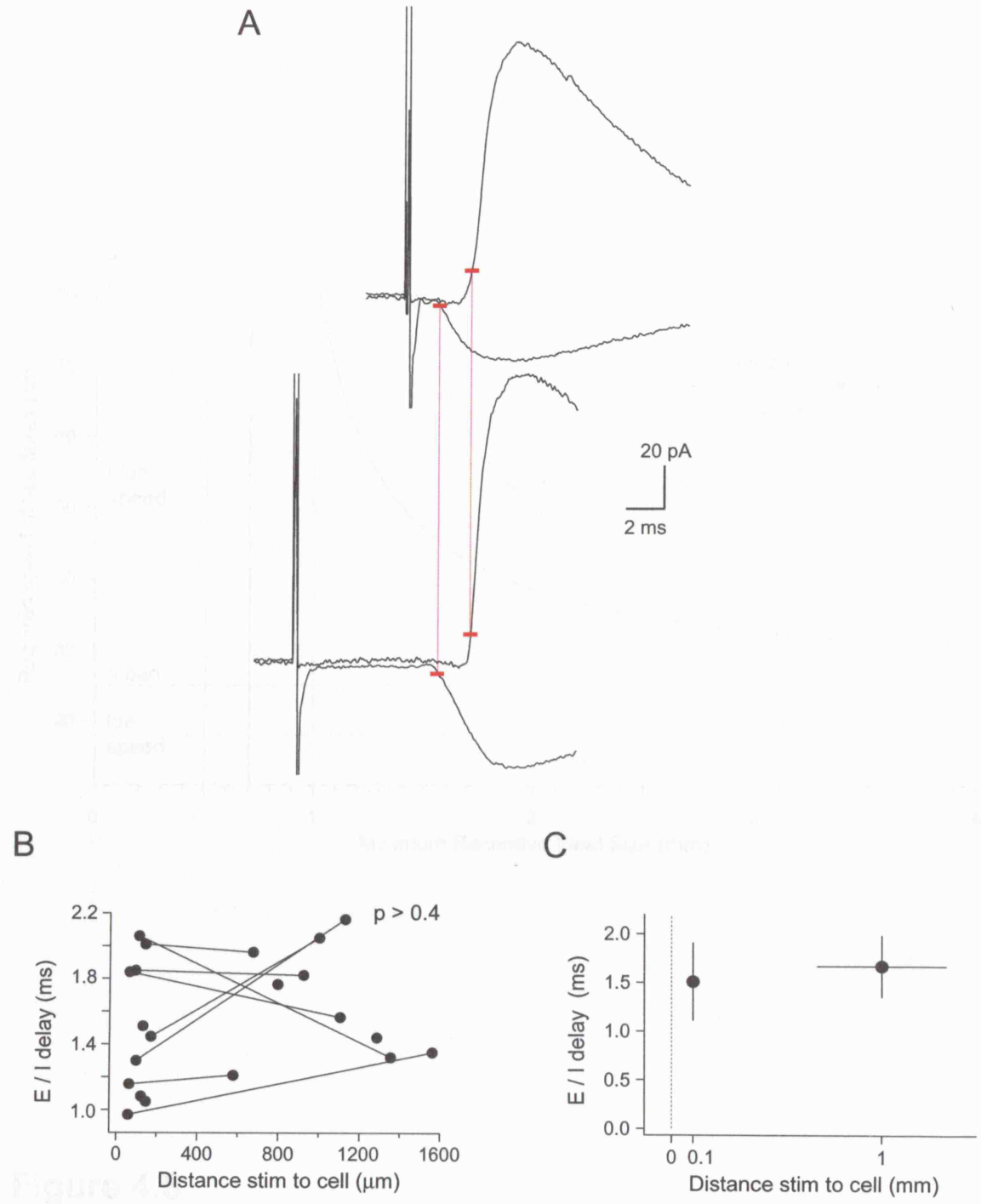

Figure 4.7

Distance dependence on the delay of FFI

A EPSC and IPSC from close and far stimulations are shown, aligned to the 10% rise of the EPSC. The delay between EPSC and IPSC of close and far stimulation is similar. Same cell as figure 4.3. **B** Plot of the delay as function of distance for all experiments. Data points from two different stimulus locations recorded in a single PC are connected and were used for statistical tests (p-values are indicated). Including single unconnected data points from experiments with only a single successful stimulation did not change the significance level (unpaired Student's *t*-test; not shown). **C** Average delay for close and far stimulation. The delay is independent of stimulation distance.

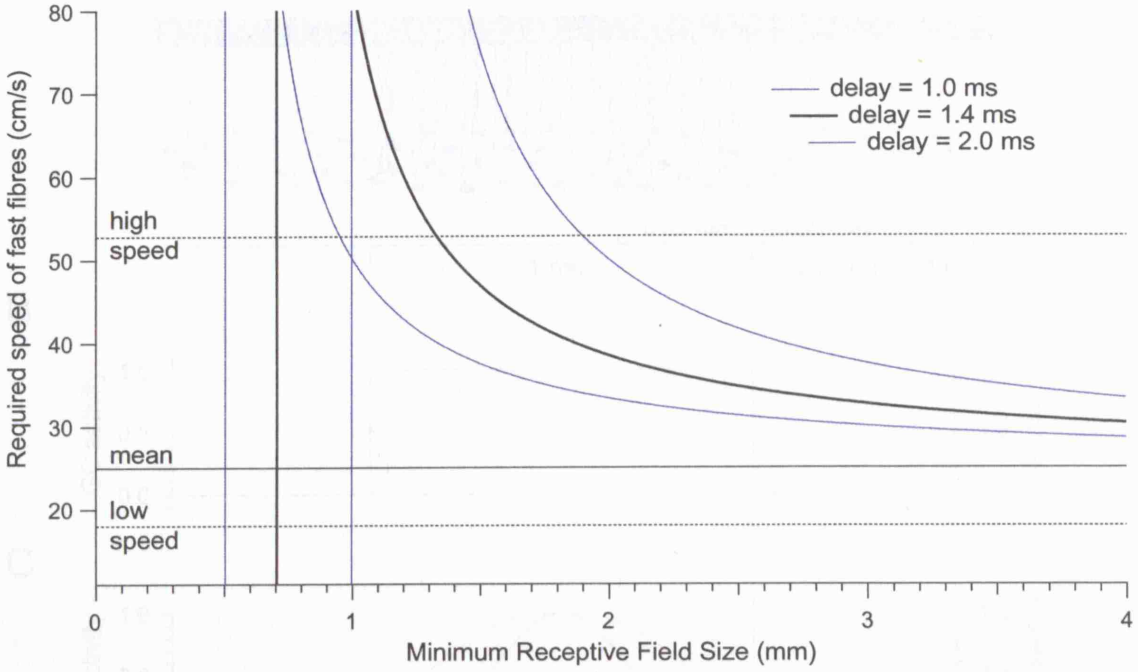

Figure 4.8

Speed of fast PFs required for **Bower's theory**
In order to achieve a PC patch limited to the length given on the abscissa, the fast fibers have to gain a lead equal to the delay of FFI in that length. This means, the smaller the field the faster the fastest fibers have to be. The formula for the function is given in the text and is plotted for the average delay measured in chapter 4 (black) as well as for the maximum and minimum (blue). Note the singularities in the functions. If a PC patch reaches a length for which the average PFs need a travelling time equal to the delay of FFI, then the fast PFs have to cross this length in infinitely short time requiring infinite speed. If the length of the field is crossed faster than the FFI delay by the average PFs, fast PFs have to cross the field in negative times, which is obviously impossible.

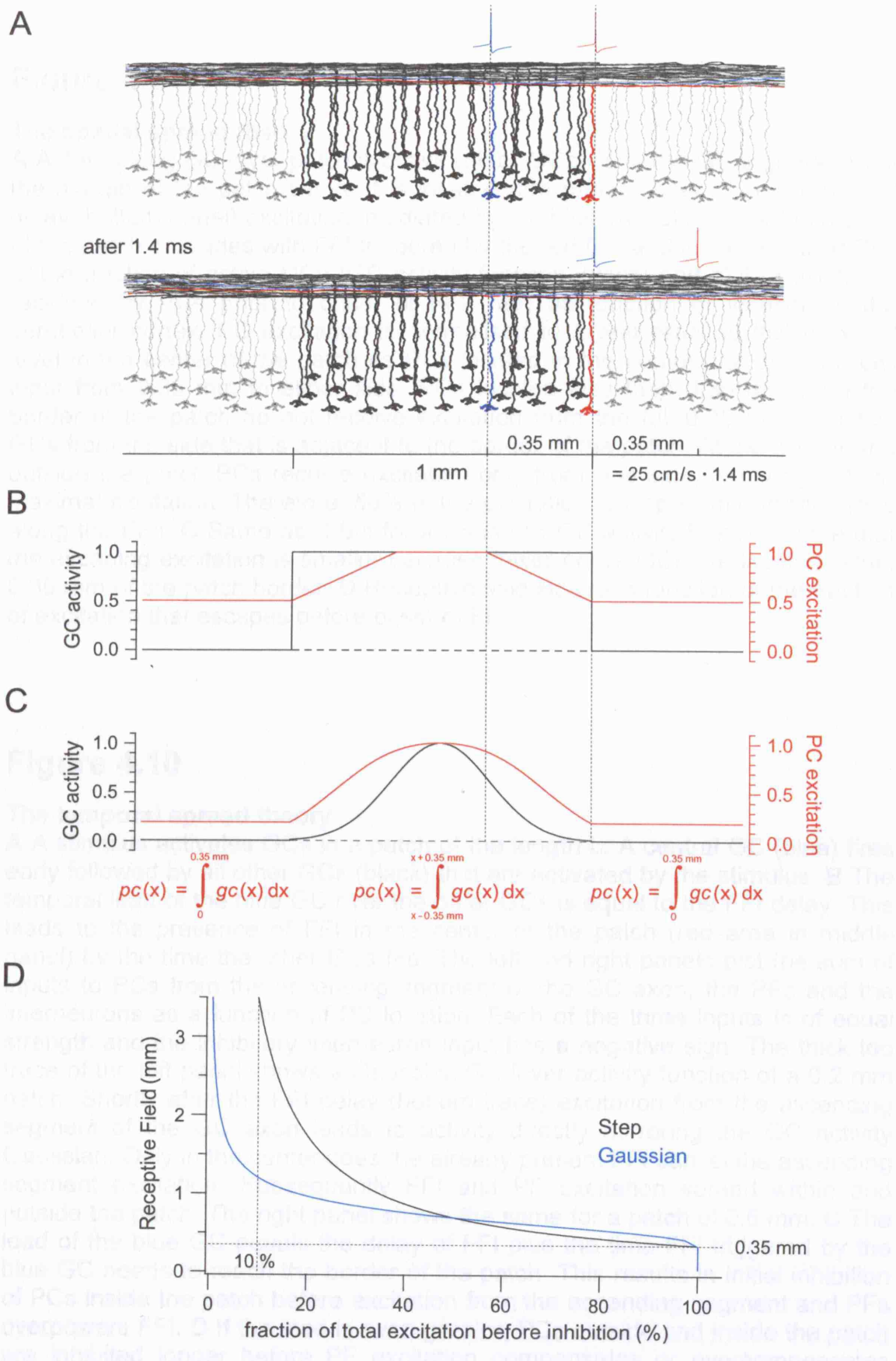

Figure 4.9

Legend overleaf.

Figure 4.9

The **spatial spread theory**
A A 1 mm long GC layer patch is active (black GCs). The red GC triggers FFI at the margin of the patch where it is located (top panel). After 1.4 ms (one FFI delay, bottom panel) excitation, mediated by the blue GC, of a PC at the margin of the patch coincides with FFI triggered by the red GC and is cancelled. **B** Plot of the fraction of active GCs (GC activity function, black) and plot of excitation received by PCs prior to onset of FFI (red) as function of location in the cerebellar cortex. PC excitation is normalised to 1 and reaches this maximal level in the center of the patch as PCs located in the center can draw on GC input from 0.35 mm to either side. PCs located less than 0.35 mm from the border of the patch do not receive excitation from the full 0.35 mm of active GCs from the side that is adjacent to the border of the patch. At the border and outside the patch PCs receive excitation only from one side, resulting in half-maximal excitation. Therefore, 50% of the excitation 'escapes' and excites PCs along the PFs. **C** Same as B but for a Gaussian GC activity function. Note that the escaping excitation is smaller because fewer active GCs are located within 0.35 mm of the patch border. **D** Receptive field size as a function of the fraction of excitation that escapes before onset of FFI.

Figure 4.10

The **temporal spread theory**
A A stimulus activates GCs in a patch of the length L. A central GC (blue) fires early followed by all other GCs (black) that are activated by the stimulus. **B** The temporal lead of the blue GC over the other GCs is equal to the FFI delay. This leads to the presence of FFI in the center of the patch (red area in middle panel) by the time the other GCs fire. The left and right panels plot the sum of inputs to PCs from the ascending segment of the GC axon, the PFs and the interneurons as a function of PC location. Each of the three inputs is of equal strength and the inhibitory interneuron input has a negative sign. The thick top trace of the left panel shows a Gaussian GC layer activity function of a 0.2 mm patch. Shortly after the FFI delay (bottom trace) excitation from the ascending segment of the GC axon leads to activity directly mirroring the GC activity Gaussian. Only in the center does the already present FFI cancel the ascending segment excitation. Subsequently FFI and PF excitation spread within and outside the patch. The right panel shows the same for a patch of 0.6 mm. **C** The lead of the blue GC equals the delay of FFI plus the time FFI triggered by the blue GC needs to reach the border of the patch. This results in initial inhibition of PCs inside the patch before excitation from the ascending segment and PFs overpowers FFI. **D** If the lead is even greater, PCs outside and inside the patch are inhibited longer before PF excitation compensates or overcompensates inhibition, respectively.

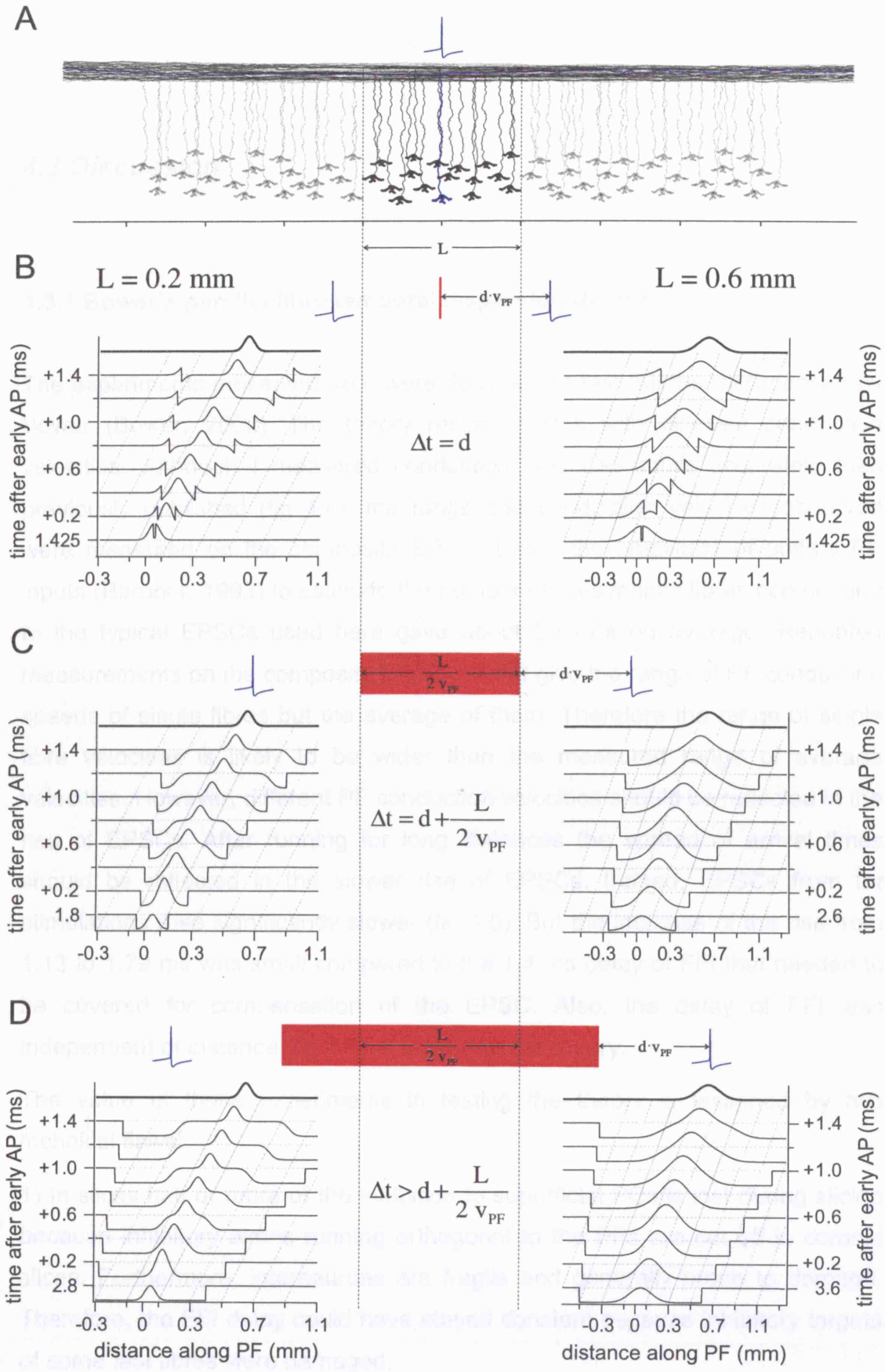

Figure 4.10

Legend on previous page.

4.3 Discussion

4.3.1 Bower's parallel fibre temporal dispersion theory

The experiments presented here were designed to test the theory proposed by Bower (Bower, 2002). The theory relies on PFs with different conduction velocities. Although I measured conduction velocities more accurately than previously published (fig 4.4), the range and conduction velocities observed were measured on the composite EPSC. Using the amplitude of unitary PF inputs (Barbour, 1993) to estimate the number of presynaptic fibres contributing to the typical EPSCs used here gave about 20 PFs on average. Repeated measurements on the composite EPSC will not give the range of PF conduction speeds of single fibres but the average of them. Therefore the range of single fibre velocities is likely to be wider than the measured range of average velocities. However, different PF conduction velocities should be reflected in the rise of EPSCs. After running for long distances the spread of arrival times should be reflected in the slower rise of EPSCs. Indeed, EPSCs from far stimulations rose significantly slower (fig 4.5). But the increase of the rise from 1.13 to 1.79 ms was small compared to the 1.4 ms delay of FFI that needed to be covered for compensation of the EPSC. Also, the delay of FFI was independent of distance (fig 4.7) at odds with the theory.

The value of these experiments in testing the theory is lessened by two technical flaws:

1) In slices half or more of the inhibition to superficial PCs is lost during slicing because inhibitory axons running orthogonal to the PFs are cut off in coronal slices. Furthermore, interneurons are fragile and generally prone to damage. Therefore, the FFI delay could have stayed constant because inhibitory targets of some fast fibres were damaged.

2) Although stimulating electrodes with large tip sizes were used, stimulation was confined to a particular depth of the molecular layer. If there is a systematic trend towards faster conduction velocities close to the PC layer (Palay & Chan-Palay, 1974; Vranesic *et al.*, 1994; Wyatt *et al.*, 2005) these experiments could have activated a population of PFs with a narrower range of conduction velocities than present in the molecular layer.

Because of these concerns, the presented experiments could have provided substantial support if consistent with Bower's theory but are not entirely sufficient for a falsification.

However, theoretical considerations presented in chapter 4.2.3 show that with Bower's theory PC fields would be much bigger than previously observed. Even if myelination would provide for some very fast fibres (Kandel, 2000) contrary to the lack of myelination observed in rats (Wyatt *et al.*, 2005), PC receptive fields would still be too large, because the function plotted in figure 4.8 has a singularity at 0.7 mm. Spikes travelling with the average PF conduction velocity need a travelling time equal to the delay of FFI to cross 0.7 mm. That means that in order to be faster by the delay, PFs have to be indefinitely fast and therefore, even with myelination, PFs receptive fields cannot be smaller than this limit. The size of the underlying GC layer patch has to be added to the limit. Aside from minimum PC receptive field sizes bigger than previously measured, PCs would show activity outside the borders of the active GC patch inconsistent with the data (Bower & Woolston, 1983). I conclude the mechanism of preventing PC beams by temporal dispersion in PFs, as suggested by Bower, does not hold.

4.3.2 The spatial spread theory

The main advantage of the spatial spread model over the Bower model is that PC receptive fields only overly patches of active GC layer like Bower himself established (Bower & Woolston, 1983).

As mentioned in chapter 4.2.3, with GC patches of 0.7 mm the fraction of "escaping" excitation over total excitation will be 50% for symmetrical GC activity functions. This limit of 0.7 mm is only dependent on FFI delay and conduction velocity, which dictate that 0.35 mm on the border of the patch will escape before FFI kicks in. Therefore 0.35 mm of sparse GC activity is required to both sides of the center. At first look this is difficult to reconcile with measurements of GC receptive fields already mentioned (fig 4.1). However, it is important to keep in mind that these fields are measured with extra-cellular electrodes that pick up field potentials. GC patches could be much larger than measured because sparse GC activity will not be picked up by the recording. If fields are in reality much larger than measured because of low probability margins these fields would lead to little escaping excitation. In the extreme case, a 0.1 mm wide, highly active GC patch, flanked on each side by a single active GC at 0.35 mm distance would count as 0.8 mm wide field in the theory but would only be found to be 0.1 mm wide experimentally. The bigger GC fields predicted by the spatial spread theory can therefore be consistent with previous measurements.

The theory that spatial spread of GC activity triggers FFI that cancels PF excitation outside the PC receptive field relies on functions of GC activity that show long, low probability tails and narrow, high-probability centers. On what basis can sensory evoked GC activity distributions be assumed? That GC field potentials show smaller peak amplitudes, less modulation and smaller integrals of the (rectified) field potentials (Shambes *et al.*, 1978b; Bower & Woolston, 1983) towards the margins of the patch was already mentioned. However, it is difficult to extract quantitative information from these recordings as they only indirectly reflect GC spiking activity.

The distribution of mossy fibre terminals as basis for assuming GC spike probability functions comes with similar problems. On top of a complex morphology, anatomical data only indirectly relates to spiking activity. It is clear, that mossy fibres converge to specific areas of the GC layer (Bower *et al.*, 1981), which is necessary for the patch-like activity in that layer. Furthermore, double retrograde labelling of mossy fibres of small separate areas of cerebellar cortex show only single labelled spatially segregated populations of pontine

cells (Odeh *et al.*, 2005). This indicates that mossy fibre projections are confined to small patches of cerebellar GC layer thereby generating the fractured somatotopic map. This is difficult to reconcile with the distribution of single mossy fibre terminals from the lateral reticular nucleus which spread up to 1 mm within a folium and to most folia in the vermis (Wu *et al.*, 1999). A quantitative description of the location of terminals activated by sensory stimulation is missing and it is going to be difficult to derive GC activity functions from the qualitative data available. However, mossy fibre terminals are distributed and cover much larger areas than the measured GC layer patches and thus meet the required assumptions of the model.

As mentioned earlier (chapter 4.2.4), any synchronous activation of GCs will lead to a minimum PC receptive field of 0.7 mm because FFI kicks in only after spikes in PFs already travelled 0.35 mm in both directions. This limitation only depends on delay of FFI and PF conduction velocity. Still, the spatial spread theory is able to produce PC receptive field down to that limit with reasonable assumptions and PC activity is confined to the area of the active GC patch consistent with the data.

4.3.3 The temporal spread theory

Instead of synchronous spatially spread GC activity a few GCs could fire earlier than others leading to hardly noticeable excitation in PCs and FFI that is present when the majority of the GCs are active. As already mentioned, in this model excitation has to overpower inhibition, which requires the ascending segment. Apart from higher metabolic costs, this model would sacrifice the effects of FFI. In the spatial spread model, PCs overlying the active GC layer patch received excitation with normal FFI. Outside the patch weak excitation is followed by stronger inhibition, which is cancelled by subsequent excitation. In the temporal spread model a few GCs firing ahead of the majority of GCs activated by a stimulus can cause inhibition throughout the patch. This happens if their lead is longer than the delay of FFI plus the time the PFs of the early GCs need to reach the borders of the patch (fig 4.10 C, D). Therefore PCs will

first be inhibited followed by a rapid compensation through the ascending segment by the time the majority of GCs fires. Afterwards PFs will lead to a net excitation. The EPSP caused by the PFs will be slow rising because the PFs will arrive within the time given in equation 4.8 for PCs located in the center and up to twice that time for PCs located in the margins. The EPSP will last a long time because it is not shortened by FFI and the PC membrane time constant is slow. Therefore, the timing of spikes in PCs within the active patch is not going to be precise.

If the early GCs would be ahead by the delay of FFI or less (fig 4.10 B), an early, very brief excitation from the ascending segment would be compensated by inhibition followed by the slow rising PF EPSP. This would be an interesting scenario, as the first excitation might allow very precise spiking, followed by a phase of increased firing rate.

Excitation provided by the PFs will be faster in the center than in the margins. This might lead to a sharpening of the PC receptive field because neurons in the center will fire earlier and with higher temporal precision.

In the temporal spread model, either some excitation or some inhibition escapes and runs along the beam. Depending on the exact timing of early GC activity, excitation with sufficient amplitude will lead to activation of PCs along their course. For the example shown in figure 4.10 A the escaping excitation has a half-maximal amplitude but only lasts for 0.4 ms for the 0.2 mm field, making it questionable whether this time is sufficient for PCs to trigger spikes. For the larger GC patch this time increases to 1.2 ms which is within the range of measured FFI delays and long enough for efficient spike triggering (chapter 3.2.4). Escaping inhibition of similar amplitude and time before cancellation by PF excitation will be less consequential, as it can only delay a spike by that time but not generate one. For a cell that spiking at 40 Hz, escaping inhibition could only change spike timing by delaying of a spike by 0.4 or 1.2 ms for a 0.2 or 0.6 mm field, respectively. Excitation could change spike timing by up to 25 ms if a spike is triggered, although realistically this value is closer to 20 ms due to refractoriness and a pronounced after-hyperpolarisation (Llinas & Sugimori, 1980 ; chapter 5). However, for

increasingly early triggered inhibition, inhibitory beams would spread through the cerebellum, which has not yet been observed, but would be more difficult to detect than excitatory beams.

What temporal spread of GC firing is realistic? Recently, whole-cell patch clamp recordings have been made from GCs during sensory stimulation (Chadderton *et al.*, 2004) and EPSCs as well as spikes fall into relatively narrow time windows. The standard deviation of first spike and first EPSC latencies can be as low as 2.2 ms. Some cells show much larger standard deviations (65 ms and 35 ms for first spike and first EPSP latencies, respectively ; Chadderton, P. personal communication). The variation of the first spike latency is measured in different trials within the same cell. One has to be careful with the commonly made assumption that a temporal average is equal to a spatial average. In other words, presenting the same stimulus to a GC a hundred times does not mean that during a single trial hundred GCs give the same responses as the single GC. If the source of variability lies at an upstream processing stage common to the different GCs, the spatial variability in the GC population during a single trial will be much lower than the temporal variability across multiple trials in a single cell. If variability is introduced at a processing stage not shared by the individual GCs the spatial average in the GC population will be similar to the temporal average of multiple trials within a single cell.

The function of the temporal spread of GC firing was collapsed into a single parameter (Δt) for simplicity. If a continuous function with low probabilities towards early times is used instead, GC activity of most cells will be shifted with respect to inhibition. Specifically, those GCs firing after the earliest GCs and before the average GC spike time are likely to escape inhibition. I decided not to use a continuous function for the temporal spread 1) because this function is unknown and 2) because in the model all inhibition is triggered by the first firing GCs. This is most certainly incorrect (discussed in chapter 4.3.4). However, the use of a continuous function for the temporal spread would be pointless as it would require a more complex representation of the triggering of inhibition (see below).

4.3.4 Role of parallel fibres and balance of excitation and inhibition

For all three models where the lack of beam like PC excitation is explained by temporal dispersion of spike conduction, spatial spread of GC activity and temporal spread of GC activity FFI is assumed to be triggered in an all-or-none fashion by one or very few active GCs. This assumption is of course unrealistic, as the first, or first few, GCs would have to make synaptic contacts to all interneurons. Even the space filling geometry of the PC dendrite samples only about 50% of the PFs (Harvey & Napper, 1991) whereas this value must be far lower for the much less dense and more spread out geometry of interneuron dendrites (Palay & Chan-Palay, 1974). Also, the results of Carter & Regehr (2002) that a unitary PF input can trigger a spike in an interneuron relies on their measurements of -127 pA average peak amplitude for minis and injection of -150 pA with dynamic clamp for triggering spikes. These values are high compared to other studies (Liu & Cull-Candy, 2002) and two or three PF inputs for generation of a spike is a safer assumption, although the spike triggering efficacy depends on where in the phase of spontaneous spiking of the interneuron the input occurs (see chapter 5). Furthermore, activity in the GC layer is treated like a single action potential and bursting activity of GCs during sensory stimulation (Chadderton *et al.*, 2004) is ignored.

All these complications are difficult to understand analytically. Therefore, either a network model or experiments are needed to test the theories. However, experimental proof for these theories is going to be difficult to obtain:

1) Measurements of temporal and spatial activity in the GC layer would require simultaneous single unit recordings. With electrophysiological methods this is going to be difficult because GC single unit activity can only be measured with patch clamp recordings (Chadderton *et al.*, 2004) and double *in vivo* patch clamp recordings have not yet been reported. Two photon calcium imaging of GC somata might be more promising but the small size of the soma and the limited depth penetration make this technically challenging (Helmchen & Waters, 2002).

2) *In vivo* PC voltage clamp recordings of synaptic currents should be able to resolve the timing of inhibitory and excitatory currents when separated by their reversal potential. At least subthreshold potentials measured in current clamp could give estimates of synaptic input. However, PCs are difficult to voltage clamp due to their electrical structure (Roth & Häusser, 2001). Current clamp recordings so far did not resolve clear sub-threshold potentials (Loewenstein *et al.*, 2005) ; Mahon, S. personal communication) and are complicated by bistability. To test the presented theories, PC recordings would have to be put into perspective with the receptive field of the GC and/or PC layer, or, ideally, allow a comparison between a PC inside and outside the receptive field.

3) The most promising experimental design to test the theories could be gained from *in vivo* recordings from interneurons, where synaptic currents can be easily resolved (chapter 3). These recordings can establish whether early GCs activate interneurons ahead of the bulk of the excitation if located outside the PC receptive field.

As these experiments are technically challenging and (apart from the first) are unable to distinguish between spatial or temporal spread as basis for the lack of beam-like excitation, a network model could be used to test the feasibility of the suggested theories. A relatively simple model could ignore an individual representation of GCs and only use spatio-temporal distributions of GC spike times as input to PCs and interneurons. Cells would have to be distributed with realistic densities to represent a stretch of cerebellar cortex extending a few millimetres in the direction of the PFs. Interneurons could be modelled as integrate-and-fire. Many parameters for such a model are already known or can easily be measured. Probabilities of PF → PC, PF → interneuron and interneuron → interneuron connections are available (Palay & Chan-Palay, 1974) and data for the conversion of inputs to spikes in interneurons are published (Carter & Regehr, 2002). Synaptic dynamics are necessary for this model and data on the short-term plasticity of the involved synapses have been published (Atluri & Regehr, 1996; Pouzat & Hestrin, 1997; Rancillac & Barbara, 2005). A computationally costly and for this purpose over-complicated representation of PCs (De Schutter & Bower, 1994a, b) could be avoided in

favour of a passive single compartment model with realistic synaptic dynamics (Atluri & Regehr, 1996; Pouzat & Hestrin, 1997) which could provide PC synaptic currents as output. With this approach it should be possible to 1) test whether different spatio-temporal patterns result in realistic PC receptive fields, 2) show how burst-firing of GCs changes the ratio of excitation over inhibition and 3) whether inhibition saturates at high levels of GC activity. The last point is especially important since it addresses the question what function PFs serve, as so far I only tried to compensate their action in the theories presented in this chapter. From the distribution pattern of GC receptive fields (Shambes *et al.*, 1978a; Shambes *et al.*, 1978b), the spread of single mossy fibre terminals (Wu *et al.*, 1999) and other compartmentalization of the cerebellum (Chen *et al.*, 1996; Odeh *et al.*, 2005; Pijpers *et al.*, 2005) I want to speculate that combinations of sensory stimuli will result in PF activity overcoming inhibition outside the respective fields of the single sensory stimuli and thus form the basis for PCs tuned to the detection of patterns of sensory stimulation.

5 Synaptic plasticity in the feed-forward circuit

5.1 Introduction

5.1.1 Motor learning in the cerebellum

Early theoretical work and most subsequent theories interpreted the single powerful CF input to PCs as a 'teaching signal' for the tens of thousands of modifiable PF inputs (Marr, 1969; Albus, 1971), whose synaptic strengths were seen as the correlate for motor memory. A decade after the formulation of this theory, it was partially confirmed when CF activation was shown to induce LTD of PF inputs (Ito *et al.*, 1982; Sakurai, 1987; Hartell, 1996b, a; Reynolds & Hartell, 2000; Ito, 2001; Karachot *et al.*, 2001; Hartell, 2002; Sims & Hartell, 2005), which today is one of the best studied forms of plasticity in the brain (chapter 1.3.1). According to the theory, CF-induced learning leads to a reduction in PC spike output, releasing the DCN from inhibition, which is necessary for the role of the cerebellum in modulating movements.

5.1.2 Classical eye blink conditioning as model for motor learning

Today, classical eye blink conditioning provides the best-studied example of cerebellar motor learning. Rabbits learn to avoid an air puff to the eye by accurately timed closure of their nictitating membrane when they hear a previously meaningless tone followed by the air puff with a fixed delay. Application of the AMPA type glutamate receptor blocker CNQX to the cerebellar cortex reversibly prevents expression of the previously learned behaviour (Attwell *et al.*, 1999; Attwell *et al.*, 2001) as well as acquisition (Attwell *et al.*, 2001). The CF seems to be necessary for acquisition (Turker &

Miles, 1986) and prevents extinction of the previously learned behaviour (Medina *et al.*, 2002b). These experiments give substantial support to the Marr-Albus-Ito model of motor learning, although a reduction of PC spike output as consequence of motor learning has never been shown directly.

5.1.3 Plasticity in the molecular layer feed-forward inhibitory circuit

In chapter 3 I characterized the feed-forward inhibitory circuit formed by PFs and inhibitory molecular layer interneurons that caused PF EPSPs in PCs to be cut short by FFI (Mittmann *et al.*, 2005). Both excitatory and inhibitory inputs from this circuit were shown to undergo plasticity triggered by the CF (Ito *et al.*, 1982; Kano *et al.*, 1992) ; chapter 1.3.5). Activation of the CF leads to LTP of spontaneous IPSCs in PCs, a form of plasticity termed 'rebound potentiation' because IPSCs usually 'run down' in the course of the recording. Co-activation of an input with the CF results in PF LTD. Both PF LTD and interneuron LTP should reduce spike output in response to an excitatory input followed by FFI, which leads to disinhibition of the DCN. Thus, although plasticity at two different synapses is involved, the result is consistent with the Marr-Albus-Ito theory, which assumed only the PFs to be plastic (Marr, 1969). The synergistic effect of both forms of plasticity might be the reason that rebound potentiation was largely ignored by cerebellar learning theories. However, the spontaneous spiking of PCs (Häusser & Clark, 1997; Raman & Bean, 1997, 1999) makes it probable that inhibitory synaptic plasticity is reflected in the spike output independent of excitatory input. Integration of synaptic inputs in the context of spontaneous spiking, as well as the expected changes to the spike output by CF induced plasticity remain unclear. What is the net effect of CF learning on the spiking behaviour of PCs?

I addressed this question by inducing plasticity separately to the excitatory and inhibitory components of feed-forward inputs. Subsequently I combined the two components with different ratios and amplitudes. Against expectation I found LTD of both components that maintained the balance of excitation and inhibition. The resulting spike output was increased for inputs dominated by FFI.

5.2 Results

5.2.1 Input – Output function of Purkinje cells

First, I looked at the excitatory and inhibitory component of typical feed-forward inputs to PCs separately to investigate how they interact with spontaneous spiking. I isolated EPSPs by blocking inhibition with SR (Hamann *et al.*, 1988). IPSPs could not be separated from PF EPSPs pharmacologically because this would have also blocked the CF response (Audinat *et al.*, 1990) necessary for physiological plasticity inducing protocols (Ito *et al.*, 1982; Hartell, 1996b; Wang *et al.*, 2000; Coesmans *et al.*, 2004). However, in parasagittal slices used here, stimulation of inhibitory fibres running across the folium outside the area of the PC dendritic tree is possible without activating PF inputs to the recorded PC. In experiments with evoked IPSPs no excitatory components were visible and blocking inhibition with SR after the experiment did not reveal any (n = 10). The latency, measured as time between the beginning of the stimulus and 10% rise of the potential, for EPSPs was 1.69 ± 0.09 ms and 2.13 ± 0.16 ms for IPSPs. Although EPSP and IPSP latencies differed significantly ($p < 0.01$, n = 40 EPSPs, 21 IPSPs, unpaired *t*-test) the difference was only 0.44 ms instead of 1.4 ms expected for disynaptic IPSPs, indicating direct activation. The difference could be due to faster EPSP rise times (EPSP: 3.54 ± 0.16 ms ; IPSP: 4.33 ± 0.31 ms) or a longer axonal delay for inhibition, which was stimulated further away than excitation (see methods).

PCs spike spontaneously *in vivo* (Granit & Phillips, 1956; Eccles *et al.*, 1967; Thach, 1968; Bell & Grimm, 1969; Armstrong & Rawson, 1979a; Nitz & Tononi, 2002) and in slice preparations (Häusser & Clark, 1997). I investigated how synaptic inputs interact with spontaneous spiking by evoking EPSPs and IPSPs of different sizes at random times during the spike train. For excitation EPSPs of different size could be evoked in the same cell by adjusting stimulation strength (fig 5.1 A). Stimulation during spontaneous spiking resulted in an

elevated spike probability briefly after the stimulation during the rising phase of the EPSP (fig 5.1 B top 3 traces). However, even if no spike occurred during rise or peak of the EPSP, the first spike after the stimulus occurred earlier than expected from the spontaneous inter spike interval (fig 5.1 B bottom trace), presumably due to the excitatory synaptic current contributing to the depolarisation of the membrane by intrinsic currents responsible for spontaneous spiking. I normalised the first spike latencies to the average delay to the next spike from a random point in time. Since for a regular spiking cell the next spike occurred between 0 ms and the inter spike interval with even probability, the normalisation factor was equal to half the inter spike interval. The average normalised latency reflects how much a spike is shifted due to an input compared to baseline spiking and is termed 'spike shift'. Histograms of normalised latencies are shown in figure 5.1 D and the spike shift as function of PSP amplitude is shown for several cells in figure 5.1 F. The spike shift was saturating for EPSPs larger than 6 mV as might be expected since large EPSPs always crossed threshold regardless of their position in the interspike trajectory and therefore always triggered spikes during their rising phase so that increasingly larger EPSPs did not result in shorter latencies.

Since there is no clear distinction between 'evoked' spikes and spontaneous spikes (Santamaria *et al.*, 2002) I measured the 'net spike output' that occurred due to an input by averaging the 'corrected cumulative spike output' over at least 100 ms after stimulation (fig 5.1 C, methods ; Mittmann *et al.*, 2005). Both measures of spike output, spike shift and net spike output, scaled with the size of the EPSP within cells (fig 5.1 C, D) as well as across cells (fig 5.1 E, F).

Comparing the effect of EPSPs and IPSPs of different amplitudes on PC spiking revealed that IPSPs had a stronger influence on spike shift and net spike output. Part of this effect was due to a significant increase in driving force between IPSPs measured at -65 mV (23 mV driving force) and the average membrane potential during spontaneous spiking (-50.4 ± 0.47 mV ; n = 5 ; 38 mV driving force). This driving force increase of 65% would increase the IPSP amplitude by a similar percentage. For the spike difference, a line fit restricted to go through zero and limited to the range of 0 to 4 mV for excitation

gave slopes of 0.45 ± 0.06 and 0.13 ± 0.01 spikes/mV for inhibition and excitation respectively (fig 5.1 E). For the spike shift the slopes were -0.96 ± 0.12 and -0.25 ± 0.02 shift/mV (fig 5.1 F).

5.2.2 Climbing fibre induced LTD of excitation and inhibition

I measured directly how synaptic plasticity translates into changes of the spike response by interleaving hyperpolarised trials to measure EPSP amplitude with trials where the EPSP occurred during the spontaneous spiking. Unlike other protocols designed to investigate mechanisms of plasticity, I aimed to recreate a realistic learning paradigm by using a Cs-free internal solution, measuring responses in current clamp during the entire experiment and using physiological CF-induced depolarisation for plasticity induction.

After the EPSP amplitude (range 1.2 to 5.3 mV) stayed stable for 10 minutes the CF was activated with a 1 ms delay after PF stimulation for 300 times at 1 Hz (Karachot *et al.*, 1994). This pairing protocol led to a small but robust long-lasting depression of the EPSP (fig 5.2 A) observed in all cells (fig 5.2 B), consistent with previous studies (Ito *et al.*, 1982; Ito, 2001; Sims & Hartell, 2005). If the pairing protocol was omitted, no such depression could be observed (fig 5.2 A, C). The small potentiation in control was not significant compared to the baseline period (103 ± 8%, $p > 0.4$, $n = 7$) as opposed to a significant depression after the pairing protocol (67 ± 4%, $p < 0.01$, $n = 7$; fig 5.2 B, 5.4 C). The comparison between the late phase of control and paired amplitude changes was also significant ($p < 0.01$, $n = 7$, unpaired *t*-test).

The sister experiment with inhibition was performed as described above. At -65 mV IPSPs were hyperpolarising and had amplitudes ranging from -0.2 to -1.3 mV (average -0.71 ± 0.05 mV). With the internal solution used here, the reversal potential was -88 ± 1.9 mV ($n = 4$) similar to perforated patch measurements (Chavas & Marty, 2003). Risetimes ranged from 0.9 – 5.6 ms (average 2.7 ± 0.2 ms). After 10 minutes of stable IPSP amplitude the same CF pairing protocol as for the EPSP was applied. This led to long lasting depression of IPSPs in all cells (fig 5.3 A, B). I did not observe a spontaneous

run-down of synaptic responses or CF induced LTP as previously reported (Kano *et al.*, 1996). I further controlled for non-specific effects like run-down or input resistance changes by omitting the pairing protocol and found a small, insignificant 'run-up' in IPSP amplitude (111.6 ± 7.6%, $p > 0.2$, $n = 10$, fig 5.3 A, C), compared to significant changes after the pairing protocol (74.6 ± 4.9%, $p < 0.01$, $n = 13$, fig 5.3 B, 5.4 D) and significant changes between late phase of control and pairing ($p < 0.01$, $n = 10$ and 14, unpaired *t*-test). This is the first time this form of plasticity, iLTD, has been observed in the cerebellum.

I evoked IPSPs by stimulating either in the upper or lower third of the molecular layer, thus predominantly recruiting stellate or basket cell inputs, respectively (Palay & Chan-Palay, 1974). These two inputs behaved identically in terms of IPSP amplitudes (basket cells -0.69 ± 0.08 mV, stellate cells -0.73 ± 0.12 mV, $p > 0.3$, unpaired *t*-test) or amount of depression after pairing (basket cells 77.9 ± 7.2%, stellate cells 70.8 ± 7.1%, $p > 0.2$, unpaired *t*-test) but had different risetimes (basket cells 2.0 ± 0.2 ms, stellate cells 3.3 ± 0.2 ms, $p < 0.01$, unpaired *t*-test).

The degree of LTD of excitation and inhibition was similar and not statistically significant ($p > 0.3$, unpaired *t*-test).

5.2.3 Climbing fibre learning is reflected in Purkinje cell spike output

After CF-induced LTD, EPSPs were less effective in accelerating the next spike, resulting in fewer spikes occurring within in the first few milliseconds after stimulation. An example of sub- and superthreshold traces is shown in figure 5.4 A (right panels). If the cell had more time to recover from the previous spike and the subsequent afterhyperpolarisation, both baseline and depressed EPSPs resulted in short-latency spikes. This was visible in histograms of the spike shift where the difference between baseline and pairing was mainly restricted to the tail (fig 5.4 Ab). The reduction in spike shift and the reduced shortening of the inter spike interval of the second spike were also reflected in the net spike output (fig 5.4 Ac). If pairing EPSP and CF was omitted, no such changes occurred (fig 5.4 Aa, Ab, Ac left panels).

The inverse of these observations was true for iLTD; the power of the IPSP to delay the next spike was reduced along with its size (fig 5.4 Ba). The histogram was shifted to the left to smaller spike shifts and shorter latencies (fig 5.4 Bb). Spikes that occurred shortly after stimulation were preceded by voltages very close to threshold and these spikes could not be prevented by the initial rise of the IPSP. The shortening of the first spike latency was reflected in the upward shift of the corrected cumulative spike output. The net spike output was increased as a consequence of CF-induced depression (fig 5.4 Bc). Omitting the induction protocol did not lead to any changes in the IPSP, spike latency or net spike output (fig 5.4 B, right panels).

In summary, PF EPSP amplitudes (control: 103 ± 8%, $p > 0.4$, $n = 7$; LTD: 67.3 ± 4.4%, $p < 0.01$, $n = 7$, fig 5.4 C) were mirrored by a reduction of the net spike output for LTD experiments and only a small insignificant increase in control (control: 115 ± 10% $p > 0.15$; LTD: 70.6 ± 4.9%, $p < 0.02$). Spike shifts increased for PF LTD, but not for control (control: 96 ± 4.7%, $p > 0.4$; CF pairing: 137.0 ± 10%, $p < 0.01$).

The reduction of IPSP amplitudes by CF pairing and even the small, insignificant run-up of the control (control: 111.6 ± 7.7%, $p > 0.2$, $n = 10$; iLTD: 74.6 ± 4.9% $p < 0.01$, $n = 13$) were reflected in a small, insignificant increase of the normalised net spike output in control and a decrease for iLTD (control: 109.5 ± 10.8%, $p > 0.3$; iLTD: 70.4 ± 6.8%, $p < 0.01$. Normalisation results in a decrease of the normalised spike output for an increase of the net spike output because the net spike output is negative.) Similarly, the spike shift was not changed in control but was reduced for iLTD (control: 102.3 ± 2.4%, $p > 0.3$ iLTD 88.6 ± 2.6%, $p < 0.01$). These results show for the first time a direct link between synaptic plasticity and spike output of the cerebellar cortex.

5.2.4 Changes in spike output induced by plasticity of feed-forward inputs

I have shown that pairing the CF with excitation or inhibition results in LTD of both inputs with opposite effects on the spike output. PF LTD led to increased latency and decreased net spike output, whereas iLTD led to a decrease in

latency and an increase in net spike output. To determine which form of plasticity dominated the CF induced changes in spike output it was necessary to know the quotient of the IPSP and EPSP amplitudes (I/E ratio) that is typical for physiologically meaningful PC inputs under *in vivo* conditions. Although *in vivo* whole-cell recordings from PCs have been published recently (Loewenstein *et al.*, 2005; Schonewille *et al.*, 2006) the nature and composition of these inputs remains unknown. I decided to simulate PF EPSPs with current injection and IPSPs with dynamic clamp to mimic excitatory currents arriving at the soma from electronically remote PF synaptic inputs and conductance changes from activated perisomatic inhibitory synapses. By avoiding real synapses, data acquisition was not restricted by the slow synaptic recovery and I could collect spike data for many different I/E ratios with a baseline and a depressed input (mimicked by a 20% decrease of both components) with a high number of sweeps for each condition (~300 sweeps).

The timecourses of simulated excitation and inhibition (EPSC: τ_{Rise}= 0.8 ms ; τ_{Decay}= 5 ms ; IPSG: τ_{Rise}= 1 ms τ_{Decay}= 8 ms) were comparable to feed-forward currents measured in P14 PCs separated pharmacologically (EPSC: τ_{Rise}= 0.70 ± 0.03 ms ; τ_{Decay}= 5.15 ± 0.36 ms ; IPSC: τ_{Rise}= 131 ± 8% $\tau_{Rise(EPSC)}$; τ_{Decay}= 162 ± 38% $\tau_{Decay(EPSC)}$; data shown in chapter 4). For the delay between excitation and inhibition 1.4 ms was used (chapter 3 ; Mittmann *et al.*, 2004). A typical example of baseline and depressed inputs is shown in figure 5.5 A for two I/E ratios. Depending on where in the spike cycle the input occurred, three scenarios could be distinguished: 1) The input fell into the late phase of the spike cycle (i.e. shortly before a spontaneous spike) and both baseline and depressed inputs triggered a spike during the rising phase or peak of the EPSP ('early spike' ; fig 5.5 B top traces). The inhibition only had a weak effect on the second spike, presumably because of shunting by the first spike and reduction of driving force through the afterhyperpolarisation. 2) The input occurred earlier in the spike cycle and the reduction in amplitude of the depressed but not the baseline input resulted in the EPSP failing to trigger an early spike and the first spike after the input occurred much later ('late spike' ; fig 5.5 B middle traces). In case of a pure excitatory input, failing to trigger a spike during the rising phase would still speed up its occurrence because the excitatory current would

contribute to the spontaneous charging of the membrane (fig 5.4 Aa). Here however, excitation was rapidly followed by inhibition, which governed spike timing (fig 5.5 B middle traces). 3) The input occurred early in the spike cycle and neither baseline nor depressed input could trigger a spike during the rising phase and the inhibitory component determined the timing of the spike, comparable to pure inhibitory inputs (fig 5.4 B bottom traces).

In spike rasters (fig 5.5 C) it was difficult to see differences between baseline and depressed inputs. Sorting spike rasters according to the timing of the last baseline spike displayed these differences more clearly (fig 5.5 D). The three scenarios are easily visible, 1) the upper sweeps showing early spikes for both inputs until 2) the depressed input started to fail to trigger early spikes in a short middle region of the raster followed by 3) sweeps where the cell was too far from threshold for either input to trigger early spikes. The effect of iLTD on spike timing was clearly visible in the timing of the second spikes after the input in the first scenario and the timing of late first spikes in the third scenario, especially for the input with stronger inhibition. From the corresponding PSTH (fig 5.5 E) I computed corrected cumulative spike outputs (fig 5.5 F). These had values around zero for the 0.5 I/E ratio and negative values for the I/E ratio of 1.5. CF learning led to an increase of the net spike output for I/E ratios larger than 0.5.

On average the number of early spikes was significantly decreased for depressed inputs at all I/E ratios (fig 5.5 G) and their latency increased with depression for I/E ratios < 1 (fig 5.5 H). The asymptotic reduction of the latency with increasing inhibition, as well as the decreasing difference in latency between baseline and depressed inputs, could be explained by the increasing inhibition narrowing the time window for early spikes. The latency of late spikes differed significantly at all ratios (fig 5.5 I). Depression increased the latency of late spikes for pure EPSPs as predicted by the synaptic data (fig 5.1 D, 5.4 Ab) because less excitatory current contributed to the spontaneous charging of the membrane to threshold. Even for I/E ratios as small as 0.25, the plasticity of the inhibitory component overcompensated this effect and determined spike timing. Excitatory inputs led to an increased spike output but small inhibitory components with an I/E ratio of 1/2 were sufficient to cancel the increase in spike output resulting in a net spike output around zero. Larger inhibitory

components resulted in a negative spike output (fig 5.5 J). Consequently, CF learning for inputs with little or no inhibition led to a reduction of PC spike output as predicted by classical theories of cerebellar learning. In contrast inputs with inhibitory components equal or bigger than the excitatory components led to an increased spike output.

I confirmed that the above results are valid for a wider range of amplitudes by testing different EPSP / IPSP amplitudes and keeping the I/E ratio constant at 1 (fig 5.6). CF learning had similar effects on spiking for all amplitudes tested, with more pronounced differences for large amplitudes (fig 6 A, B). Note that for larger inputs the first scenario, where either input triggered a spike, is expanded at the expense of the last scenario where neither input triggered spikes (fig 5.6 D). This was reflected in a higher PSTH peak and the resulting corrected cumulative spike count (fig 5.6 E, F). On average the number of early spikes was reduced by plasticity over all amplitudes tested (fig 5.6 G), implying that FFI prevented the spike readout from saturating and loosing its sensitivity to small changes in input strength, unlike the situation for pure excitatory inputs (fig 5.1 E, F). The plasticity-induced changes in first spike latencies were not significant at all amplitudes (fig 5.6 H). An I/E ratio of 1 was just at the border of significant changes in first spike latencies before overpowering inhibition cut the time window for first spikes too short for plasticity-induced differences in first spike latencies to be detectable (fig 5.5 H). Latencies of late spikes were reduced by iLTD at all amplitudes as expected (fig 5.6 I). A significant increase in spike output was observed at all amplitudes but at 1 mV, where the net spike output was too small for statistically significant differences (fig 5.6 J).

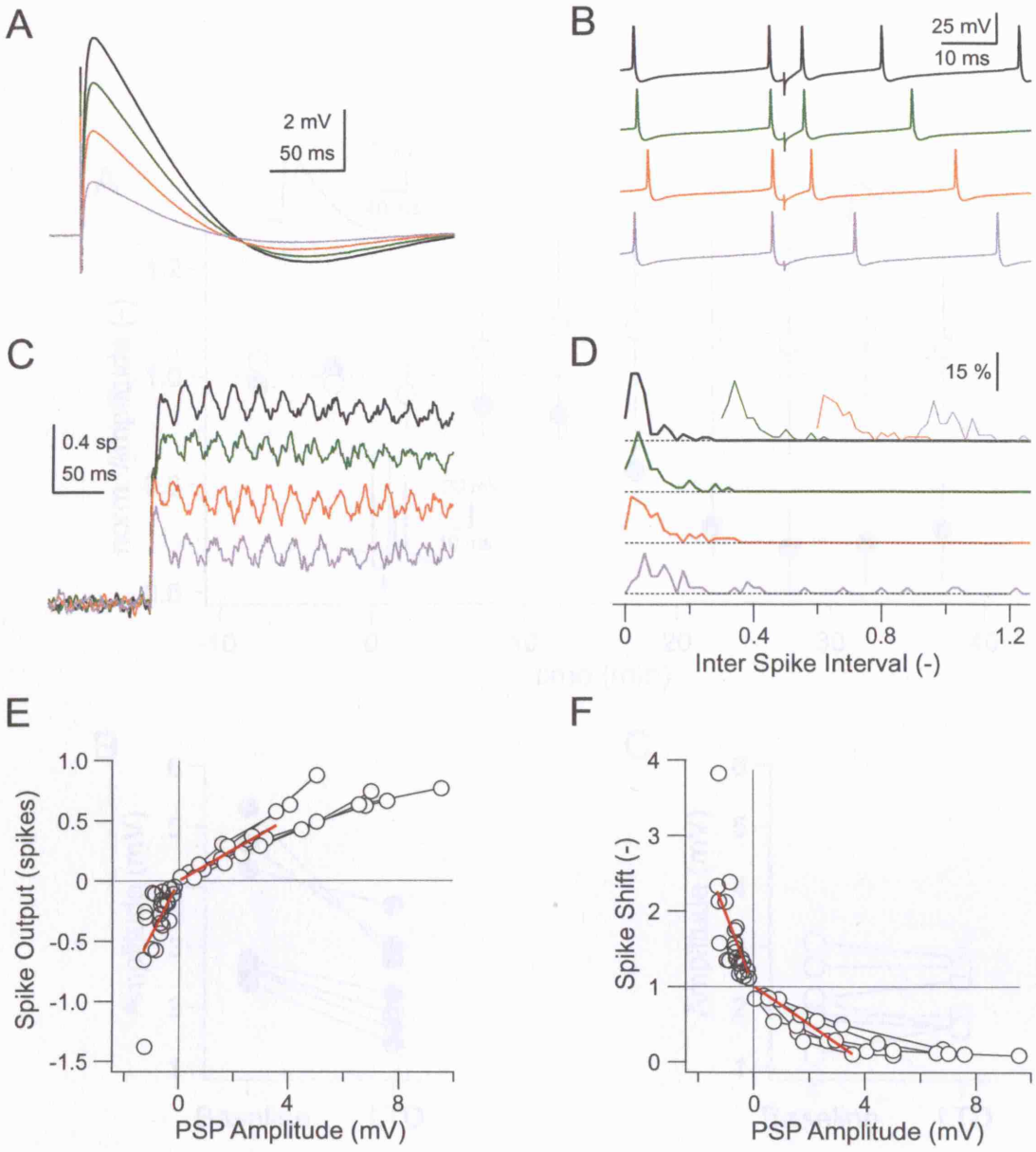

Figure 5.1

Net spike output and **spike shift** for excitatory and inhibitory inputs
PF EPSPs (**A**) changed the timing of the first and second spike after stimulation. This is visible in the single trials shown in **B**, where spike timing is determined by EPSP amplitude. **C** Corrected cumulative spike output. When the EPSP was evoked at random times during spontaneous spiking the spikes fired on top of the spontaneous firing scaled with the size of the EPSP. **D** Histogram of the latency of the first spike after stimulation normalised by the baseline ISI. The thin top traces are for comparison of histogram amplitude. The amplitude of the EPSP determined the first spike latency. **E** Fits to the constant regions of the corrected cumulative spike output ('net spike output') in response to EPSPs and IPSPs for several experiments. Connected data points were from the same cell. Note the different slopes of the red line fits to EPSPs and IPSPs. **F** The average first spike latency ('spike shift') for the same experiments shown in E. Note the difference in the slopes of the red line fits.

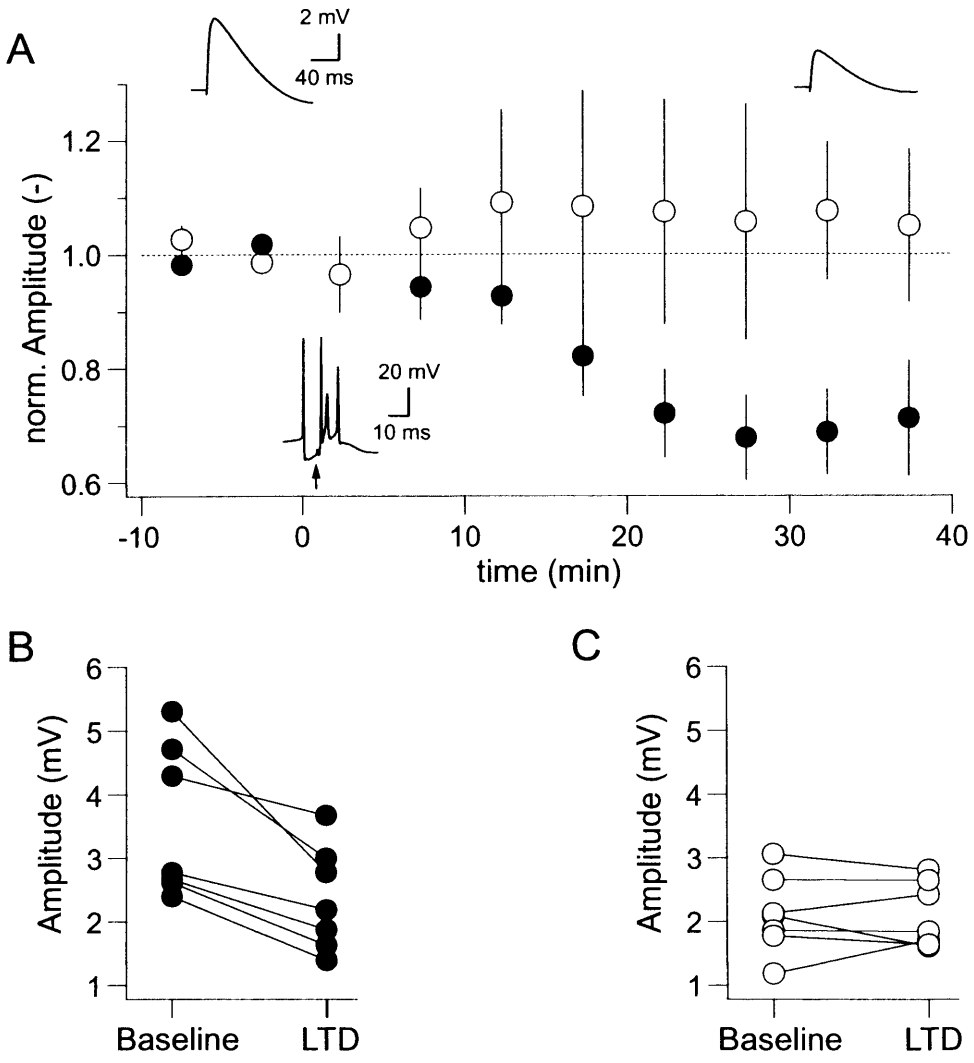

Figure 5.2

PF LTD

A PF EPSPs underwent LTD when paired with the CF. Filled circles show normalised EPSP amplitudes for 7 cells. Open circles show controls (7 cells) where omission of the induction did not lead to LTD. Insets show an example of the averaged EPSP before and after pairing and the response to CF stimulation (single trial). **B** EPSP amplitude before and after CF pairing shown for single cells. **C** Same as B for control.

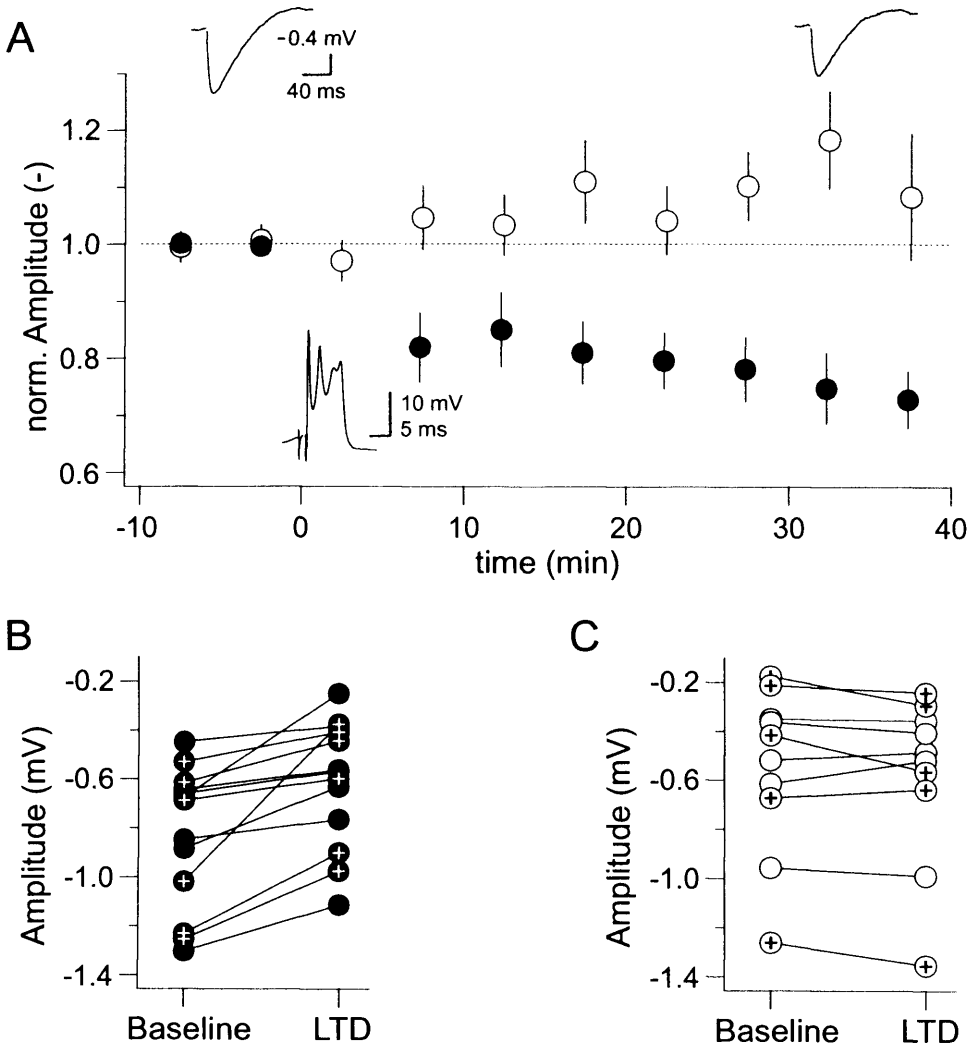

Figure 5.3

LTD of inhibitory PC input after CF pairing
A Evoked IPSPs underwent LTD when paired with CF stimulation. Filled circles show normalised EPSP amplitudes for 13 cells. Open circles show controls (10 cells) without pairing. Insets show an example of an averaged IPSP before and after pairing and a complex spike (single trial). **B** IPSP amplitude before and after pairing with the CF shown for single cells. Circles with a cross were stellate cell inputs, solid circles were from basket cells. **C** Same as B for control.

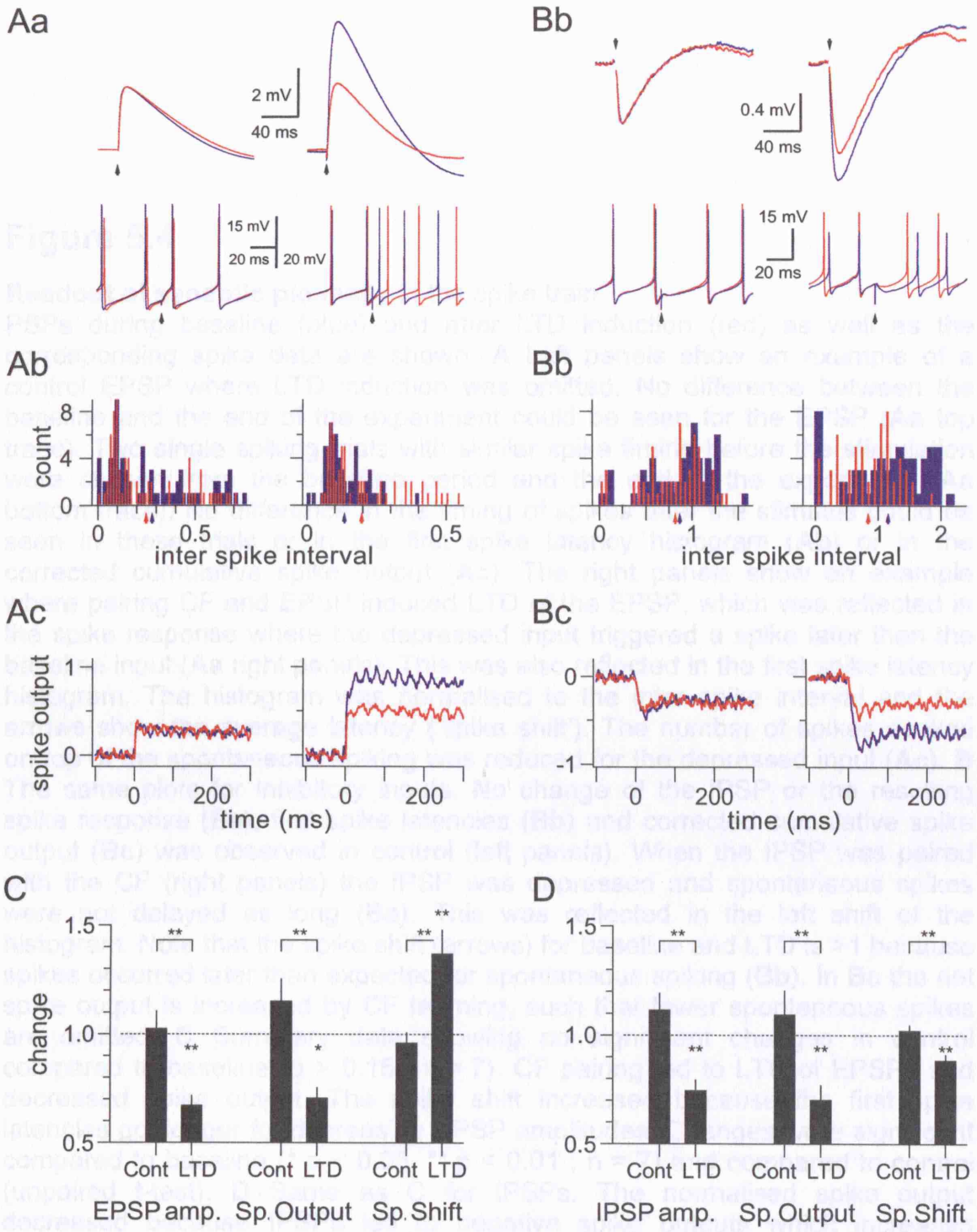

Figure 5.4

Legend overleaf.

Figure 5.4

Readout of synaptic plasticity in the spike train
PSPs during baseline (blue) and after LTD induction (red) as well as the corresponding spike data are shown. **A** Left panels show an example of a control EPSP where LTD induction was omitted. No difference between the baseline and the end of the experiment could be seen for the EPSP (**Aa** top trace). Two single spiking trials with similar spike timing before the stimulation were chosen from the baseline period and the end of the experiment (**Aa** bottom trace). No difference in the timing of spikes after the stimulus could be seen in these trials or in the first spike latency histogram (**Ab**) or in the corrected cumulative spike output (**Ac**). The right panels show an example where pairing CF and EPSP induced LTD of the EPSP, which was reflected in the spike response where the depressed input triggered a spike later than the baseline input (**Aa** right panels). This was also reflected in the first spike latency histogram. The histogram was normalised to the inter spike interval and the arrows show the average latency ('spike shift'). The number of spikes evoked on top of the spontaneous spiking was reduced for the depressed input (**Ac**). **B** The same plots for inhibitory inputs. No change of the IPSP or the resulting spike response (**Ba**), first spike latencies (**Bb**) and corrected cumulative spike output (**Bc**) was observed in control (left panels). When the IPSP was paired with the CF (right panels) the IPSP was depressed and spontaneous spikes were not delayed as long (**Ba**). This was reflected in the left shift of the histogram. Note that the spike shift (arrows) for baseline and LTD is >1 because spikes occurred later than expected for spontaneous spiking (**Bb**). In **Bc** the net spike output is increased by CF learning, such that fewer spontaneous spikes are omitted. **C** Summary data showing no significant changes in control compared to baseline ($p > 0.15$; $n = 7$). CF pairing led to LTD of EPSPs and decreased spike output. The spike shift increased because the first spike latencies got longer for decreasing EPSP amplitudes. Changes were significant compared to baseline (* $p < 0.05$, ** $p < 0.01$; $n = 7$) and compared to control (unpaired t-test). **D** Same as C for IPSPs. The normalised spike output decreased because IPSPs led to negative spike outputs which increased towards zero through iLTD. The spike shift decreased because latencies decreased with smaller IPSPs.

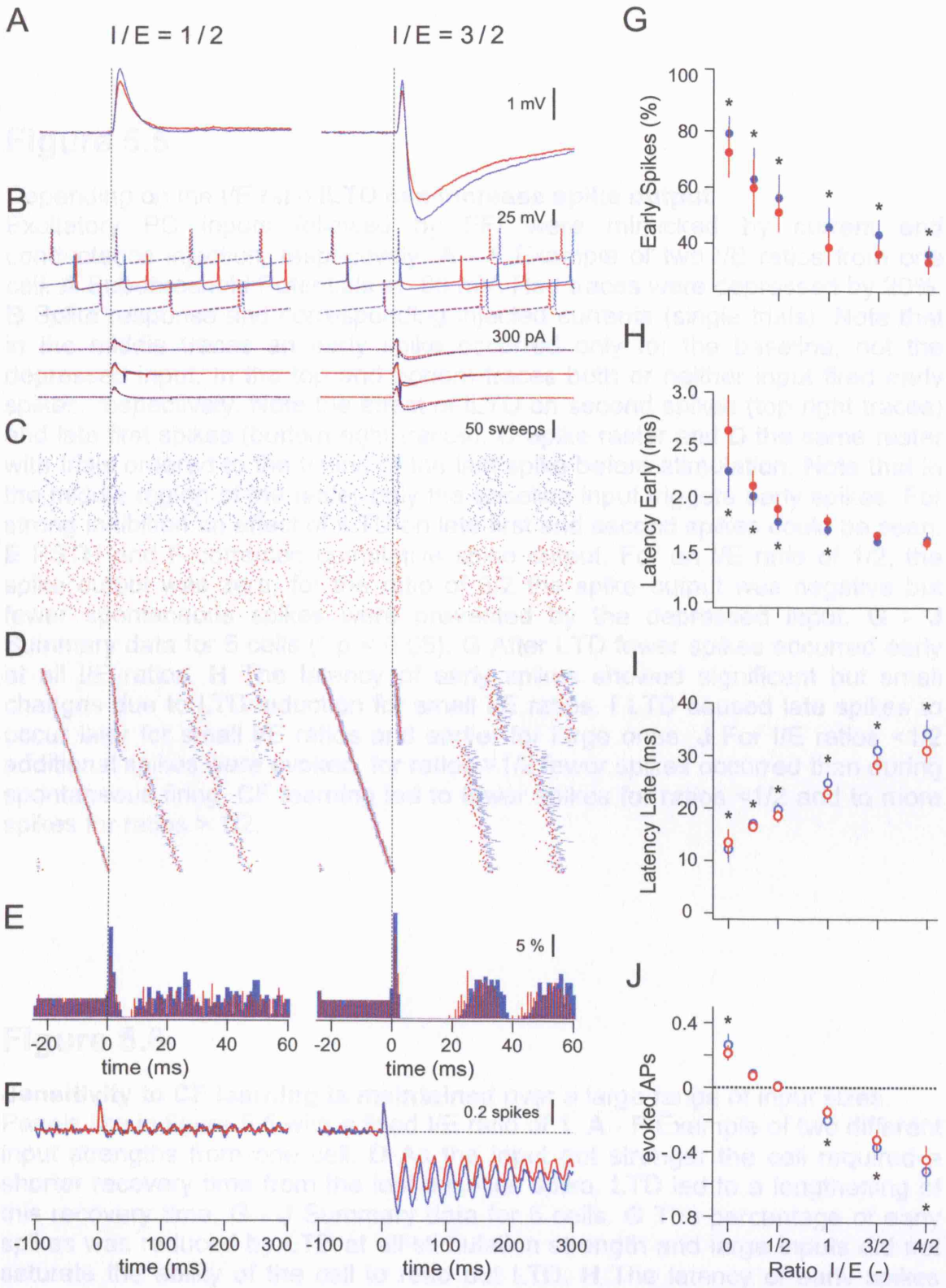

Figure 5.5

Legend overleaf.

Figure 5.5

Depending on the I/E ratio **iLTD can increase spike output**
Excitatory PC inputs followed by FFI were mimicked by current and conductance injection, respectively. **A - F** Example of two I/E ratios from one cell. **A** Sub-threshold Potentials at -65 mV. Red traces were depressed by 20%. **B** Spike response and corresponding injected currents (single trials). Note that in the middle traces an early spike occurred only for the baseline, not the depressed input. In the top and bottom traces both or neither input fired early spikes, respectively. Note the effect of iLTD on second spikes (top right traces) and late first spikes (bottom right traces). **C** Spike raster and **D** the same raster with trials ordered to the timing of the last spike before stimulation. Note that in the middle region of the raster only the baseline input triggers early spikes. For strong inhibition an effect of iLTD on late first and second spikes could be seen. **E** PSTH and **F** corrected cumulative spike output. For an I/E ratio of 1/2, the spike output was zero, for the ratio of 3/2 the spike output was negative but fewer spontaneous spikes were prevented by the depressed input. **G - J** Summary data for 5 cells (* $p < 0.05$). **G** After LTD fewer spikes occurred early at all I/E ratios. **H** The latency of early spikes showed significant but small changes due to LTD induction for small I/E ratios. **I** LTD caused late spikes to occur later for small I/E ratios and earlier for large ones. **J** For I/E ratios <1/2 additional spikes were evoked, for ratios >1/2 fewer spikes occurred than during spontaneous firing. CF learning led to fewer spikes for ratios <1/2 and to more spikes for ratios > 1/2.

Figure 5.6

Sensitivity to CF learning is maintained over a large range of input sizes.
Panels like in figure 5.5 with a fixed I/E ratio of 1. **A - F** Example of two different input strengths from one cell. **D** As the input got stronger the cell required a shorter recovery time from the last baseline spike. LTD led to a lengthening of this recovery time. **G - J** Summary data for 5 cells. **G** The percentage of early spikes was reduced by LTD at all stimulation strength and large inputs did not saturate the ability of the cell to read out LTD. **H** The latency of early spikes also did not saturate with large inputs although this was not significant at all input strength. **I** The latency of late first spikes was decreased for all inputs as it depended mainly on inhibition. **J** At all input strength the spike output was negative and CF learning led to an increase in spiking.

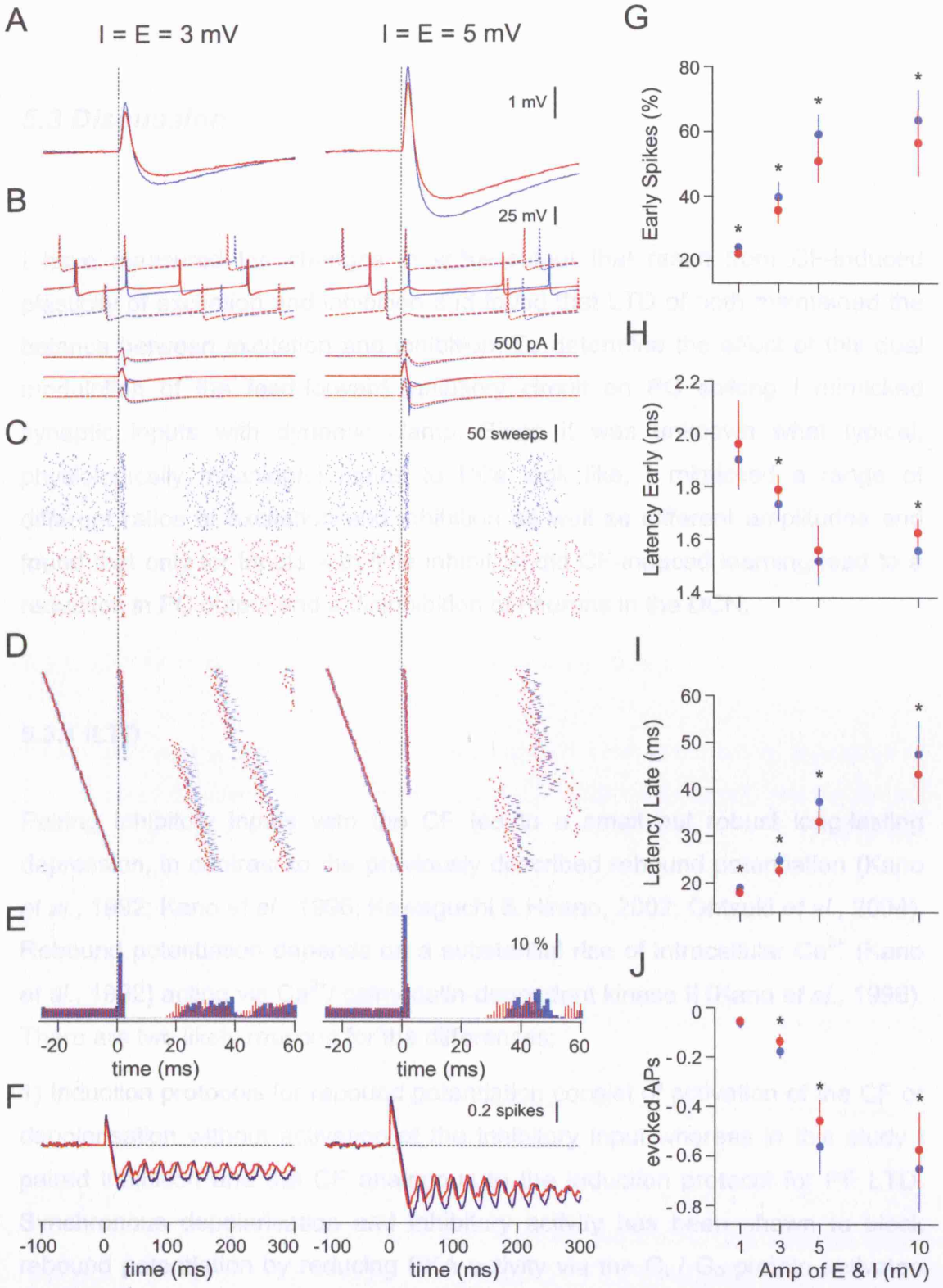

Figure 5.6

Legend on previous page.

5.3 Discussion

I have measured the changes in spike output that result from CF-induced plasticity of excitation and inhibition and found that LTD of both maintained the balance between excitation and inhibition. To determine the effect of this dual modulation of the feed-forward inhibitory circuit on PC spiking I mimicked synaptic inputs with dynamic clamp. Since it was unknown what typical, physiologically meaningful inputs to PCs look like, I mimicked a range of different ratios of excitation and inhibition as well as different amplitudes and found that only for inputs with little inhibition did CF-induced learning lead to a reduction in PC output and a disinhibition of neurons in the DCN.

5.3.1 iLTD

Pairing inhibitory inputs with the CF led to a small but robust long-lasting depression, in contrast to the previously described rebound potentiation (Kano *et al.*, 1992; Kano *et al.*, 1996; Kawaguchi & Hirano, 2002; Ohtsuki *et al.*, 2004). Rebound potentiation depends on a substantial rise of intracellular Ca^{2+} (Kano *et al.*, 1992) acting via Ca^{2+}/ calmodulin-dependent kinase II (Kano *et al.*, 1996). There are two likely reasons for the differences:

1) Induction protocols for rebound potentiation consist of activation of the CF or depolarisation without activation of the inhibitory input whereas in this study I paired inhibition and the CF analogous to the induction protocol for PF LTD. Synchronous depolarisation and inhibitory activity has been shown to block rebound potentiation by reducing PKA activity via the G_i / G_0 protein activated by postsynaptic $GABA_B$ receptors (Kawaguchi & Hirano, 2000; Kawaguchi & Hirano, 2002) ; fig 1.4). The signalling pathway for blocking rebound potentiation is known (Kawaguchi & Hirano, 2002) and it is not unlikely that instead of merely blocking rebound potentiation this pathway could lead to

iLTD. If iLTD does share the same pathway it was probably overlooked in those studies due to differences in induction protocols (depolarisation to 0 mV for 500 ms versus pairing of inhibitory input and CF at 1 Hz) or different internal solutions (see below).

2) Alternatively, iLTD was discovered here because I used a potassium based internal solution, which does not interfere with K^+ channel activation (Bezanilla & Armstrong, 1972) and therefore leads to a more physiological Ca^{2+} signalling through fast hyperpolarisation after the CF input. Previously, cesium based internal solutions were used for rebound potentiation experiments (Kano *et al.*, 1992; Kano *et al.*, 1996; Kawaguchi & Hirano, 2002; Ohtsuki *et al.*, 2004) and in some cases the block of rebound potentiation by the intracellularly applied Ca^{2+}chelator BAPTA led to a long lasting depression, similar in magnitude to iLTD (Kano *et al.*, 1992).

5.3.2 Inhibition exerts a powerful influence on spiking

When comparing inputs by their amplitude, IPSPs were more powerful in influencing PC spiking than EPSPs (fig 5.1). This effect could not be solely attributed to a stronger driving force for IPSPs during spiking. The ratio of the slopes of the line fits to inhibition / excitation for both spike measures was higher than the increase in driving force (spike difference: 351% I/E ; spike shift: 382% I/E ; driving force: 165%).

These differences might be due to the low net spike output for large EPSPs because during undisturbed spiking the next spike occurred on average after half the inter spike interval. Therefore, even with antidromic stimulation, a maximum of +0.5 net spike output was expected. That the net spike output converged to a value higher than 0.5 was due to incomplete shunting of the EPSP (Häusser *et al.*, 2001) by the first spike leading to the second spike occurring earlier than one normal baseline inter spike interval after the first spike (fig 5.1 B, upper trace). Stimulation strength was adjusted to avoid stereotyped bursts. These bursts are one mechanism to escape these restrictions and to increase the net spike output to higher values (chapter 6). In

contrast to excitation, which can only accelerate the first spike by half the inter spike interval, inhibition was not subject to a saturating spike shift and was less likely to be weakened by shunting because the spike probability during the inhibitory conductance is reduced. This is consistent with previous modelling and experimental work (Jaeger & Bower, 1999) where spike triggered averaging revealed a strong influence of inhibition on spiking compared to a weak influence of excitation. However, the authors point out that part of this effect can be explained by fluctuating inhibitory input and less variable excitatory input acting more like a DC current. Instead of uncorrelated input leading to steady currents, I used correlated inputs making a comparison difficult.

Induction of plasticity led to a modest depression of both excitation and inhibition. For silent neurons the effect of changes in input size on spike output is easy to understand (Otmakhov *et al.*, 1993), whereas the situation for the spontaneously spiking PC is more complicated, especially when interaction between synaptic current and intrinsic, voltage sensitive conductances in the dendrite are taken into account (Jaeger *et al.*, 1997). However, although the plastic changes were small, the timing of spikes and number of spikes evoked by the input clearly reflected the underlying changes in synaptic strength.

5.3.3 Relevance of climbing fibre induced changes to the spike output

I showed that LTD of both excitation and inhibition is read out by the spike output of PCs. How will the changes in the spike output induced by CF learning affect the DCN if excitation and inhibition is combined in a typical feed-forward manner? First, the number of early spikes, evoked during the brief excitatory phase was reduced. This reduction was independent of the I/E ratio and reflected LTD of the excitatory component because at this time the inhibition was not yet active or very small. This is visible in the middle region of the sorted spike rasters of figure 5.5 D and 5.6 D and corresponds to the second scenario where recovery from the previous spike only allowed the undepressed input to fire a spike. This scenario took place only for a short time window of preceding spikes due to the small amount of depression used here. For stronger levels of

depression the second scenario would be extended at the cost of the first scenario (where both inputs used to fire a spike) because an increasingly weaker depressed input would require an even longer recovery of the PC from the previous spike in order to reach threshold. Although inhibition exerts a very powerful influence on the net spike output (see below), this direct readout of PF LTD might be crucial in governing synchronisation of PCs, which receive similar input via the PF system. Second, for the first and third scenario, where either both or neither input fired a spike, the length of the pause from the first spike (first scenario) or the stimulus (second scenario) to the next spike might act as a readout of iLTD. In the spontaneously active Purkinje population a pause of a defined length could be a signal as important to the downstream targets as synchronous activation, or even more important because it is less dependent on the timing of the spike prior to the input (fig 5.5 C, D and fig 5.6 C, D). However, the timing of the spikes after the pause is not nearly as precise as the timing of early spikes and iLTD of smaller inhibitory components (<= 50%) is not reflected in the length of the pause (fig 5.5 C, D left). Third, even if the precise timing of these later spikes or the length of the pause is not used as a signal, iLTD does govern the net spike output for inputs with I / E ratios bigger than 0.5. If the net spike output for a given input was positive, CF learning led to a reduction in spike output and vice versa because both components of the input were depressed by the same amount. Therefore, CF-evoked plasticity of inputs with large inhibitory components contradict the Marr-Albus-Ito theory because CF learning would lead to stronger inhibition of DCN neurons in response to the input.

5.3.4 Physiological inputs

Do PCs ever see inputs with large inhibitory components? There is little data available on sub threshold responses to sensory stimulation despite some recordings from PC dendrites *in vivo* (Jaeger & Bower, 1994) and recent patch clamp studies (Loewenstein *et al.*, 2005; Schonewille *et al.*, 2006). Sensory stimulation does evoke precisely timed mossy fibre EPSCs in GCs causing them to spike with high temporal precision and short latencies (Chadderton *et*

al., 2004). Sensory evoked extracellular PC spiking activity shows sharp increases of spike probability followed by longer decreases (Bower & Woolston, 1983) resulting in PSTHs similar to those shown here. Taken together with the properties of the hard-wired inhibitory feed-forward network in the cerebellar cortex (chapter 3 ; Mittmann *et al.*, 2005) this indicates that PCs receive feed-forward inputs within the range tested here, at least in some physiological conditions.

Single PF inputs to PCs are much smaller than unitary inhibitory inputs (Barbour, 1993; Häusser & Clark, 1997; Isope & Barbour, 2002). In slice, directly evoked inhibition was much smaller than excitation (fig 5.1 E, F, 5.2 B, C and 5.3 B, C). When PFs were stimulated FFI was smaller than excitation, especially for strong stimulation indicating that many PFs activated few inhibitory inputs. I expect that PCs receive a lot more inhibition *in vivo* because in slice a significant fraction of inhibition is cut off independent of slice orientation as inhibitory axons run along and across the folium (Palay & Chan-Palay, 1974). Furthermore, focal stimulation used in slice is likely to bias PC inputs towards excitation: electrical stimulation in the PFs likely results in a beam with a high proportion of active fibres activating nearly all interneurons within the beam even at low stimulation intensities because few inputs are sufficient to bring an interneuron to threshold (Carter & Regehr, 2002). Recruitment of more PFs will result in stronger excitatory input to PCs with little increase in inhibition. Compared to the situation in slice, sensory evoked inputs are likely to result in a much more dispersed PF activation pattern favouring inhibition and with little tendency towards saturation. A network model to test some of these predictions is described in chapter 4.3.4.

6 Coding through input induced spike pauses

6.1 Introduction

In chapter 5.1 the role of the cerebellum in motor learning and the Marr-Albus-Ito theory was introduced. According to the theory, erroneous elements of movements signalled by the CF act as a teaching signal leading to LTD of PF synapses, which serve as the correlate for motor memory. PF LTD reduces the excitatory drive to PCs leading to a reduced PC spike output representing the learned information. This theory gained experimental support from studies of eye-blink conditioning as a model for motor learning (chapter 5.1.2). The structures involved in eye-blink conditioning are identified and parts of this process, like PF LTD, are understood on a molecular level. Unfortunately our understanding of the whole process has a modular character; while some modules are understood in themselves, the connection to other modules or the contribution to the overall process remain unclear. In this chapter I address how information stored in PF synaptic weights is transmitted to the PC targets and what features of the spike output of PCs can be used to extract that information.

6.1.1 Transmission of climbing fibre induced plastic changes to strong inputs

If strong PF inputs to PCs undergo CF-induced learning, how is this change transmitted to the PC targets, the DCN?

PCs have many more excitatory PF → PC synapses (150,000; Harvey & Napper, 1991) than inhibitory interneuron → PC synapses (a few hundred;

Palay & Chan-Palay, 1974; Shepherd, 2004). This imbalance is only partially compensated by the smaller unitary PF input (PF: 8.4 pA equivalent to 0.07 mV; Isope & Barbour, 2002) compared to unitary inhibitory inputs (0.25 mV ; Häusser & Clark, 1997). During phases of strong GC activity, it is likely that inhibition does not scale with excitation but reaches a maximum because interneurons can be recruited with few PFs (Carter & Regehr, 2002).

In chapter 5 I showed that LTD of excitatory inputs leads to changes in the first spike latencies. Although the absolute time differences are small for an efficient neural code, FFI can intensify these time differences as seen in the previous chapter. However, for strong excitatory inputs, the changes in first spike latencies saturate (fig 5.1 F). If inputs operate in a regime where FFI is saturated and EPSPs are too big for plasticity to change the first spike latency, the net spike output (number of spikes on top of spontaneous spiking) might serve as a signal for PC targets. The spike output also showed some saturation (fig 5.1), but this was a consequence of rejecting inputs that cause bursts when activated during spontaneous spiking. As discussed in chapter 5.3.2 inputs that cause bursts are expected to strongly increase spike output.

Therefore, the prediction is that CF-induced LTD of strong PF inputs reduces the number of spikes fired in response to this input. Consistent with motor learning theories of the cerebellum (Marr, 1969; Albus, 1971) this would make the "novel" and "learned" input recognisable for the neurons of the DCN that would be disinhibited.

6.1.2 Modeling results

Steuber & De Schutter tested the prediction that the number of spikes fired in response to a strong PF input is reduced by LTD. They used a PC model to establish whether this feature of the spike train can be used to distinguish between baseline and depressed PF inputs (personal communication). Since the experiments presented in this chapter were designed to test predictions of this modelling study, their results are briefly introduced here.

Steuber & De Schutter used a multi-compartmental PC model with active dendrites and soma (De Schutter & Bower, 1994a, b) where PF synapses were modelled with an AMPA conductance on the spine head compartments. Random background PF and inhibitory input led to PC spiking with 48 Hz. During this baseline spiking a randomly chosen set of 1000 synapses were activated either with 0.7 nS synaptic conductance or with half that value to mimic a baseline and depressed inputs, respectively. Example traces and spike rasters for novel and stored patterns are shown in figure 6.1. After a burst of three spikes there is a pause in spiking longer than the inter-spike-interval (only called "pause" henceforth). In addition to the number of spikes in the burst, two other features were measured: the first spike latency and length of the pause.
The depressed input showed only a small decrease in the number of spikes compared to the novel input (novel: 2.8 ± 0.4 spikes ; depressed: 2.7 ± 0.5 spikes ; $p < 0.01$). The spike latency also showed a small difference between novel and stored inputs (novel: 1.8 ± 0.8 ms ; depressed: 2.3 ± 1.3 ms; $p < 0.01$). In contrast, the pause showed robust changes from 57 ± 3 ms to 39 ± 6 ms ($p < 0.01$). The signal to noise ratio (s/n ratio) indicates whether a feature could be used to distinguish between novel and stored inputs and was high for the pause (15.6) but low for the other features (< 1).

The mechanism underlying the pause was a negative feedback process in the PC dendrite. Strong PF inputs led to depolarisation sufficient to activate voltage gated calcium channels, causing Ca^{2+} to enter the cell (Eilers *et al.*, 1995). The synaptic input together with the Ca^{2+} current caused a burst of spikes, after which activation of Ca^{2+}-dependent potassium channels resulted in an afterhyperpolarisation (Fox & Gruol, 1993; Etzion & Grossman, 1998; Cingolani *et al.*, 2002) that caused the pause by inhibiting spike generation. The duration of the pause depended on the cytoplasmic Ca^{2+} concentration. Because the Ca^{2+} influx varied with the size of the synaptic input, the pause duration was decreased through LTD.

6.2 Results

6.2.1 Bursts of spikes are not followed by pauses in whole-cell recordings

To test the predictions of the model experimentally I performed whole-cell current clamp recordings from PCs in sagittal slices. PF inputs of varying size were evoked with a stimulus electrode buried in the slice beneath the dendrite of the recorded PC. To avoid pauses evoked by FFI, inhibition was blocked with bath applied SR. In most cells (10/14 ; fig 6.2) bursts could be evoked when large inputs (> 10 mV) were given during spontaneous spiking. Failure to evoke bursts was due to CF activation at high stimulation strength, which obscured PF responses.

Bursts were not followed by pauses that were longer than the inter spike interval. In figure 6.2 a typical experiment is shown. A burst is evoked with an EPSP of 15 mV but no pause occurs even with an EPSP twice that size.

6.2.2 Confirmation of model predictions with extracellular recordings

In contrast to the whole-cell recordings, pauses were observed with extracellular and cell-attached recordings. Pause duration changed with stimulation strength, consistent with the model. An example is shown in figure 6.3 A. Note that at low stimulation strength (top panel) a burst of three or four spikes was followed by the normal spontaneous spiking of the cell. At higher PF stimulation strength a pause developed after the burst, which further increased with larger stimulation strengths. These pause durations were similar to those observed in the model (fig 6.1). Because extracellular recordings do not resolve the size and properties of the underlying EPSPs I subsequently patched the same PC in whole-cell mode and recorded the EPSP during hyperpolarizing current steps (fig 6.3 B). This also allowed confirmation that the

spike response was due to PFs and not the CF. In this (fig 6.3 C) and other cells (fig 6.3 D, E) I consistently found that the amplitude of the PF EPSP determined the length of the pause measured either as absolute time or normalized by the spontaneous inter spike interval. In all cells at least two different stimulation strengths produced pauses of different length ($p < 0.01$, $n = 10$), both longer than the spontaneous inter spike interval. All but one cell (9/10) responded to the next smaller EPSP with a significantly shorter pause (red connections in fig 6.3 D, E). The average increase in pause duration was 42.7 ± 10.0% for an underlying increase in EPSP amplitude of 52.1 ± 22.5% ($n = 24$ stimulation strengths in 9 cells). Pauses at different EPSP sizes did not differ significantly if the change in EPSP size was small (-6.1 ± 2.1%, $n = 10$ stimulation strengths in 5 cells).

In some cells (n=4) spike responses were measured first in cell-attached then in whole-cell mode. The change in the recording configuration reduced the number of spikes in the burst in half of the cells (fig 6.4), in the other half the burst was unaffected. The pauses observed in extracellular recordings were completely abolished after establishing whole-cell mode. Spikes following the burst occurred after the normal inter spike interval or less (fig 6.4). The time from entrance into whole-cell mode to the first spike response in which the pause was abolished was brief. Although not directly measured, in two cells that time was only between 5 – 10 seconds.

6.2.3 LTD induction reduces pause duration

I addressed the predictions of the model more directly by testing whether the same PF input would lead to a shorter pause after induction of LTD. I searched for CF responses with an additional stimulation electrode before starting to record the baseline period. CF responses could easily be distinguished from spontaneous spikes or bursts evoked by PF EPSPs (fig 6.5 C) by their small spike amplitude, their brief inter spike intervals within the burst (Monsivais *et al.*, 2005), their small variability and their all or nothing response. After a baseline period of 8 – 10 minutes PF and CF were paired with a lag of 1 ms for 300

times at 1 Hz (Sims & Hartell, 2005). Following 30 – 40 minutes of extracellular monitoring of the spike response, I re-patched the same cell and recorded PF EPSPs and CF bursts in whole-cell mode to confirm the synaptic cause of the bursts. This standard LTD induction protocol resulted in a reduction of the pause that developed in the first few minutes after the induction (fig 6.5 A, B, D). The average normalized pause duration of all cells decreased to 57.3 ± 17.2% of baseline (fig 6.5 D), corresponding to a reduction from 89.9 ± 25.8 ms to 44.8 ± 11.1 ms. The change in the length of the pause was significant in all but one case ($p < 0.001$; fig 6.5 E left) where the pause length increased. The s/n ratio for discrimination of pauses before and after the LTD induction protocol was 5.4 ± 1.5. Only the cell with an increase in pause length had a s/n ratio smaller than 4 (fig 6.5 E right). Consistent with the model, other features of the spike train were poorer candidates for pattern recognition. The s/n ratios for the number of spikes in the burst (baseline: 4.1 ± 0.5 spikes; after induction: 3.5 ± 0.6 spikes) or the first spike latency (baseline: 2.0 ± 0.2 ms; after induction: 2.3 ± 0.4 ms) were below 2 in all but one cell. The average s/n ratio was 1.1 ± 0.5 (outlier excluded) for the number of spikes in the burst and 0.42 ± 0.2 (outlier excluded) for the first spike latencies (fig 6.5 E).

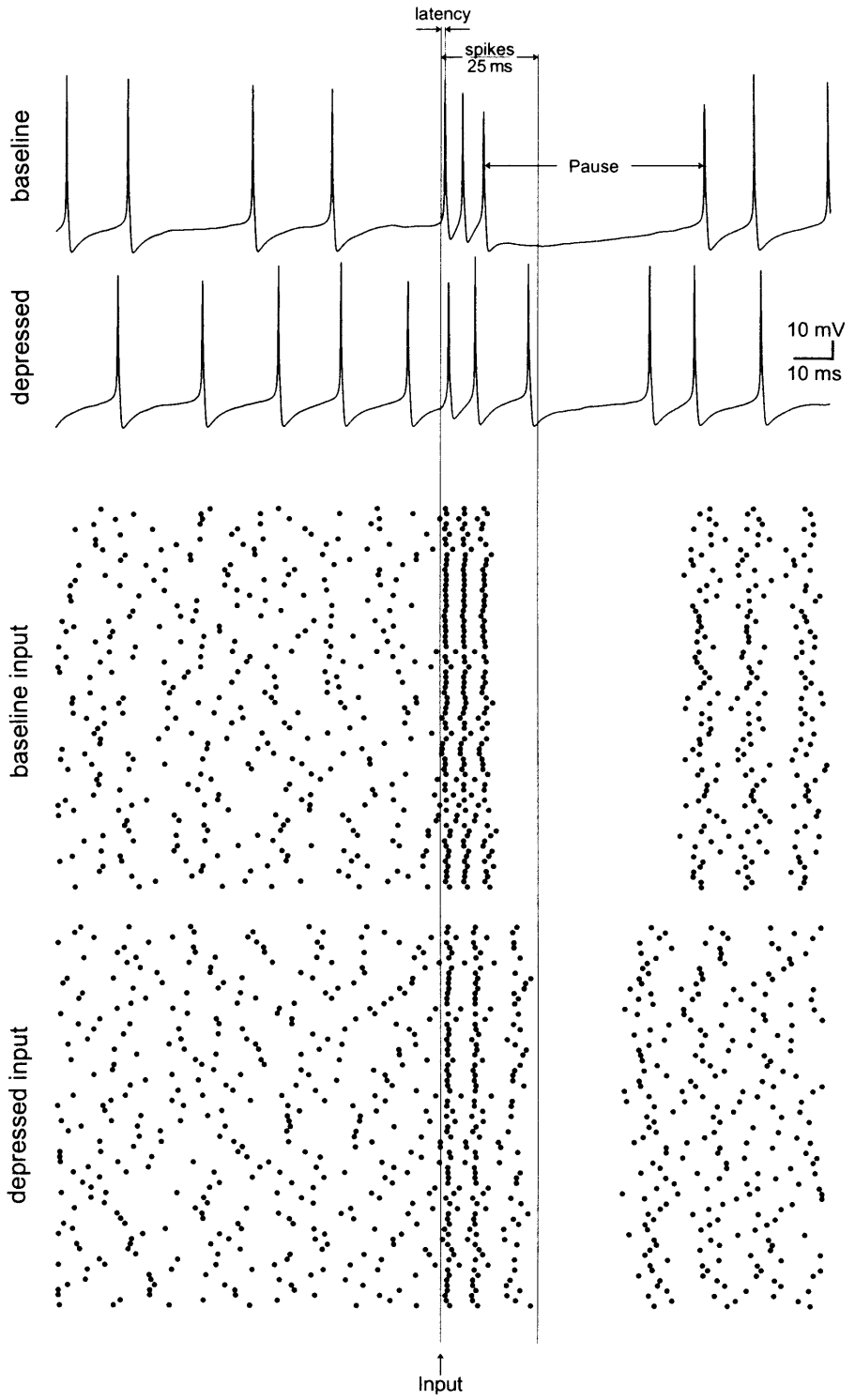

Figure 6.1

The model responds to strong PF input with a **Burst followed by a Pause**
A baseline (top trace) and a depressed (bottom trace) PF input are presented at the vertical line and evoke a burst of spikes followed by a pause. The pause duration is reduced for the depressed input. Raster plots showing the presentation of 75 baseline and 75 depressed inputs consisting of 1000 synchronously activated PF synapses with 50% smaller conductance for the depressed inputs. Same time scale as traces. Data from Steuber & De Schutter.

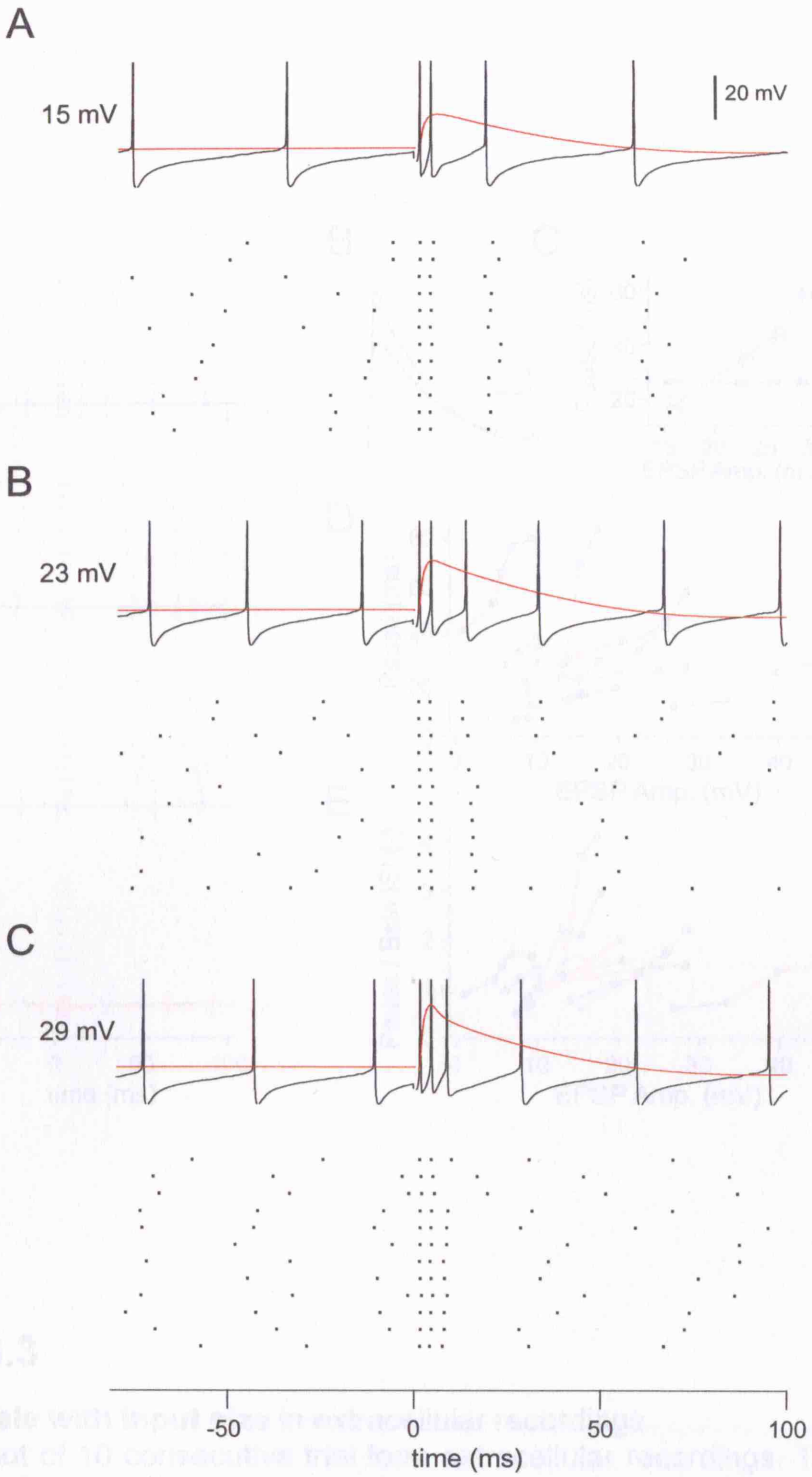

Figure 6.2

Strong PF inputs evoke bursts but **no pauses in whole cell recordings**
PF input was stimulated when the PC was hyperpolarised to -85 mV (red) and during spontaneous spiking. Example traces (black) and spike rasters of 12 consecutive trials are shown. **A** An EPSP of 15 mV evokes a burst of two or three spikes. The third spike shows more variable timing but is not followed by a pause. Instead the fourth spike follows after less than the baseline inter spike interval. Increasing the EPSP to 23 mV (**B**) or 29 mV (**C**) leads to reduced latencies of the third and fourth spike but no pauses are observed. Spikes are truncated and stimulus artefacts omitted. Data from a single PC.

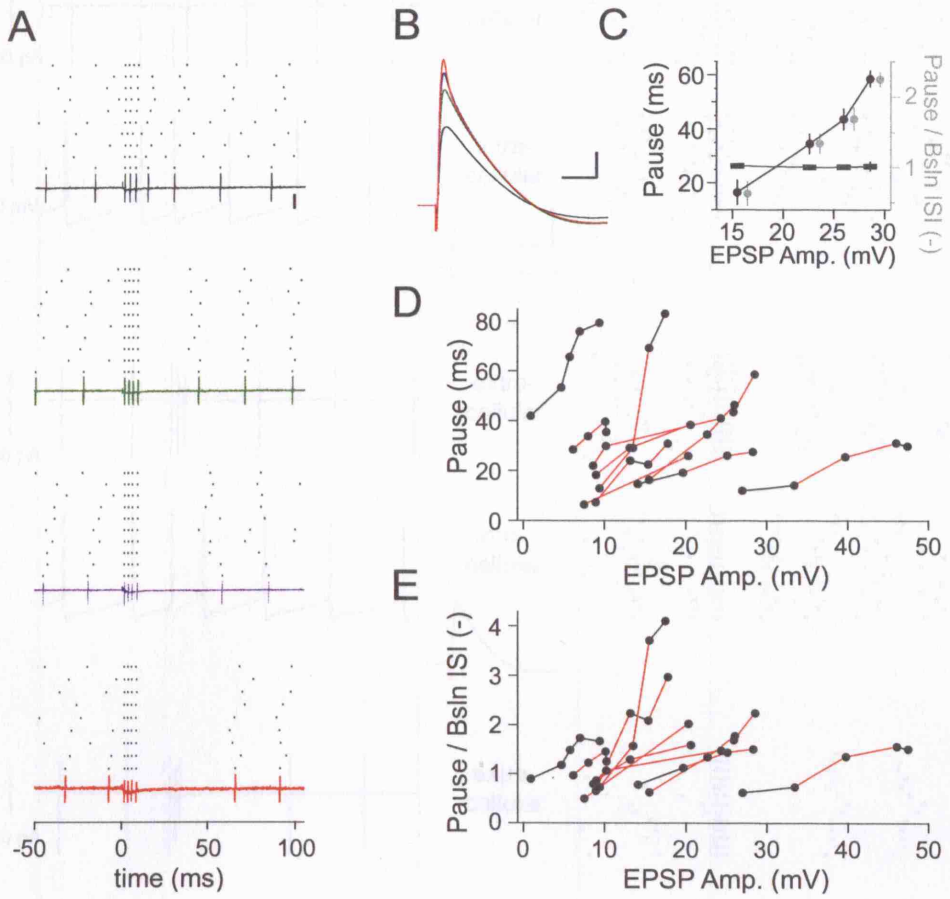

Figure 6.3

Pauses scale with input size in extracellular recordings
A Raster plot of 10 consecutive trial form extracellular recordings. The first trial in each raster is also shown as a raw trace. Scale bar is 200 pA and 100 pA for the last raw trace. The underlying EPSP amplitude for each raster was recorded in whole-cell mode after collection of extracellular data and was (top to bottom) 15.5, 22.6, 26.0, 28.6 mV. Note the increase in pause duration for bigger EPSPs. **B** EPSPs recorded in whole-cell mode. **C** Summary plot for cell shown in A. Pause duration as function of EPSP amplitude (black circles), baseline inter spike interval (rectangles) and pause divided by the inter spike interval (shifted to the right for better visibility) are shown. **D** Pause as function of EPSP amplitude in 10 cells. Red connecting lines indicate statistical significance ($p < 0.01$). (E) Same data as in D, but normalised by the baseline inter spike interval.

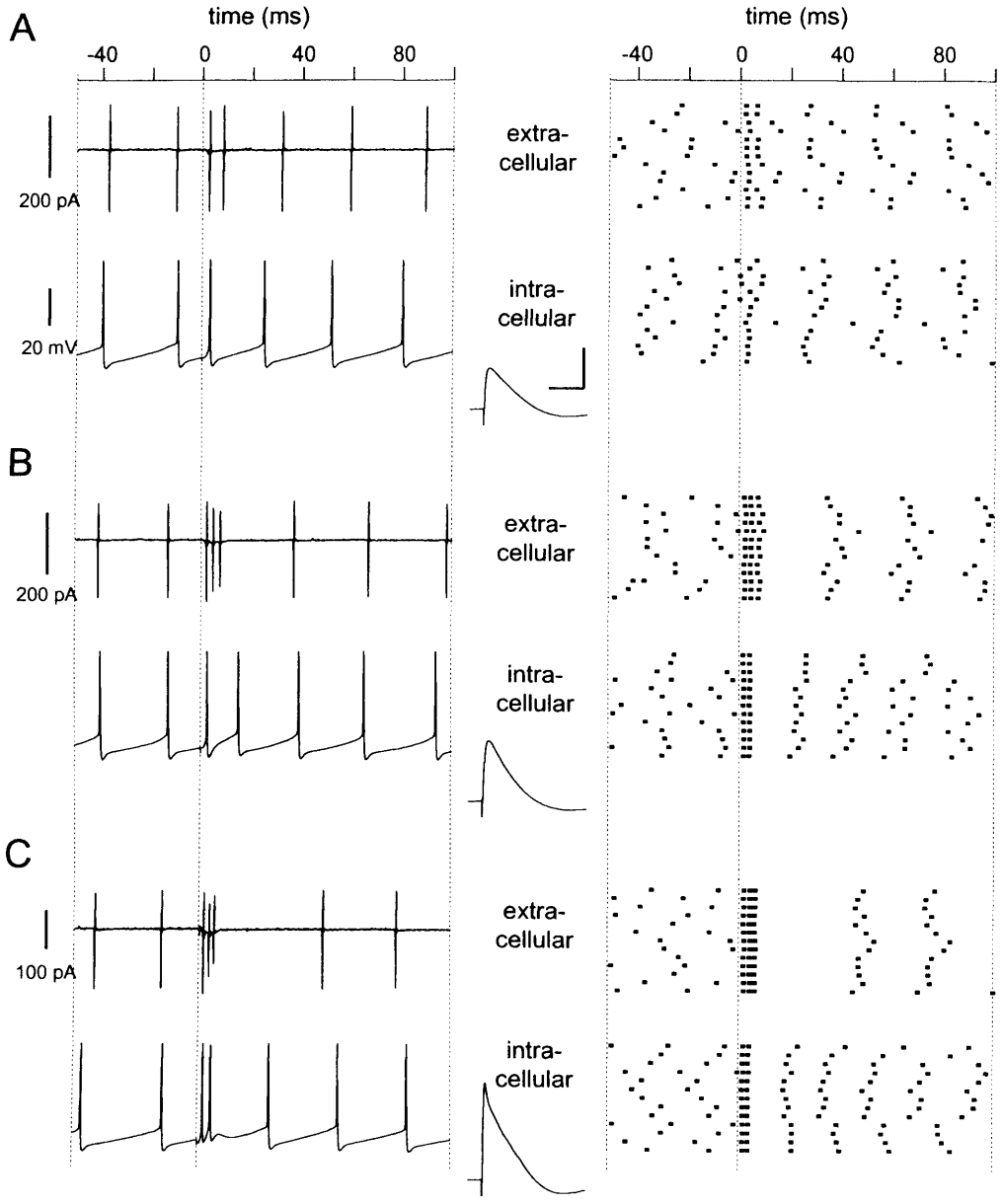

Figure 6.4

The **whole-cell configuration prevents the pause**
Example of a PC where PF input was given during spontaneous spiking. The top traces (single trials) and top raster plots in **A-C** show the spike response recorded extracellularly. Subsequently the same PC was patched in whole-cell mode and the spike response (bottom traces and raster plots) as well as the EPSP (middle traces; scale bar 10 mV, 50 ms) was recorded. For an EPSP of 10.2 mV (**A**) the whole-cell spike response is somewhat weaker but the EPSP is to weak to evoke a pause in either recording configuration. **B** An EPSP of 15.1 mV evokes a burst of three spikes followed by a pause slightly longer than the inter spike interval. The whole-cell recording of the same input shows a burst of only two spikes that is not followed by a pause. This discrepancy between the recording configurations is even stronger for the largest EPSP in **C** (24.3 mV) where a long pause is completely abolished in the whole-cell recording.

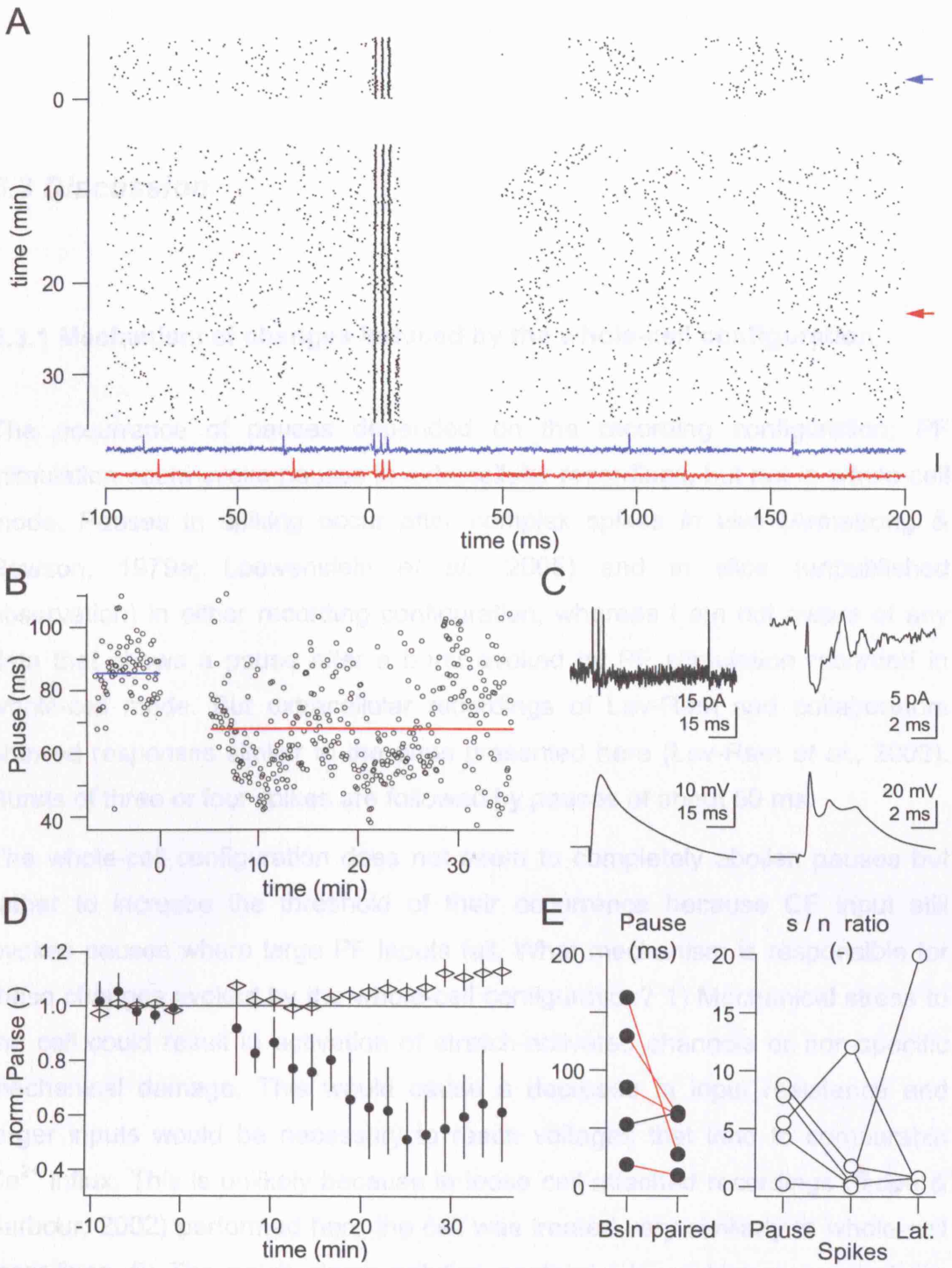

Figure 6.5

Induction of **LTD leads to shortening of the pause**.
A Spike raster and two example traces at times indicated by the arrows. Scale bar is 40 pA. PF input was paired with the CF at time 0. **B** The pause as a function of time and **C** extracellularly recorded PF (single trial) and CF induced spikes and PF EPSP and CF spike recorded in whole-cell mode after collection of extracellular data. **D** Averaged normalised pause duration (circles) and baseline inter spike interval for 5 cells. **E** Change of pause for single cells (red connection indicates statistical significance) and s/n ratio of pause, number of spikes and latency. Note that the cell with a low s/n ratio for the pause is the same cell that did not show a decrease in pause duration in the left plot.

6.3 Discussion

6.3.1 Mechanism of changes induced by the whole-cell configuration

The occurrence of pauses depended on the recording configuration; PF stimulation could evoke pauses in extracellular recordings, but not in whole-cell mode. Pauses in spiking occur after complex spikes *in vivo* (Armstrong & Rawson, 1979a; Loewenstein *et al.*, 2005) and in slice (unpublished observation) in either recording configuration, whereas I am not aware of any data that shows a pause after a burst evoked by PF stimulation recorded in whole-cell mode. But extracellular recordings of Lev-Ram and collaborators showed responses similar to the ones presented here (Lev-Ram *et al.*, 2003). Bursts of three or four spikes are followed by pauses of about 50 ms.

The whole-cell configuration does not seem to completely abolish pauses but rather to increase the threshold of their occurrence because CF input still evokes pauses where large PF inputs fail. What mechanism is responsible for these changes evoked by the whole-cell configuration? 1) Mechanical stress to the cell could result in activation of stretch-activated channels or non-specific mechanical damage. This would cause a decrease in input resistance and larger inputs would be necessary to reach voltages that lead to comparable Ca^{2+} influx. This is unlikely because in loose cell attached recordings (Isope & Barbour, 2002) performed here the cell was treated very similarly to whole-cell recordings. 2) The patch clamp solution contained K^+ at high concentrations (137 mM) mimicking the intracellular composition of the cell. Before formation of the seal internal solution was squirted onto the cell which leads to strong depolarisation (Hille, 2001). This depolarisation or subsequent Ca^{2+} influx could change properties of channels participating in the generation of the pause (e.g. depression of AMPA receptors). Alternatively, other parts of the cell could undergo changes leading to decreases in input resistance or enhance currents counteracting currents that lead to the pause. This possibility could be tested

experimentally by recording pauses extracellularly followed by application of internal solution with a second electrode. 3) Dialysis of the cell in whole-cell mode could evoke the above changes. This could either happen through specific actions of compounds of the internal solution on proteins (e.g. on Ca^{2+} channels) or by gradual washout of soluble endogenous components (e.g. calmodulin) that regulate activity of parts of the signalling cascade leading to the pause. No specific agonistic or antagonistic action of compounds of the internal solution has been established but this remains possible. The principle anion, methanesulfonate, would be the likeliest candidate because of the high concentration (130 mM). This could be tested by substitution with different anions. A washout of internal components is less likely because the effect of entry into the whole-cell configuration is rapid (5 – 10 s).

Whatever the reasons for the differences between the two recording configurations, extracellular recordings of spike responses have to be taken as a more accurate reflection of the physiological behaviour of PCs given that they do not interfere with the intracellular medium of the recorded cell.

6.3.2 LTD induction

Since intracellular recordings could not be used I was forced to use extracellular recordings that do not resolve the size of the PF EPSP. Although the EPSP could be recorded at the end of the experiment it was not possible to measure changes of EPSP amplitude evoked by the induction protocol. However, it is likely that the EPSP underwent LTD because the same induction protocol was previously shown to induce LTD (Hartell, 1996b) and was used for LTD induction in chapter 5. Furthermore, the decrease in pause duration observed after LTD induction (fig 6.5) indicates LTD of the EPSP, because reducing EPSP size through decreased stimulus intensity reduced pause duration (fig 6.3). On average, reducing the EPSP size by 25% led to a 26% decrease in pause duration. In LTD experiments the pause duration was reduced by 43% indicating that the underlying depression was considerably larger than 25%.

I did not observe a change of pause duration during baseline, indicating stable EPSP amplitude. Previous evidence suggested that strong EPSPs, like the

ones used here, can trigger LTD independently of the CF (Hartell, 1996b). However, at the monitoring frequency of 0.2 Hz used here, Hartell showed that no LTD occurred, consistent with a stable pause duration during baseline.

Lev-Ram and co-workers used the number of spikes in the burst to monitor amplitudes of PF EPSPs (Lev-Ram et al., 2003) with extracellular recordings. After LTD induction they observed a 35% decrease. Here, the number of spikes was reduced by only 15% after LTD induction. It is not clear whether this difference is only due to a different analysis; in the study by Lev-Ram et al spikes are counted over a fixed interval of 50 ms, including spikes after the burst. In the raw data they show (fig 1 and fig 4 inset ; Lev-Ram *et al.*, 2003) PCs did not spike spontaneously or only at very low frequencies (<10 Hz) and PF input increased spiking for seconds after the input. I did not observe such long lasting effects of the PF input and PCs fired with frequencies of about 46 Hz, making it difficult to compare with the study by Lev-Ram *et al.* Their experiments were performed at room temperature and with different protocols for plasticity induction, which might be the reason for differences in the burst or spontaneous activity.

6.3.3 Comparison of experimental and modeling results

Spike output measured with cell-attached recordings showed responses similar to the model (compare fig 6.1 and fig 6.3, fig 6.5). As in the model, the pause showed the highest s/n ratio before and after LTD induction compared to the other spike features. In the model, conductances of depressed synapses were reduced by 50% which led to a 32% reduction of the pause duration. Experiments measuring pause duration and EPSP amplitude in response to a range of stimulus intensities (fig 6.3) revealed that a 25% decrease in EPSP amplitude caused a 26% decrease in pause duration. This indicates that real PCs are similarly or even more sensitive to PF LTD than the model.

The presented experiments replicated all the key findings of the model although real PCs with a range of passive and active properties were used. Despite the

good agreement, the comparison of s/n ratios of different features of the spike train remains difficult. In the model s/n ratios were calculated between different baseline and depressed inputs. Because experimentally it is impossible to activate many different inputs, s/n ratios of the experiments were calculated on responses to many presentations of the same input before and after LTD induction.

6.3.4 Physiological consequences

The physiological consequences of a reduction in pause duration by CF learning should be identical to those where pauses are evoked by inhibition and modulated by synaptic plasticity. These are discussed in the previous chapter (chapter 5.3.3).

Changes in the burst were small and showed a low s/n ratio. That the number of spikes in the burst is exploited to discriminate between inputs is made even less likely by the short-term depression of the synapses between PC and deep cerebellar nucleus neurons (Telgkamp & Raman, 2002).

Changes in the latency of the first spike were small for the large EPSPs used here as predicted by results shown in figure 5.1. In themselves, these changes will not be useful for distinguishing between inputs. However, with strong FFI these latency changes might have an effect. Depending on the relative timing of the first spike and onset of FFI, spikes in the burst could be inhibited or activation of voltage-gated channels responsible for the pause could be altered. In the model, excitatory and inhibitory activity was not correlated and the normal background rate of inhibition prevailed during strong excitatory inputs. To mimic these conditions I blocked inhibition so neither model nor experiments showed any FFI. The conclusions from these experiments rely on the assumption that no FFI is present. While this assumption is unrealistic for smaller inputs it is likely to apply for the large inputs used here, as mentioned in the introduction (chapter 6.1.1). The network model outlined in chapter 4.3.4 could be used to test whether saturation of FFI is likely.

7 General Discussion

The basic structure of the cerebellar cortex is conserved across the entire subphylum of vertebrates, suggesting that it performs an important function. PC axons form the only output of the cerebellar cortex and spikes in these fibres carry the results of information processing performed by the cerebellar cortex. In the work presented in this thesis I have focused on the feed-forward inhibitory microcircuit of the molecular layer. I characterised the properties of this circuit and showed how FFI influences timing and level of spike output. I also looked at the possibility that FFI shapes the spatial distribution of sensory processing and concluded that a temporal dispersion of activity in the GC layer but not a spread of PF conduction velocities is the likely basis for the fractured somatotopic map of the cerebellar cortex. Finally, I examined plasticity in the feed-forward response triggered by CF input and its potential consequences for Purkinje cell output. This is relevant to cerebellar learning, in that sensory feedback conveyed to the cerebellum is thought to involve signalling of erroneous movements via the CFs.

The physiological relevance of my findings as well as further experiments are discussed at the end of each chapter. Here I would like to discuss the nature of sensory evoked input to PCs, and how the resulting output is interpreted by neurons of the DCN whose influence on motor targets ultimately ensures smooth movements. A better understanding of synaptic integration of PC input to the DCN would put my results into a wider context and contribute to a clearer framework of cerebellar function.

7.1 Sensory – evoked subthreshold potentials in Purkinje cells

Extracellular recordings from PCs in awake animals have shown that spike probability is correlated with movements (Thach, 1968; Armstrong & Edgley, 1988) and sensory input (Eccles *et al.*, 1972a, b). Experiments measuring PC spike probability in response to sensory stimulation reveal a variety of different responses. Some PCs show only reduced spike probability, others show brief increases in probability followed by decreases and some cells show prolonged increases (Bower & Woolston, 1983). These responses are consistent with PCs receiving IPSPs, EPSPs curtailed by FFI and EPSPs, respectively. Observed sharp rises in spike probability are likely to be a consequence of large fast rising EPSPs. Such EPSPs would require a high degree of PF synchrony.

Unfortunately, intracellular recordings from Purkinje cells *in vivo* are extremely difficult and therefore rare. As a consequence, the synaptic events underlying changes in spiking associated with movements and sensory stimulation remain poorly characterised despite some sharp electrode recordings from PC dendrites *in vivo* (Jaeger & Bower, 1994). Recent whole-cell recordings from Purkinje cells in anaesthetized animals have not reported large spontaneous or sensory-evoked EPSPs or IPSPs (Loewenstein et al., 2005) as would be expected from synchronous granule cell activity. This is consistent with the proposal of some researchers that PF activity is asynchronous, acting like a tonic current (Santamaria *et al.*, 2002). Clear data on subthreshold sensory responses of PCs would aid in the understanding of the cerebellar circuit and provide a blueprint for realistic inputs in experiments studying synaptic transmission in PCs. In chapter 5 for example, the ultimate effect of CF-induced plasticity on spiking depended on the unknown **ratio** of inhibition to excitation. Furthermore, some contradictory results in studies of synaptic plasticity may be a consequence of the different inputs employed, and an input blueprint could help to resolve these issues. This applies to input **size** (Hartell, 1996b) as well as input **frequency** (Lev-Ram *et al.*, 2002). In almost all slice studies, PF

EPSPs are elicited by a single electrical shock to the PFs, which results in PF synchrony and fast rising EPSPs. The **risetime** of sensory-evoked EPSPs could be much slower, which is important for studies of synaptic integration as this changes the conductance profile over time and also leads to less effective spike triggering and less precise FFI.

7.2 Readout of Purkinje cell activity by deep cerebellar nucleus neurons

As pointed out in the introduction, the entire cerebellar cortex can be viewed as the inhibitory component of the mossy fibre feed–forward loop terminating on the DCN neurons (fig 1.1). This means that during the final integration stage of cerebellar processing Purkinje cell output is interpreted by neurons of the DCN, whose axons form the output of the cerebellum. Spike trains in these axons should therefore be necessary and sufficient for whatever the cerebellum does. However, the role of the DCN in expression of previously learned motor responses is unclear. Activity in neurons of the DCN is clearly correlated with expression of previously learned delayed eye blinks (Gruart *et al.*, 2000). Activity in the DCN is well timed for a role in triggering the eye blink and correlates with the occurrence of eye blinks. However, stimulation of these neurons does not lead to full eye blinks and does not seem to determine their timing (Gruart *et al.*, 2000), leaving the problem of the exact role of the DCN unsolved.

Spike output from the DCN is primarily controlled by 5 factors: 1) intrinsic currents, 2) local connections 3) input from the CF 4) inhibitory input from PCs and 5) excitatory input from mossy fibre collaterals.

DCN neurons spike spontaneously in the absence of synaptic input. Spontaneous spiking and the pronounced "rebound spiking" of DCN neurons following hyperpolarising inputs are due to intrinsic currents and have been studied recently (Aizenman & Linden, 1999; Raman *et al.*, 2000). This rebound

spiking likely occurs after burst – pause sequences of PC input (McKay *et al.*, 2005), which is exactly what was observed after strong PF input (chapter 6).
The excitatory neurons of the DCN, which form the principal output of the cerebellum (Chan-Palay, 1977) also receive some local connections but not much is known about the contribution of these for the spike output. The DCN also receives excitatory input from CF collaterals. While this input might play an important role for learning (chapter 7.3), it is not necessary for the expression of learned behaviour (Medina *et al.*, 2002b).

The inhibitory input to the DCN is provided by the Purkinje cell axons, i.e. the output of the cerebellar cortex. As explored in this thesis, the factors determining PC output patterns are now relatively well understood. Taken together with work on the synaptic properties of the PC → DCN connections (Telgkamp & Raman, 2002; Pedroarena & Schwarz, 2003) the input to the DCN provided by the inhibitory part of the cerebellar mossy fibre feed-forward loop is relatively well characterized.

In contrast, much less is known about the direct mossy fibre → DCN connection, the excitatory part of the mossy fibre feed-forward inhibitory loop. The importance of this connection as the primary storage site for motor memories has been proposed by the trigger-and-storage model (Medina *et al.*, 2002a). Also, experimental data shows sharp increases in firing rate following sensory stimulation indicating direct excitation by the mossy fibre → DCN connection rather than disinhibition (Armstrong & Rawson, 1979b; Rowland & Jaeger, 2005). Mossy fibre excitation driving spiking followed by FFI via the cerebellar cortex that tunes the duration and level of spike output offers advantages over disinhibition of spontaneous DCN activity leading to rebound spiking: it is faster and probably more precise. This is clearly demonstrated by a first spike latency of more than 100 ms after termination of a hyperpolarising current pulse compared to a latency of 1 ms in response to a depolarising current pulse of the same magnitude (Aizenman & Linden, 1999; Raman *et al.*, 2000). However, the importance of the mossy fibre → DCN connection is controversial as blocking excitatory synaptic transmission in the DCN does not interfere with expression of previously learned behaviour (Attwell *et al.*, 2002).

In order to understand the role of the mossy fibre → DCN connection and the functional properties of the mossy fibre circuit, the following experiments would be desirable:

1. Whole-cell recordings from DCN neurons and activation of the loop by stimulation of mossy fibres should yield the relative timing of direct excitation and inhibition coming from the cortex. The change in relative strength of excitation and inhibition when stimulating mossy fibres at different frequencies would help to establish the basic properties of this pathway. To obtain this data will be difficult as slice preparations are unlikely to contain all parts of the circuit. *In vivo* recordings from neurons of the DCN and electrical stimulation of mossy fibres are possible but recordings will be impeded by the depth of the target cells and the high density of myelinated fibres.

2. It will be important to resolve synaptic currents and potentials with whole-cell recordings during expression of a learned movement. Furthermore it will be interesting to see whether exciting or silencing a single DCN cell can generate or influence a movement, similar to what has been observed in motor cortex (Brecht *et al.*, 2004).

7.3 Plasticity in the feed-forward inhibitory mossy fibre circuit

In chapter 5 and chapter 6 I used the CF to induce plasticity of PC inputs. This form of plasticity is generally accepted to be required for motor learning as exemplified for eye blink conditioning (Attwell *et al.*, 2001). The controversial role of the mossy fibre → DCN connection for expression of learned behaviour is discussed in the previous chapter, but whether this synapse and/or the inhibitory PC → DCN synapse is required for learning is even more controversial (for review see Attwell *et al.*, 2002; Lavond, 2002; Medina *et al.*, 2002a). If an engineer had just finished building the cerebellar cortex with multiple forms of plasticity enabling the cortex to learn any given PC spike output, his motivation to continue construction by equipping the PC → DCN synapse for memory storage should be low. Plasticity of the mossy fibre →

DCN synapse, the excitatory branch of the feed-forward inhibitory mossy fibre circuit would be much more interesting as it offers an additional degree of freedom to control the DCN output.

As described in the general introduction (fig 1.1), the CF does not only contact PCs but also provides direct excitatory input to neurons of the DCN. What are the CF collaterals to the DCN good for? Anatomical work has shown that CFs target areas of the cortex and DCN that are connected by the PC axons (Ruigrok, 1997; De Zeeuw *et al.*, 1998; Pijpers *et al.*, 2005). The existence of the CF → DCN connection, its specific mapping, the fact that the CF is not necessary for expression of learned behaviour (Medina *et al.*, 2002b) and the possible computational advantages of a plastic mossy fibre → DCN synapse suggests associative plasticity at that synapse mediated by CF activation, similar to the situation in the cortex. This possibility could be tested with experiments in slices.

Knowledge of the functional role and the properties of the feed-forward inhibitory mossy fibre circuit would aid understanding of how the PC activity patterns studied in this thesis are processed in the DCN and ultimately what computation is performed by the cerebellar circuitry. Investigating plasticity at the mossy fibre → DCN synapse and the possible involvement of the CF will establish whether and how CF error signalling teaches motor memory-storing synapses at two different computational layers. Together with a better characterisation of cerebellar inputs this might solve the enigma surrounding a fifth of the mammalian brain in the not so distant future.

8 References

Aiba A, Kano M, Chen C, Stanton ME, Fox GD, Herrup K, Zwingman TA & Tonegawa S. (1994). Deficient cerebellar long-term depression and impaired motor learning in mGluR$_1$ mutant mice. *Cell* **79,** 377-388.

Aizenman CD & Linden DJ. (1999). Regulation of the rebound depolarization and spontaneous firing patterns of deep nuclear neurons in slices of rat cerebellum. *J Neurophysiol* **82,** 1697-1709.

Albus J. (1971). A theory of cerebellar function. *Math Biosci* **28,** 167-171.

Allen GI, Azzena GB & Ohno T. (1974). Somatotopically organized inputs from fore- and hindlimb areas of sensorimotor cortex to cerebellar Purkyne cells. *Exp Brain Res* **20,** 255-272.

Andersen P, Eccles JC & Loyning Y. (1963). Recurrent inhibition in the hippocampus with identification of the inhibitory cell and its synapses. *Nature* **198,** 540-542.

Armstrong DM & Edgley SA. (1988). Discharges of interpositus and Purkinje cells of the cat cerebellum during locomotion under different conditions. *J Physiol* **400,** 425-445.

Armstrong DM & Rawson JA. (1979a). Activity patterns of cerebellar cortical neurones and climbing fibre afferents in the awake cat. *J Physiol* **289,** 425-448.

Armstrong DM & Rawson JA. (1979b). Responses of neurones in nucleus interpositus of the cerebellum to cutaneous nerve volleys in the awake cat. *J Physiol* **289,** 403-423.

Atluri PP & Regehr WG. (1996). Determinants of the time course of facilitation at the granule cell to Purkinje cell synapse. *J Neurosci* **16,** 5661-5671.

Attwell PJ, Ivarsson M, Millar L & Yeo CH. (2002). Cerebellar mechanisms in eyeblink conditioning. *Ann N Y Acad Sci* **978,** 79-92.

Attwell PJ, Rahman S, Ivarsson M & Yeo CH. (1999). Cerebellar cortical AMPA-kainate receptor blockade prevents performance of classically conditioned nictitating membrane responses. *J Neurosci* **19,** RC45.

Attwell PJ, Rahman S & Yeo CH. (2001). Acquisition of eyeblink conditioning is critically dependent on normal function in cerebellar cortical lobule HVI. *J Neurosci* **21,** 5715-5722.

Audinat E, Knopfel T & Gahwiler BH. (1990). Responses to excitatory amino acids of Purkinje cells' and neurones of the deep nuclei in cerebellar slice cultures. *J Physiol* **430,** 297-313.

Barbour B. (1993). Synaptic currents evoked in Purkinje cells by stimulating individual granule cells. *Neuron* **11,** 759-769.

Baude A, Nusser Z, Roberts JD, Mulvihill E, McIlhinney RA & Somogyi P. (1993). The metabotropic glutamate receptor ($mGluR_{1\alpha}$) is concentrated at perisynaptic membrane of neuronal subpopulations as detected by immunogold reaction. *Neuron* **11,** 771-787.

Bell CC & Grimm RJ. (1969). Discharge properties of Purkinje cells recorded on single and double microelectrodes. *J Neurophysiol* **32,** 1044-1055.

Ben-Ari Y. (2002). Excitatory actions of gaba during development: the nature of the nurture. *Nat Rev Neurosci* **3,** 728-739.

Bezanilla F & Armstrong CM. (1972). Negative conductance caused by entry of sodium and cesium ions into the potassium channels of squid axons. *J Gen Physiol* **60,** 588-608.

Bienenstock EL, Cooper LN & Munro PW. (1982). Theory for the development of neuron selectivity: orientation specificity and binocular interaction in visual cortex. *J Neurosci* **2,** 32-48.

Bliss TV & Lomo T. (1973). Long-lasting potentiation of synaptic transmission in the dentate area of the anaesthetized rabbit following stimulation of the perforant path. *J Physiol* **232,** 331-356.

Blomfield S & Marr D. (1970). How the cerebellum may be used. *Nature* **227,** 1224-1228.

Bower JM. (2002). The organization of cerebellar cortical circuitry revisited: implications for function. *Ann N Y Acad Sci* **978,** 135-155.

Bower JM, Beermann DH, Gibson JM, Shambes GM & Welker W. (1981). Principles of organization of a cerebro-cerebellar circuit. Micro-mapping the projections from cerebral (S1) to cerebellar (granule cell layer) tactile areas of rats. *Brain Behav Evol* **18,** 1-18.

Bower JM & Woolston DC. (1983). Congruence of spatial organization of tactile projections to granule cell and Purkinje cell layers of cerebellar hemispheres of the albino rat: vertical organization of cerebellar cortex. *J Neurophysiol* **49,** 745-766.

Boxall AR & Garthwaite J. (1996). Long-term depression in rat cerebellum requires both NO synthase and NO-sensitive guanylyl cyclase. *Eur J Neurosci* **8,** 2209-2212.

Boxall AR, Lancaster B & Garthwaite J. (1996). Tyrosine kinase is required for long-term depression in the cerebellum. *Neuron* **16,** 805-813.

Boyden ES, Katoh A & Raymond JL. (2004). Cerebellum-dependent learning: the role of multiple plasticity mechanisms. *Annu Rev Neurosci* **27,** 581-609.

Braitenberg V & Atwood RP. (1958). Morphological observations on the cerebellar cortex. *J Comp Neurol* **109,** 1-33.

Brecht M, Schneider M, Sakmann B & Margrie TW. (2004). Whisker movements evoked by stimulation of single pyramidal cells in rat motor cortex. *Nature* **427,** 704-710.

Brickley SG, Cull-Candy SG & Farrant M. (1996). Development of a tonic form of synaptic inhibition in rat cerebellar granule cells resulting from persistent activation of $GABA_A$ receptors. *J Physiol* **497,** 753-759.

Brunel N, Hakim V, Isope P, Nadal JP & Barbour B. (2004). Optimal information storage and the distribution of synaptic weights: perceptron versus Purkinje cell. *Neuron* **43,** 745-757.

Brunig I, Scotti E, Sidler C & Fritschy JM. (2002). Intact sorting, targeting, and clustering of γ-aminobutyric acid A receptor subtypes in hippocampal neurons in vitro. *J Comp Neurol* **443,** 43-55.

Carter AG & Regehr WG. (2002). Quantal events shape cerebellar interneuron firing. *Nat Neurosci* **5,** 1309-1318.

Carter AG, Vogt KE, Foster KA & Regehr WG. (2002). Assessing the role of calcium-induced calcium release in short-term presynaptic plasticity at excitatory central synapses. *J Neurosci* **22,** 21-28.

Casado M, Isope P & Ascher P. (2002). Involvement of presynaptic N-methyl-D-aspartate receptors in cerebellar long-term depression. *Neuron* **33,** 123-130.

Cathala L, Brickley S, Cull-Candy S & Farrant M. (2003). Maturation of EPSCs and intrinsic membrane properties enhances precision at a cerebellar synapse. *J Neurosci* **23,** 6074-6085.

Chadderton P, Margrie TW & Häusser M. (2004). Integration of quanta in cerebellar granule cells during sensory processing. *Nature* **428,** 856-860.

Chan-Palay V. (1977). *Cerebellar Dentate Nucleus: Organization, Cytology, and Transmitters.* Springer, Berlin.

Chavas J & Marty A. (2003). Coexistence of excitatory and inhibitory GABA synapses in the cerebellar interneuron network. *J Neurosci* **23,** 2019-2031.

Chen C & Thompson RF. (1995). Temporal specificity of long-term depression in parallel fiber-Purkinje synapses in rat cerebellar slice. *Learning and Memory* **2,** 185-198.

Chen G, Hanson CL & Ebner TJ. (1996). Functional parasagittal compartments in the rat cerebellar cortex: an in vivo optical imaging study using neutral red. *J Neurophysiol* **76,** 4169-4174.

Cingolani LA, Gymnopoulos M, Boccaccio A, Stocker M & Pedarzani P. (2002). Developmental regulation of small-conductance Ca^{2+}-activated K^+ channel expression and function in rat Purkinje neurons. *J Neurosci* **22,** 4456-4467.

Clark BA & Cull-Candy SG. (2002). Activity-dependent recruitment of extrasynaptic NMDA receptor activation at an AMPA receptor-only synapse. *J Neurosci* **22,** 4428-4436.

Clark DA, Mitra PP & Wang SS. (2001). Scalable architecture in mammalian brains. *Nature* **411,** 189-193.

Coesmans M, Weber JT, De Zeeuw CI & Hansel C. (2004). Bidirectional parallel fiber plasticity in the cerebellum under climbing fiber control. *Neuron* **44,** 691-700.

Cohen D & Yarom Y. (1998). Patches of synchronized activity in the cerebellar cortex evoked by mossy-fiber stimulation: questioning the role of parallel fibers. *Proc Natl Acad Sci U S A* **95,** 15032-15036.

Cohen D & Yarom Y. (2000). Cerebellar on-beam and lateral inhibition: two functionally distinct circuits. *J Neurophysiol* **83,** 1932-1940.

Conquet F, Bashir ZI, Davies CH, Daniel H, Ferraguti F, Bordi F, Franz-Bacon K, Reggiani A, Matarese V, Conde F & et al. (1994). Motor deficit and impairment of synaptic plasticity in mice lacking $mGluR_1$. *Nature* **372,** 237-243.

Coutinho V, Mutoh H & Knopfel T. (2004). Functional topology of the mossy fibre-granule cell--Purkinje cell system revealed by imaging of intrinsic fluorescence in mouse cerebellum. *Eur J Neurosci* **20,** 740-748.

Cowan WM, Südhof TC & Stevens CF. (2001). *Synapses*. Johns Hopkins University Press, Baltimore.

Crepel F, Dhanjal SS & Sears TA. (1982). Effect of glutamate, aspartate and related derivatives on cerebellar purkinje cell dendrites in the rat: an in vitro study. *J Physiol* **329,** 297-317.

Daniel H, Hemart N, Jaillard D & Crepel F. (1993). Long-term depression requires nitric oxide and guanosine 3':5' cyclic monophosphate production in rat cerebellar Purkinje cells. *Eur J Neurosci* **5,** 1079-1082.

De Schutter E & Bower JM. (1994a). An active membrane model of the cerebellar Purkinje cell II. Simulation of synaptic responses. *J Neurophysiol* **71,** 401-419.

De Schutter E & Bower JM. (1994b). An active membrane model of the cerebellar Purkinje cell. I. Simulation of current clamps in slice. *J Neurophysiol* **71,** 375-400.

de Zeeuw CI, Holstege JC, Ruigrok TJ & Voogd J. (1989). Ultrastructural study of the GABAergic, cerebellar, and mesodiencephalic innervation of the cat medial accessory olive: anterograde tracing combined with immunocytochemistry. *J Comp Neurol* **284,** 12-35.

De Zeeuw CI, Simpson JI, Hoogenraad CC, Galjart N, Koekkoek SK & Ruigrok TJ. (1998). Microcircuitry and function of the inferior olive. *Trends Neurosci* **21,** 391-400.

Delaney AJ & Jahr CE. (2002). Kainate receptors differentially regulate release at two parallel fiber synapses. *Neuron* **36,** 475-482.

Destexhe A, Rudolph M & Pare D. (2003). The high-conductance state of neocortical neurons in vivo. *Nat Rev Neurosci* **4,** 739-751.

Diana MA & Marty A. (2003). Characterization of depolarization-induced suppression of inhibition using paired interneuron--Purkinje cell recordings. *J Neurosci* **23,** 5906-5918.

DiGregorio DA, Nusser Z & Silver RA. (2002). Spillover of glutamate onto synaptic AMPA receptors enhances fast transmission at a cerebellar synapse. *Neuron* **35,** 521-533.

Dittman JS & Regehr WG. (1997). Mechanism and kinetics of heterosynaptic depression at a cerebellar synapse. *J Neurosci* **17,** 9048-9059.

Dugue GP, Dumoulin A, Triller A & Dieudonne S. (2005). Target-dependent use of co-released inhibitory transmitters at central synapses. *J Neurosci* **25,** 6490-6498.

Dumoulin A, Triller A & Dieudonne S. (2001). IPSC kinetics at identified GABAergic and mixed GABAergic and glycinergic synapses onto cerebellar Golgi cells. *J Neurosci* **21,** 6045-6057.

Dunbar RL, Chen G, Gao W, Reinert KC, Feddersen R & Ebner TJ. (2004). Imaging parallel fiber and climbing fiber responses and their short-term interactions in the mouse cerebellar cortex in vivo. *Neuroscience* **126,** 213-227.

Ebner TJ, Chen G, Gao W & Reinert K. (2005). Optical imaging of cerebellar functional architectures: parallel fiber beams, parasagittal bands and spreading acidification. *Prog Brain Res* **148,** 125-138.

Eccles JC. (1973). The cerebellum as a computer: patterns in space and time. *J Physiol* **229,** 1-32.

Eccles JC, Faber DS, Murphy JT, Sabah NH & Taborikova H. (1971). Investigations on integration of mossy fibre inputs to Purkyne cells in the anterior lobe. *Exp Brain Res* **13,** 54-77.

Eccles JC, Ito M & Szenthagothai J. (1967). *The Cerebellum as a Neuronal Machine.*

Eccles JC, Llinás R & Sasaki K. (1966). The mossy fibre-granule cell relay of the cerebellum and its inhibitory control by Golgi cells. *Exp Brain Res* **1,** 82-101.

Eccles JC, Sabah NH, Schmidt RF & Taborikova H. (1972a). Cutaneous mechanoreceptors influencing impulse discharges in cerebellar cortex. II. In Purkyne cells by mossy fiber input. *Exp Brain Res* **15,** 261-277.

Eccles JC, Sabah NH, Schmidt RF & Taborikova H. (1972b). Integration by Purkyne cells of mossy and climbing fiber inputs from cutaneous mechanoreceptors. *Exp Brain Res* **15,** 498-520.

Eilers J, Augustine GJ & Konnerth A. (1995). Subthreshold synaptic Ca^{2+} signalling in fine dendrites and spines of cerebellar Purkinje neurons [see comments]. *Nature* **373,** 155-158.

Ekerot CF & Kano M. (1985). Long-term depression of parallel fibre synapses following stimulation of climbing fibres. *Brain Res* **342,** 357-360.

Endo S, Suzuki M, Sumi M, Nairn AC, Morita R, Yamakawa K, Greengard P & Ito M. (1999). Molecular identification of human G-substrate, a possible downstream component of the cGMP-dependent protein kinase cascade in cerebellar Purkinje cells. *Proc Natl Acad Sci U S A* **96,** 2467-2472.

Etzion Y & Grossman Y. (1998). Potassium currents modulation of calcium spike firing in dendrites of cerebellar Purkinje cells. *Exp Brain Res* **122,** 283-294.

Farrant M & Nusser Z. (2005). Variations on an inhibitory theme: phasic and tonic activation of GABA(A) receptors. *Nat Rev Neurosci* **6,** 215-229.

Fetz EE & Gustafsson B. (1983). Relation between shapes of post-synaptic potentials and changes in firing probability of cat motoneurones. *J Physiol* **341,** 387-410.

Finch EA & Augustine GJ. (1998). Local calcium signalling by inositol-1,4,5-trisphosphate in Purkinje cell dendrites. *Nature* **396,** 753-756.

Forsythe ID & Clements JD. (1990). Presynaptic glutamate receptors depress excitatory monosynaptic transmission between mouse hippocampal neurones. *J Physiol* **429,** 1-16.

Fox EA & Gruol DL. (1993). Corticotropin-releasing factor suppresses the afterhyperpolarization in cerebellar Purkinje neurons. *Neurosci Lett* **149,** 103-107.

Fredette BJ & Mugnaini E. (1991). The GABAergic cerebello-olivary projection in the rat. *Anat Embryol (Berl)* **184,** 225-243.

Freund TF & Buzsaki G. (1996). Interneurons of the hippocampus. *Hippocampus* **6,** 347-470.

Gao W, Chen G, Reinert KC & Ebner TJ. (2005). Cerebellar molecular layer inhibition in crus II: relation to zebrin II bands and peripheral responses. *SFN Abstracts* **Program No. 179.7**.

Garthwaite J, Charles SL & Chess-Williams R. (1988). Endothelium-derived relaxing factor release on activation of NMDA receptors suggests role as intercellular messenger in the brain. *Nature* **336,** 385-388.

Garwicz M & Andersson G. (1992). Spread of synaptic activity along parallel fibres in cat cerebellar anterior lobe. *Exp Brain Res* **88,** 615-622.

Granit R & Phillips CG. (1956). Excitatory and inhibitory processes acting upon individual Purkinje cells of the cerebellum in cats. *J Physiol* **133,** 520-547.

Gruart A, Guillazo-Blanch G, Fernandez-Mas R, Jimenez-Diaz L & Delgado-Garcia JM. (2000). Cerebellar posterior interpositus nucleus as an enhancer of classically conditioned eyelid responses in alert cats. *J Neurophysiol* **84,** 2680-2690.

Gulledge AT & Stuart GJ. (2003). Excitatory actions of GABA in the cortex. *Neuron* **37,** 299-309.

Gundappa-Sulur G, De Schutter E & Bower JM. (1999). Ascending granule cell axon: an important component of cerebellar cortical circuitry. *J Comp Neurol* **408,** 580-596.

Hamann M, Desarmenien M, Desaulles E, Bader MF & Feltz P. (1988). Quantitative evaluation of the properties of a pyridazinyl GABA derivative (SR 95531) as a $GABA_A$ competitive antagonist. An electrophysiological approach. *Brain Res* **442,** 287-296.

Hamori J & Somogyi J. (1983). Formation of new synaptic contacts by Purkinje axon collaterals in the granular layer of deafferented cerebellar cortex of adult rat. *Acta Biol Hung* **34,** 163-176.

Hansel C, Linden DJ & D'Angelo E. (2001). Beyond parallel fiber LTD: the diversity of synaptic and non-synaptic plasticity in the cerebellum. *Nat Neurosci* **4,** 467-475.

Harsch A & Robinson HP. (2000). Postsynaptic variability of firing in rat cortical neurons: the roles of input synchronization and synaptic NMDA receptor conductance. *J Neurosci* **20,** 6181-6192.

Hartell NA. (1994). cGMP acts within cerebellar Purkinje cells to produce long term depression via mechanisms involving PKC and PKG. *Neuroreport* **5,** 833-836.

Hartell NA. (1996a). Inhibition of cGMP breakdown promotes the induction of cerebellar long-term depression. *J Neurosci* **16,** 2881-2890.

Hartell NA. (1996b). Strong activation of parallel fibers produces localized calcium transients and a form of LTD that spreads to distant synapses. *Neuron* **16,** 601-610.

Hartell NA. (2001). Receptors, second messengers and protein kinases required for heterosynaptic cerebellar long-term depression. *Neuropharmacology* **40,** 148-161.

Hartell NA. (2002). Parallel fiber plasticity. *Cerebellum* **1,** 3-18.

Harvey RJ & Napper RM. (1991). Quantitative studies on the mammalian cerebellum. *Prog Neurobiol* **36,** 437-463.

Häusser M & Clark BA. (1997). Tonic synaptic inhibition modulates neuronal output pattern and spatiotemporal synaptic integration. *Neuron* **19,** 665-678.

Häusser M, Major G & Stuart GJ. (2001). Differential shunting of EPSPs by action potentials. *Science* **291,** 138-141.

Hebb D. (1949). *The organization of behavior: a neuropsychological theory.* Wiley, New York.

Helmchen F & Waters J. (2002). Ca^{2+} imaging in the mammalian brain in vivo. *Eur J Pharmacol* **447,** 119-129.

Hille B. (2001). *Ion Channels of Excitable Membranes.* Sinauer Associates, Inc, Sunderland, USA.

Hoffmeister B, Janig W & Lisney SJ. (1991). A proposed relationship between circumference and conduction velocity of unmyelinated axons from normal and regenerated cat hindlimb cutaneous nerves. *Neuroscience* **42,** 603-611.

Holmes G. (1939). The cerebellum of man. *Brain* **40,** 1-30.

Isope P & Barbour B. (2002). Properties of unitary granule cell-->Purkinje cell synapses in adult rat cerebellar slices. *J Neurosci* **22,** 9668-9678.

Isope P, Franconville R, Barbour B & Ascher P. (2004). Repetitive firing of rat cerebellar parallel fibres after a single stimulation. *J Physiol* **554,** 829-839.

Ito M. (2001). Cerebellar long-term depression: characterization, signal transduction, and functional roles. *Physiol Rev* **81,** 1143-1195.

Ito M & Kano M. (1982). Long-lasting depression of parallel fiber-Purkinje cell transmission induced by conjunctive stimulation of parallel fibers and climbing fibers in the cerebellar cortex. *Neurosci Lett* **33,** 253-258.

Ito M, Sakurai M & Tongroach P. (1982). Climbing fibre induced depression of both mossy fibre responsiveness and glutamate sensitivity of cerebellar Purkinje cells. *J Physiol* **324,** 113-134.

Ivry R. (1997). Cerebellar timing systems. *Int Rev Neurobiol* **41,** 555-573.

Ivry RB & Spencer RM. (2004). The neural representation of time. *Curr Opin Neurobiol* **14,** 225-232.

Jacoby S, Sims RE & Hartell NA. (2001). Nitric oxide is required for the induction and heterosynaptic spread of long-term potentiation in rat cerebellar slices. *J Physiol* **535,** 825-839.

Jaeger D. (2003). No parallel fiber volleys in the cerebellar cortex: evidence from cross-correlation analysis between Purkinje cells in a computer model and in recordings from anesthetized rats. *J Comput Neurosci* **14,** 311-327.

Jaeger D & Bower JM. (1994). Prolonged responses in rat cerebellar Purkinje cells following activation of the granule cell layer: an intracellular in vitro and in vivo investigation. *Exp Brain Res* **100,** 200-214.

Jaeger D & Bower JM. (1999). Synaptic control of spiking in cerebellar Purkinje cells: dynamic current clamp based on model conductances. *J Neurosci* **19,** 6090-6101.

Jaeger D, De Schutter E & Bower JM. (1997). The role of synaptic and voltage-gated currents in the control of Purkinje cell spiking: a modeling study. *J Neurosci* **17,** 91-106.

Jorntell H & Ekerot CF. (2003). Receptive field plasticity profoundly alters the cutaneous parallel fiber synaptic input to cerebellar interneurons in vivo. *J Neurosci* **23,** 9620-9631.

Joseph JW, Shambes GM, Beermann DH, Welker W, Gibson JM & Welker W. (1978). Tactile projections to granule cells in caudal vermis of the rat's cerebellum. *Brain Behav Evol* **15,** 141-149.

Kakegawa W & Yuzaki M. (2005). A mechanism underlying AMPA receptor trafficking during cerebellar long-term potentiation. *Proc Natl Acad Sci U S A* **102,** 17846-17851.

Kampa BM, Clements J, Jonas P & Stuart GJ. (2004). Kinetics of Mg^{2+} unblock of NMDA receptors: implications for spike-timing dependent synaptic plasticity. *J Physiol* **556,** 337-345.

Kandel ER. (2000). *Principals of Neural Science*. McGraw-Hill Medical, New York.

Kano M, Fukunaga K & Konnerth A. (1996). Ca^{2+}-induced rebound potentiation of γ-aminobutyric acid-mediated currents requires activation of Ca^{2+}/calmodulin-dependent kinase II. *Proc Natl Acad Sci U S A* **93,** 13351-13356.

Kano M & Kato M. (1987). Quisqualate receptors are specifically involved in cerebellar synaptic plasticity. *Nature* **325,** 276-279.

Kano M, Rexhausen U, Dreessen J & Konnerth A. (1992). Synaptic excitation produces a long-lasting rebound potentiation of inhibitory synaptic signals in cerebellar Purkinje cells. *Nature* **356,** 601-604.

Karachot L, Kado RT & Ito M. (1994). Stimulus parameters for induction of long-term depression in in vitro rat Purkinje cells. *Neurosci Res* **21,** 161-168.

Karachot L, Shirai Y, Vigot R, Yamamori T & Ito M. (2001). Induction of long-term depression in cerebellar Purkinje cells requires a rapidly turned over protein. *J Neurophysiol* **86,** 280-289.

Kassel J. (1980). Superior colliculus projections to tactile areas of rat cerebellar hemispheres. *Brain Res* **202,** 291-305.

Kaupmann K, Huggel K, Heid J, Flor PJ, Bischoff S, Mickel SJ, McMaster G, Angst C, Bittiger H, Froestl W & Bettler B. (1997). Expression cloning of GABA(B) receptors uncovers similarity to metabotropic glutamate receptors. *Nature* **386,** 239-246.

Kawa K. (2003). Glycine receptors and glycinergic synaptic transmission in the deep cerebellar nuclei of the rat: a patch-clamp study. *J Neurophysiol* **90,** 3490-3500.

Kawaguchi S & Hirano T. (2000). Suppression of inhibitory synaptic potentiation by presynaptic activity through postsynaptic GABA(B) receptors in a Purkinje neuron. *Neuron* **27,** 339-347.

Kawaguchi SY & Hirano T. (2002). Signaling cascade regulating long-term potentiation of GABA(A) receptor responsiveness in cerebellar Purkinje neurons. *J Neurosci* **22,** 3969-3976.

Kolb FP, Arnold G, Lerch R, Straka H & Buttner-Ennever J. (1997). Spatial distribution of field potential profiles in the cat cerebellar cortex evoked by peripheral and central inputs. *Neuroscience* **81,** 1155-1181.

Kondo S & Marty A. (1998). Synaptic currents at individual connections among stellate cells in rat cerebellar slices. *J Physiol (Lond)* **509,** 221-232.

Konnerth A, Llano I & Armstrong CM. (1990). Synaptic currents in cerebellar Purkinje cells. *Proc Natl Acad Sci U S A* **87,** 2662-2665.

Kreitzer AC & Regehr WG. (2001). Retrograde inhibition of presynaptic calcium influx by endogenous cannabinoids at excitatory synapses onto Purkinje cells. *Neuron* **29,** 717-727.

Launey T, Endo S, Sakai R, Harano J & Ito M. (2004). Protein phosphatase 2A inhibition induces cerebellar long-term depression and declustering of synaptic AMPA receptor. *Proc Natl Acad Sci U S A* **101,** 676-681.

Lavond DG. (2002). Role of the nuclei in eyeblink conditioning. *Ann N Y Acad Sci* **978,** 93-105.

Leinekugel X, Medina I, Khalilov I, Ben-Ari Y & Khazipov R. (1997). Ca^{2+} oscillations mediated by the synergistic excitatory actions of GABA(A) and NMDA receptors in the neonatal hippocampus. *Neuron* **18,** 243-255.

Leitges M, Kovac J, Plomann M & Linden DJ. (2004). A unique PDZ ligand in PKCα confers induction of cerebellar long-term synaptic depression. *Neuron* **44,** 585-594.

Lev-Ram V, Mehta SB, Kleinfeld D & Tsien RY. (2003). Reversing cerebellar long-term depression. *Proc Natl Acad Sci U S A* **100,** 15989-15993.

Lev-Ram V, Wong ST, Storm DR & Tsien RY. (2002). A new form of cerebellar long-term potentiation is postsynaptic and depends on nitric oxide but not cAMP. *Proc Natl Acad Sci U S A* **99,** 8389-8393.

Lin LL, Wartmann M, Lin AY, Knopf JL, Seth A & Davis RJ. (1993). cPLA2 is phosphorylated and activated by MAP kinase. *Cell* **72,** 269-278.

Linden DJ. (1995). Phospholipase A2 controls the induction of short-term versus long-term depression in the cerebellar Purkinje neuron in culture. *Neuron* **15,** 1393-1401.

Linden DJ & Ahn S. (1999). Activation of presynaptic cAMP-dependent protein kinase is required for induction of cerebellar long-term potentiation. *J Neurosci* **19,** 10221-10227.

Liu SJ & Cull-Candy SG. (2002). Activity-dependent change in AMPA receptor properties in cerebellar stellate cells. *J Neurosci* **22,** 3881-3889.

Llano I & Gerschenfeld HM. (1993). Inhibitory synaptic currents in stellate cells of rat cerebellar slices. *J Physiol (Lond)* **468,** 177-200.

Llano I, Leresche N & Marty A. (1991). Calcium entry increases the sensitivity of cerebellar Purkinje cells to applied GABA and decreases inhibitory synaptic currents. *Neuron* **6,** 565-574.

Llinas R & Sugimori M. (1980). Electrophysiological properties of in vitro Purkinje cell somata in mammalian cerebellar slices. *J Physiol* **305,** 171-195.

Loewenstein Y, Mahon S, Chadderton P, Kitamura K, Sompolinsky H, Yarom Y & Häusser M. (2005). Bistability of cerebellar Purkinje cells modulated by sensory stimulation. *Nat Neurosci* **8,** 202-211.

Maex R & De Schutter E. (2005). Oscillations in the cerebellar cortex: a prediction of their frequency bands. *Prog Brain Res* **148,** 181-188.

Magee JC & Johnston D. (1997). A synaptically controlled, associative signal for Hebbian plasticity in hippocampal neurons. *Science* **275,** 209-213.

Markram H, Lubke J, Frotscher M & Sakmann B. (1997). Regulation of synaptic efficacy by coincidence of postsynaptic APs and EPSPs. *Science* **275,** 213-215.

Marr D. (1969). A theory of cerebellar cortex. *J Physiol (Lond)* **202,** 437-470.

Matsuda S, Launey T, Mikawa S & Hirai H. (2000). Disruption of AMPA receptor GluR2 clusters following long-term depression induction in cerebellar Purkinje neurons. *Embo J* **19,** 2765-2774.

McDonald BJ & Moss SJ. (1994). Differential phosphorylation of intracellular domains of γ-aminobutyric acid type A receptor subunits by calcium/calmodulin type 2-

dependent protein kinase and cGMP-dependent protein kinase. *J Biol Chem* **269,** 18111-18117.

McKay BE, Molineux ML, Mehaffey WH & Turner RW. (2005). Kv1 K^+ channels control Purkinje cell output to facilitate postsynaptic rebound discharge in deep cerebellar neurons. *J Neurosci* **25,** 1481-1492.

Medina JF, Christopher Repa J, Mauk MD & LeDoux JE. (2002a). Parallels between cerebellum- and amygdala-dependent conditioning. *Nat Rev Neurosci* **3,** 122-131.

Medina JF, Nores WL & Mauk MD. (2002b). Inhibition of climbing fibres is a signal for the extinction of conditioned eyelid responses. *Nature* **416,** 330-333.

Medina JF, Nores WL, Ohyama T & Mauk MD. (2000). Mechanisms of cerebellar learning suggested by eyelid conditioning. *Curr Opin Neurobiol* **10,** 717-724.

Mellor JR & Randall AD. (1998). Voltage-dependent deactivation and desensitization of GABA responses in cultured murine cerebellar granule cells. *J Physiol* **506,** 377-390.

Midtgaard J. (1992). Membrane properties and synaptic responses of Golgi cells and stellate cells in the turtle cerebellum in vitro. *J Physiol* **457,** 329-354.

Miles R, Toth K, Gulyas AI, Hajos N & Freund TF. (1996). Differences between somatic and dendritic inhibition in the hippocampus. *Neuron* **16,** 815-823.

Mitchell SJ & Silver RA. (2000). Glutamate spillover suppresses inhibition by activating presynaptic mGluRs. *Nature* **404,** 498-502.

Mitchell SJ & Silver RA. (2003). Shunting inhibition modulates neuronal gain during synaptic excitation. *Neuron* **38,** 433-445.

Mittmann W, Chadderton P & Häusser M. (2004). Neuronal microcircuits: frequency-dependent flow of inhibition. *Curr Biol* **14,** R837-839.

Mittmann W, Koch U & Häusser M. (2005). Feed-forward inhibition shapes the spike output of cerebellar Purkinje cells. *J Physiol* **563,** 369-378.

Miyakawa H, Lev-Ram V, Lasser-Ross N & Ross WN. (1992). Calcium transients evoked by climbing fiber and parallel fiber synaptic inputs in guinea pig cerebellar Purkinje neurons. *J Neurophysiol* **68,** 1178-1189.

Miyata M, Kim HT, Hashimoto K, Lee TK, Cho SY, Jiang H, Wu Y, Jun K, Wu D, Kano M & Shin HS. (2001). Deficient long-term synaptic depression in the rostral cerebellum correlated with impaired motor learning in phospholipase C β4 mutant mice. *Eur J Neurosci* **13,** 1945-1954.

Molineux ML, Fernandez FR, Mehaffey WH & Turner RW. (2005). A-type and T-type currents interact to produce a novel spike latency-voltage relationship in cerebellar stellate cells. *J Neurosci* **25,** 10863-10873.

Monsivais P, Clark BA, Roth A & Häusser M. (2005). Determinants of action potential propagation in cerebellar Purkinje cell axons. *J Neurosci* **25,** 464-472.

Moss SJ & Smart TG. (2001). Constructing inhibitory synapses. *Nat Rev Neurosci* **2,** 240-250.

Nakazawa K, Mikawa S, Hashikawa T & Ito M. (1995). Transient and persistent phosphorylation of AMPA-type glutamate receptor subunits in cerebellar Purkinje cells. *Neuron* **15,** 697-709.

Napper RM & Harvey RJ. (1988). Number of parallel fiber synapses on an individual Purkinje cell in the cerebellum of the rat. *J Comp Neurol* **274,** 168-177.

Neher E & Sakmann B. (1992). The patch clamp technique. *Sci Am* **266,** 44-51.

Nitz D & Tononi G. (2002). Tonic rhythmic activity of rat cerebellar neurons. *Exp Brain Res* **146,** 265-270.

Nolte J. (1999). *The Human Brain: an introduction to its functional anatomy.* Mosby Inc., St. Louis.

Oancea E & Meyer T. (1998). Protein kinase C as a molecular machine for decoding calcium and diacylglycerol signals. *Cell* **95,** 307-318.

Odeh F, Ackerley R, Bjaalie JG & Apps R. (2005). Pontine maps linking somatosensory and cerebellar cortices are in register with climbing fiber somatotopy. *J Neurosci* **25,** 5680-5690.

Ohtsuki G, Kawaguchi SY, Mishina M & Hirano T. (2004). Enhanced inhibitory synaptic transmission in the cerebellar molecular layer of the GluRδ2 knock-out mouse. *J Neurosci* **24,** 10900-10907.

Otmakhov N, Shirke AM & Malinow R. (1993). Measuring the impact of probabilistic transmission on neuronal output. *Neuron* **10,** 1101-1111.

Palay SL & Chan-Palay V. (1974). *Cerebellar Cortex: Cytology and organization.* Berlin: Springer-Verlag.

Pedroarena CM & Schwarz C. (2003). Efficacy and short-term plasticity at GABAergic synapses between Purkinje and cerebellar nuclei neurons. *J Neurophysiol* **89,** 704-715.

Perkel DJ, Hestrin S, Sah P & Nicoll RA. (1990). Excitatory synaptic currents in Purkinje cells. *Proc R Soc Lond B Biol Sci* **241,** 116-121.

Pichitpornchai C, Rawson JA & Rees S. (1994). Morphology of parallel fibres in the cerebellar cortex of the rat: an experimental light and electron microscopic study with biocytin. *J Comp Neurol* **342,** 206-220.

Pijpers A, Voogd J & Ruigrok TJ. (2005). Topography of olivo-cortico-nuclear modules in the intermediate cerebellum of the rat. *J Comp Neurol* **492,** 193-213.

Pouille F & Scanziani M. (2001). Enforcement of temporal fidelity in pyramidal cells by somatic feed-forward inhibition. *Science* **293,** 1159-1163.

Pouille F & Scanziani M. (2004). Routing of spike series by dynamic circuits in the hippocampus. *Nature* **429,** 717-723.

Pouzat C & Hestrin S. (1997). Developmental regulation of basket/stellate cell-->Purkinje cell synapses in the cerebellum. *J Neurosci* **17,** 9104-9112.

Purves D, Augustine GJ, Fitzpatrick D, Hall WC, LaMantia A-S, McNamara JO & Williams SM. (2004). *Neuroscience*. Sinauer Associates, Inc., Sunderland, USA.

Raman IM & Bean BP. (1997). Resurgent sodium current and action potential formation in dissociated cerebellar Purkinje neurons. *J Neurosci* **17,** 4517-4526.

Raman IM & Bean BP. (1999). Ionic currents underlying spontaneous action potentials in isolated cerebellar Purkinje neurons. *J Neurosci* **19,** 1663-1674.

Raman IM, Gustafson AE & Padgett D. (2000). Ionic currents and spontaneous firing in neurons isolated from the cerebellar nuclei. *J Neurosci* **20,** 9004-9016.

Ramón y Cajal S. (1888). Sobre las fibras nerviosas de la capa molecular del cerebelo. *Rev trimestr Histol* **No 2,** 33 - 41.

Ramón y Cajal S. (1894). *Les nouvelles idées sur la structure du systéme nerveux chez l'homme et chez les vertébrés.* Paris.

Ramón y Cajal S. (1904). *La Textura del Sistema Nerviosa del Hombre y los Vertebrados*. Madrid.

Rancillac A & Barbara JG. (2005). Frequency-dependent recruitment of inhibition mediated by stellate cells in the rat cerebellar cortex. *J Neurosci Res* **80,** 414-423.

Reynolds T & Hartell NA. (2000). An evaluation of the synapse specificity of long-term depression induced in rat cerebellar slices. *J Physiol* **527,** 563-577.

Robinson HP & Kawai N. (1993). Injection of digitally synthesized synaptic conductance transients to measure the integrative properties of neurons. *J Neurosci Methods* **49,** 157-165.

Rossi DJ & Hamann M. (1998). Spillover-mediated transmission at inhibitory synapses promoted by high affinity α6 subunit GABA(A) receptors and glomerular geometry. *Neuron* **20,** 783-795.

Roth A & Häusser M. (2001). Compartmental models of rat cerebellar Purkinje cells based on simultaneous somatic and dendritic patch-clamp recordings. *J Physiol* **535,** 445-472.

Rowland NC & Jaeger D. (2005). Coding of tactile response properties in the rat deep cerebellar nuclei. *J Neurophysiol* **94,** 1236-1251.

Ruigrok TJ. (1997). *Cerebellar nuclei: the olivary connection.* Elsevier Science, Amsterdam.

Safo PK & Regehr WG. (2005). Endocannabinoids control the induction of cerebellar LTD. *Neuron* **48,** 647-659.

Sakurai M. (1987). Synaptic modification of parallel fibre-Purkinje cell transmission in in vitro guinea-pig cerebellar slices. *Journal of Physiology (London)* **394,** 463-480.

Salin PA, Malenka RC & Nicoll RA. (1996). Cyclic AMP mediates a presynaptic form of LTP at cerebellar parallel fiber synapses. *Neuron* **16,** 797-803.

Santamaria F, Jaeger D, De Schutter E & Bower JM. (2002). Modulatory effects of parallel fiber and molecular layer interneuron synaptic activity on purkinje cell responses to ascending segment input: a modeling study. *J Comput Neurosci* **13,** 217-235.

Schonewille M, Khosrovani S, Winkelman BH, Hoebeek FE, De Jeu MT, Larsen IM, Van Der Burg J, Schmolesky MT, Frens MA & De Zeeuw CI. (2006). Purkinje cells in awake behaving animals operate at the upstate membrane potential. *Nat Neurosci* **9,** 459-461.

Shambes GM, Beermann DH & Welker W. (1978a). Multiple tactile areas in cerebellar cortex: another patchy cutaneous projection to granule cell columns in rat. *Brain Res* **157,** 123-128.

Shambes GM, Gibson JM & Welker W. (1978b). Fractured somatotopy in granule cell tactile areas of rat cerebellar hemispheres revealed by micro-mapping. *Brain Behav Evol* **15,** 94-140.

Sharp AA, O'Neil MB, Abbott LF & Marder E. (1993). Dynamic clamp: computer-generated conductances in real neurons. *J Neurophysiol* **69,** 992-995.

Shepherd G. (2004). *The Synaptic Organization of the Brain.* Oxford University Press, New York.

Sherrington CS. (1906). *The Integrative Action of the Nervous System.* Yale University Press, New Haven.

Silver RA, Momiyama A & Cull-Candy SG. (1998). Locus of frequency-dependent depression identified with multiple-probability fluctuation analysis at rat climbing fibre-Purkinje cell synapses. *J Physiol* **510,** 881-902.

Sims RE & Hartell NA. (2005). Differences in transmission properties and susceptibility to long-term depression reveal functional specialization of ascending axon and parallel fiber synapses to Purkinje cells. *J Neurosci* **25,** 3246-3257.

Sjostrom PJ, Turrigiano GG & Nelson SB. (2001). Rate, timing, and cooperativity jointly determine cortical synaptic plasticity. *Neuron* **32,** 1149-1164.

Sjostrom PJ, Turrigiano GG & Nelson SB. (2003). Neocortical LTD via coincident activation of presynaptic NMDA and cannabinoid receptors. *Neuron* **39,** 641-654.

Smith SL & Otis TS. (2003). Persistent changes in spontaneous firing of Purkinje neurons triggered by the nitric oxide signaling cascade. *J Neurosci* **23,** 367-372.

Song S, Sjostrom PJ, Reigl M, Nelson S & Chklovskii DB. (2005). Highly nonrandom features of synaptic connectivity in local cortical circuits. *PLoS Biol* **3,** e68.

Southam E, Morris R & Garthwaite J. (1992). Sources and targets of nitric oxide in rat cerebellum. *Neurosci Lett* **137,** 241-244.

Spencer RM, Zelaznik HN, Diedrichsen J & Ivry RB. (2003). Disrupted timing of discontinuous but not continuous movements by cerebellar lesions. *Science* **300,** 1437-1439.

Stell BM, Brickley SG, Tang CY, Farrant M & Mody I. (2003). Neuroactive steroids reduce neuronal excitability by selectively enhancing tonic inhibition mediated by δ subunit-containing $GABA_A$ receptors. *Proc Natl Acad Sci U S A* **100,** 14439-14444.

Stevens CF. (1998). A million dollar question: does LTP = memory? *Neuron* **20,** 1-2.

Strack S, Barban MA, Wadzinski BE & Colbran RJ. (1997). Differential inactivation of postsynaptic density-associated and soluble Ca^{2+}/calmodulin-dependent protein kinase II by protein phosphatases 1 and 2A. *J Neurochem* **68,** 2119-2128.

Stuart G & Häusser M. (1994). Initiation and spread of sodium action potentials in cerebellar Purkinje cells. *Neuron* **13,** 703-712.

Stuart G, Spruston N & Häusser M. (1999). *Dendrites*. Oxford University Press, Oxford.

Stuart GJ, Dodt HU & Sakmann B. (1993). Patch-clamp recordings from the soma and dendrites of neurons in brain slices using infrared video microscopy. *Pflugers Arch* **423,** 511-518.

Sugihara I, Wu HS & Shinoda Y. (2001). The entire trajectories of single olivocerebellar axons in the cerebellar cortex and their contribution to Cerebellar compartmentalization. *J Neurosci* **21,** 7715-7723.

Sultan F & Bower JM. (1998). Quantitative Golgi study of the rat cerebellar molecular layer interneurons using principal component analysis. *J Comp Neurol* **393,** 353-373.

Suter KJ & Jaeger D. (2004). Reliable control of spike rate and spike timing by rapid input transients in cerebellar stellate cells. *Neuroscience* **124,** 305-317.

Takechi H, Eilers J & Konnerth A. (1998). A new class of synaptic response involving calcium release in dendritic spines. *Nature* **396,** 757-760.

Telgkamp P & Raman IM. (2002). Depression of inhibitory synaptic transmission between Purkinje cells and neurons of the cerebellar nuclei. *J Neurosci* **22,** 8447-8457.

Tempia F, Miniaci MC, Anchisi D & Strata P. (1998). Postsynaptic current mediated by metabotropic glutamate receptors in cerebellar Purkinje cells. *J Neurophysiol* **80,** 520-528.

Thach WT. (1968). Discharge of Purkinje and cerebellar nuclear neurons during rapidly alternating arm movements in the monkey. *J Neurophysiol* **31,** 785-797.

Turker KS & Miles TS. (1986). Climbing fiber lesions disrupt conditioning of the nictitating membrane response in the rabbit. *Brain Res* **363,** 376-378.

Vincent P, Armstrong CM & Marty A. (1992). Inhibitory synaptic currents in rat cerebellar Purkinje cells: modulation by postsynaptic depolarization. *J Physiol* **456,** 453-471.

Voet D & Voet JG. (1995). *Biochemistry*. John Wiley & Sons, Inc., New York.

Vos BP, Maex R, Volny-Luraghi A & De Schutter E. (1999). Parallel fibers synchronize spontaneous activity in cerebellar Golgi cells. *Journal of Neuroscience* **RC6,** 1-5.

Vranesic I, Iijima T, Ichikawa M, Matsumoto G & Knopfel T. (1994). Signal transmission in the parallel fiber-Purkinje cell system visualized by high-resolution imaging. *Proc Natl Acad Sci U S A* **91,** 13014-13017.

Wang SS-H, Denk W & Häusser M. (2000). Coincidence detection in single dendritic spines mediated by calcium release. *Nature Neuroscience*, accepted.

Wang YT & Linden DJ. (2000). Expression of cerebellar long-term depression requires postsynaptic clathrin-mediated endocytosis. *Neuron* **25,** 635-647.

Watanabe S, Takagi H, Miyasho T, Inoue M, Kirino Y, Kudo Y & Miyakawa H. (1998). Differential roles of two types of voltage-gated Ca^{2+} channels in the dendrites of rat cerebellar Purkinje neurons. *Brain Res* **791,** 43-55.

Welker C. (1971). Microelectrode delineation of fine grain somatotopic organization of (SmI) cerebral neocortex in albino rat. *Brain Res* **26,** 259-275.

Welker W. (1987). *Spatial organization of somatosensory projections to granule cell cerebellar cortex: Functional and connectional implications of fractured somatotopy*. Inc J.S. King.

Welsh JP & Llinas R. (1997). Some organizing principles for the control of movement based on olivocerebellar physiology. *Prog Brain Res* **114,** 449-461.

Williams SR, Christensen SR, Stuart GJ & Häusser M. (2002). Membrane potential bistability is controlled by the hyperpolarization-activated current I(H) in rat cerebellar Purkinje neurons in vitro. *J Physiol* **539,** 469-483.

Womack M & Khodakhah K. (2002). Active contribution of dendrites to the tonic and trimodal patterns of activity in cerebellar Purkinje neurons. *J Neurosci* **22,** 10603-10612.

Womack MD & Khodakhah K. (2004). Dendritic control of spontaneous bursting in cerebellar Purkinje cells. *J Neurosci* **24,** 3511-3521.

Woolston DC, Kassel J & Gibson JM. (1981). Trigeminocerebellar mossy fiber branching to granule cell layer patches in the rat cerebellum. *Brain Res* **209,** 255-269.

Wu HS, Sugihara I & Shinoda Y. (1999). Projection patterns of single mossy fibers originating from the lateral reticular nucleus in the rat cerebellar cortex and nuclei. *J Comp Neurol* **411,** 97-118.

Wyatt KD, Tanapat P & Wang SS. (2005). Speed limits in the cerebellum: constraints from myelinated and unmyelinated parallel fibers. *Eur J Neurosci* **21,** 2285-2290.

Frequently used abbreviations:

Abbreviation	Full Name
CF	climbing fiber
DCN	deep cerebellar nuclei
EPSC	excitatory postsynaptic current
EPSP	excitatory postsynaptic potential
FFI	feed-forward inhibition
GC	granule cell
GABA	γ-aminobutyric acid
$GABA_AR$	ionotropic γ-aminobutyric acid receptor
I / E ratio	IPSP amplitude divided by EPSP amplitude at -65 mV
IPSC	postsynaptic inhibitory current
IPSP	postsynaptic inhibitory potential
LTD	long-term depression
LTP	long-term potentiation
PC	Purkinje cell
PF	parallel fibre
PSTH	post stimulus time histogram

This table is also printed in the methods section.